AN ABSTRACT OF THE THESIS OF

STEVEN J. GANOE for the degree of MASTER OF SCIENCE

in GEOPHYSICS presented on October 20, 1982

Title: INVESTIGATION OF P_n WAVE PROPAGATION IN OREGON

Abstract approved: Redacted for Privacy

An investigation into the nature of P_n wave propagation was conducted for the portion of Oregon west of 120° W longitude. This included a determination of the velocity of propagation of the P_n wave as it travels along the Moho and an insight into the structure of the Moho.

Traveltimes from selected regional events recorded on the U.S. Geological Survey's Oregon network of short-period vertical seismometers made up the data set for this study. The locations of the events were examined in order to determine the distances associated with the traveltimes as accurately as possible and to determine the effects of errors in the distances on the subsequent analysis.

Three methods of analysis of the data were employed in this study. The first method was a traveltime analysis that included both a single and two simultaneously determined least squares straight line fits, performed on the whole region as well as on areas east and west of the Cascade Mountains. This analysis resulted in P_n velocities of 7.756 km/sec for the whole array, 7.975 km/sec west of the Cascades, and 7.751 km/sec east of the Cascades and Moho depths of 32 km average for the whole array, 22 km west, and 37 km east of the Cascades. The

second method was a time-term analysis which resulted in a crustal thickness map for the region that indicated a possible isostatic crustal root associated with the Cascades, but which does not fully compensate them. The possibility of partially molten or high temperature material in the areas of Mt. Hood and Newberry Crater was also indicated. The third method was a velocity vs. azimuth analysis which found anisotropy in the P_n velocity with the fast direction oriented generally southwest-northeast. The results of the method further supported the hypothesis that partially molten material exists in the Mt. Hood and Newberry Crater areas.

Investigation of P_n Wave Propagation in Oregon

by

Steven J. Ganoe

A THESIS

submitted to

Oregon State University

in partial fulfillment of
the requirements for the
degree of

Master of Science

Commencement June 1983

APPROVED:

Redacted for Privacy

Assistant Professor of Geophysics in charge of major

Redacted for Privacy

Dean of School of Oceanography

Redacted for Privacy

Dean of Gra[illegible]

Date thesis is presented 20 October, 1982

Typed by Donna Moore for Steven J. Ganoe

ACKNOWLEDGEMENTS

My most sincere thanks go to Mike Fehler, my major professor, for his guidance and support throughout the course of this work. His comments and suggestions during our discussions have always been insightful and thought provoking. I am grateful for the time and effort he has given me and the confidence he has shown in me.

Thanks also go to Alan Rite and Auriel (Cookie) Kollmann of the U.S. Geological Survey in Menlo Park, California for their cooperation and humor with my quest for 'the best data set possible'.

Special thanks go to my fellow students in Geophysics. Ariel Solano-Borrego helped me find out about the problems in locating earthquakes as well as giving me many enjoyable hours of 'cultural exchange' discussions about the two Americas (North and South). He and his family are special people. Dean Goodman taught me the forward toss in frisbee throwing and was always ready to help me relax and unwind. I expect to be hearing his songs on the radio very soon. Michel Bée, Haraldur Audunsson and Will Avera have given me many insights into geophysics and the world in general. Their friendship is very much appreciated.

This thesis could not have been completed without the skilled assistance of Donna Moore for her typing and administrative magic and of Josie Peper and Steven Troseth for their excellent drafting. Thanks also go to Jennifer Couch for patiently performing time consuming tasks for me and for not remaking the world just yet.

My most heartfelt thanks go to JoAnne Huppunen. JoAnne's intelligence and style have been an inspiration to me and her

understanding has helped me through some of the rough spots. I hope some day to completely master 'Huppunese'.

Last, but not least, I would like to thank my mother for always being there with encouragement and support and my father to whom this thesis is dedicated.

This research was supported in part by the Dean of Research at Oregon State University and in part by a grant from the Oregon State legislature to perform seismic monitoring in the state of Oregon.

TABLE OF CONTENTS

LIST OF FIGURES

LIST OF TABLES

INVESTIGATION OF P_n WAVE PROPAGATION IN OREGON

INTRODUCTION

This study presents the results of an investigation into the manner in which P_n waves travel beneath Oregon west of 120° west longitude. P_n waves are the compressional seismic waves which propagate along the Mohorovičić discontinuity (or Moho) that defines the separation of the crust from the mantle. The investigation into the nature of P_n wave propagation includes a determination of the velocity of propagation and some insight into the structure of the Moho. The determination of these Moho characteristics will improve the understanding of the seismic structure of the upper mantle and of the overlying crust in this region of Oregon.

The data set for this study consisted of the traveltimes from selected regional events (earthquakes and explosions) recorded on an array of short-period vertical seismometers installed by the United States Geological Survey. An examination of the locations of the events was performed in order to form the best data set possible.

The data were examined with three methods of analysis in hopes of obtaining a complementary set of results. The first method was a standard traveltime analysis which resulted in determination of P_n velocities and Moho depths for areas east and west of the Cascade Mountains and average values for the whole region. The second method was a time-term analysis which resulted in an average P_n velocity and a crustal thickness map for the region. The last method was a velocity vs. azimuth analysis in which anisotropy in the P_n velocity was determined and mapped. The investigation concluded with an

interpretation of the results obtained from the three forms of analysis and comparisons were made with the results of previous geologic and geophysical studies of the area.

It is hoped that this study can be effectively combined with future studies in this region to form a clearer picture of the structural and tectonic setting of Western Oregon.

GEOLOGIC AND TECTONIC SETTING

Western Oregon has a complex geologic and tectonic history and encompasses several physiographic provinces (see Figure 1). The provinces of main concern to this study are the Cascade Range, the Willamette Valley, the Coast Range, and the High Lava Plains.

The Cascade Range in Oregon is part of a north-south trending volcanic range which extends from British Columbia to northern California. The Range is divided into the Western Cascades and the High Cascades based on a structural and, to a lesser extent, compositional unconformity between the lavas (McBirney, 1978; Peck et al, 1964). The Western Cascades consist of gently folded and faulted flows and tuffs which were laid down from Eocene to Miocene time. It is still uncertain when activity began along the Cascade axis but by Oligocene time there were many eruptions of andesite and more siliceous rocks from centers in the area of the Western Cascades (McBirney, 1978). By far the greatest volumes of lava poured out in the Mid-Miocene 'Columbian' volcanism. In the Western Cascades this volcanism was expressed by a chain of basalt to andesite volcanoes which covered the region with thick assemblages of basalts and andesites that compose the Sardine formation. At this time Columbia River basalts were erupted from centers to the east and covered extensive areas in the northern Cascades and have also been traced to the present coast of Oregon (Beeson and Moran, 1979). Shortly after this episode of volcanism, broad folds developed along an axis that closely paralleled the trend of the Mid-Miocene volcanoes, uplifting the area of the Cascades.

The recent episode of volcanism has been responsible for the

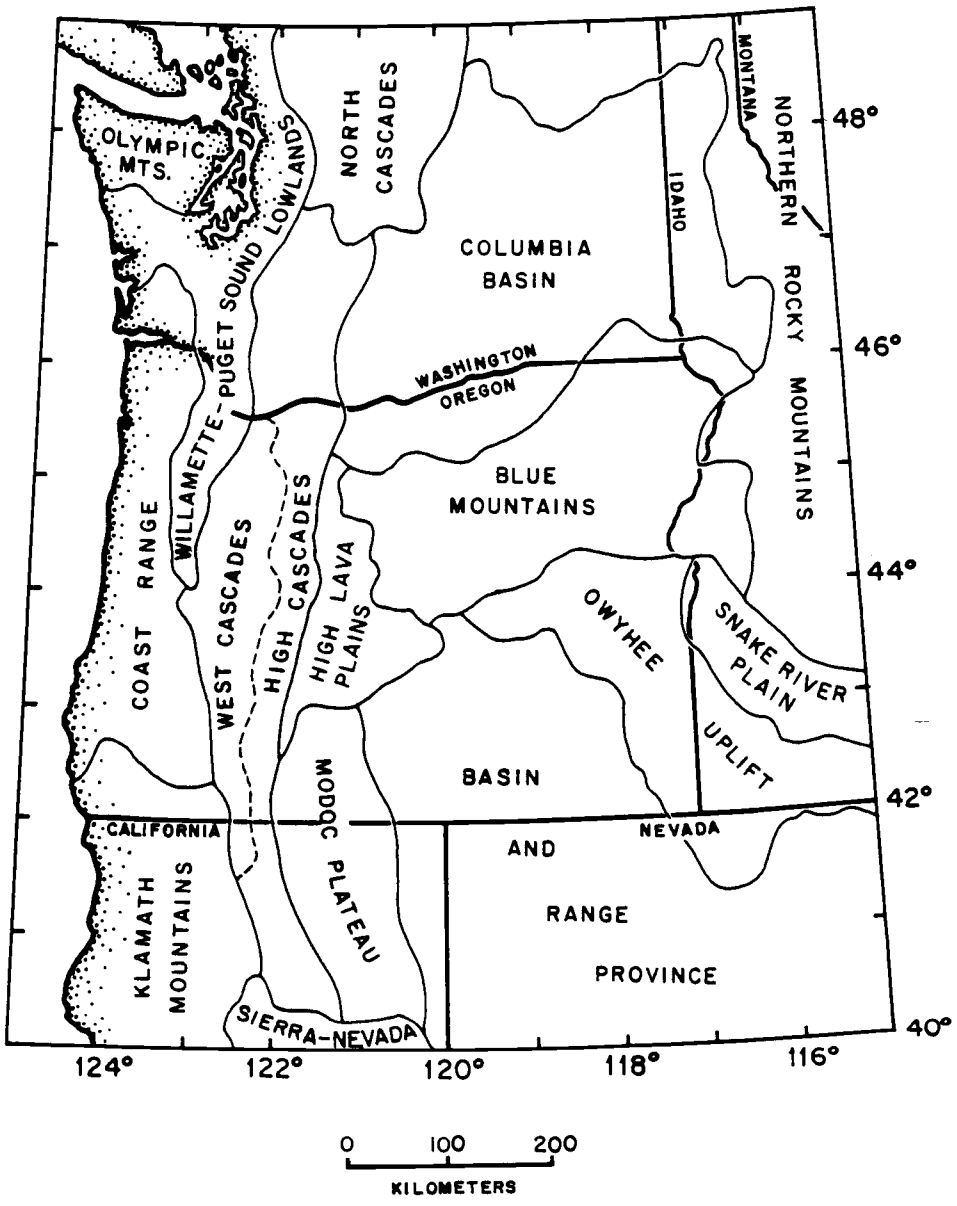

Figure 1. Physiographic provinces of the Northwest United States. After Wells and Peck (1961).

familiar volcanoes of the modern High Cascades, which form the eastern portion of the Cascade Range. This episode began in earliest Pleistocene time and its activity was characterized by basaltic cones, flows, and low overlapping shields. With time, the activity became more localized in persistent centers from which progressively more differentiated magmas were discharged. Most of the large andesitic cones that form the crest of the High Cascades began to rise about one million years ago and reached their present elevations during a brief period of intense activity. Block faulting occurred concurrently with the volcanism and resulted in uplift and westward tilting of the Western Cascades and subsidence of the basement below the High Cascades to form a shallow graben (Allen, 1966; McBirney, 1978). The total thickness of volcanics that has accumulated in the Cascade region since Eocene time has been estimated to be approximately 5000 meters (Braman, 1981).

The Coast Range is a north-south trending mountainous belt extending from the Klamath Mountains northward beyond the Columbia River into Washington. It is composed of Paleocene to Eocene submarine basalts that attain thicknesses of 4600 meters and Eocene to Pleistocene sedimentary rocks that have a combined thickness of approximately 7600 meters (Snavely et al., 1969). It is believed that the basalts were erupted from a hot spot, centered on a spreading ridge in this area, and formed a chain of submarine volcanoes. Sediments, eroded from the Cascades, intertongued and covered the volcano chain (R. Duncan, personal communication). The uplift of the area probably began in late Oligocene time and during the Miocene gabbroic and alkalic sills and dikes were emplaced and Columbia River basalt flowed

through the north part of the area from its eruptive centers to the east (Snavely et al., 1969, Thiruvathukal et al., 1970).

The Willamette Valley, which lies between the Coast Range and the Cascades, is a nearly flat alluvial plain with low hills. It is a structural depression and consists of nearly the same sequence of volcanic and sedimentary rocks as the Coast Range. Differences include a more extensive Columbia River basalt layer, intertongueing on the east side of the valley of sedimentary rock types derived from the Cascades, and a 30 to 60 meter cover of unconsolidated alluvium (Newton, 1969; Snavely et al., 1969).

The High Lava Plains consist of Plio-Pleistocene basaltic lavas, tuffs, and alluvium which have covered over the earlier Tertiary volcanics and Basin and Range structure. Basaltic cinder cones and lava buttes occur in many places but the most prominent feature of this province is the Newberry Caldera. Newberry is an extensive shield volcano which rises from the basalt plateaus of the High Lava Plains and is centered about 60 kilometers east of the crest of the Cascades. The volcano is approximately 40 kilometers in diameter and the caldera, which formed from the collapse of the top of the volcano, is approximately 13 kilometers in diameter. Rhyolite flows, ash, pumice, and obsidian flows erupted in the cladera after its collapse. The latest of these occurred approximately 1900 years ago and it is thought that there might still be a body of magma beneath this volcano (Higgins and Waters, 1968).

PREVIOUS GEOPHYSICAL STUDIES

There has been a number of investigations into the crustal structure beneath various parts of Oregon. Both gravity and seismic methods can produce models of the crust down to and including the upper mantle, and both have been employed in these previous investigations. In the case of gravity, layers and/or blocks of different constant densities are modeled to fit the observed gravity anomalies. Where possible, other geophysical constraints are included to reduce the nonuniqueness of the modeling. There are many methods to collect and interpret seismic data, but the end product is usually a model consisting of a layer or several layers with their associated thicknesses and P or S wave velocities. The velocities are usually considered to be constant within the layer, but they can vary with depth. Lateral velocity variations are sometimes modeled, but usually only on a large scale. The thicknesses of layers can vary laterally, either as a constant slope or as an undulating surface.

Gravity surveys have covered the entire State of Oregon with particular attention to the Cascades. Thiruvathukal et al. (1970) produced gravity anomaly maps of the entire state and also fit third-degree and tenth-degree polynomials to the data to obtain regional gravity variations which should correspond to crustal depths. Assuming a single layer constant density crust over the mantle, Thiruvathukal et al. (1970) employed the $(\sin x)/x$ method to obtain a crustal thickness map of Oregon and western Idaho (Figure 2). Thicknesses ranged from 20-25 km beneath the Coast Range to 40-50 km beneath eastern Oregon. The map indicates that any root that the

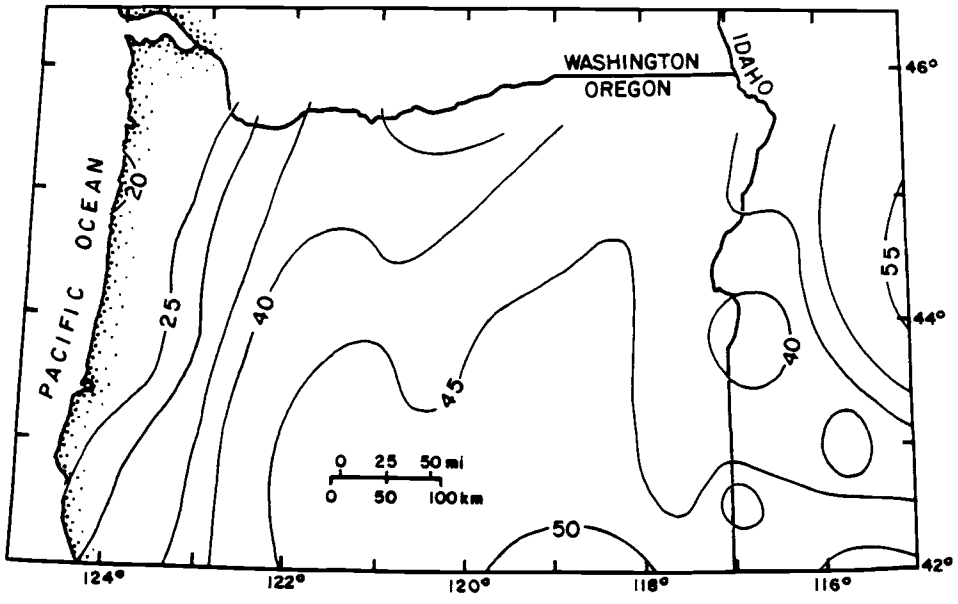

Figure 2. Crustal thickness map obtained by Thiruvathukal et al. (1970) using the (sin x)/x method on gravity data. Contour interval is 5 km.

Cascades might have, would have to be minor in depth and extent. They also speculate that a thinner crust (approximately 30 km) over a mantle of lower density would also fit the data east of the Cascades and would be more in line with a Basin and Range type structure.

Veen (1982), who performed a gravity survey of the Southern Oregon Cascades and adjoining Basin and Range province, modeled two layers in the upper mantle. Her model included a 30 km crust over a 10 km layer of 3.27 g/cm^3 density which was underlain by normal mantle of 3.32 g/cm^3. This model agrees with observations that the Basin and Range province has anomalously low densities and velocities in a shallower than normal upper mantle (see Cook, 1967; Hill and Pakiser, 1967; and Priestly and Brune, 1978).

Both Pitts (1979), who studied gravity data collected in Central Oregon Cascades, and Braman (1981), who worked in the Northern Oregon Cascades, report a general increase in crustal thickness to the southeast seen on their regional gravity maps. This agrees with the trends seen on Thiruvathukal's (1970) crustal thickness map, as do their absolute thicknesses.

Several seismic investigations, using different methods of analysis, have determined crustal structures in different areas of the Northwestern United States, including total crustal thickness and P_n velocities. Dehlinger et al. (1965) constructed traveltime curves for the Pacific Northwest states using arrival time from earthquakes in Washington, Idaho, and Montana. They showed that a linear fit to the P_n traveltimes is justified and found lower P_n velocities (7.67 km/sec) west of the Cascades than to the east (7.96 km/sec). Their intercept times indicated that the crust is 5 to 10 km thinner west

of the Cascades than to the east, though they did not resolve absolute crustal thickness.

Berg et al. (1966) obtained a crustal profile of the Oregon Coast Range from an unreversed refraction line, which had a shot point near Depoe Bay, Oregon and stations extending north into western Washington. From straight-line fits to the traveltime data they found an apparent crustal thickness of 16 km with an apparent P_n velocity of 8.0 km/sec.

Chiburis (1966), analyzing surface wave dispersion across arrays in eastern Oregon, Idaho, Washington, and Nevada, and using the P_n velocities of Dehlinger et al. (1965), found a crustal thickness of 45 km. Using Bouguer gravity anomalies and isostasy considerations he extended the model west and found a crustal thickness of 48 km beneath the Cascades and 35 km west of the Cascades.

A large chemical explosion in southern British Columbia provided the source for several unreversed refraction lines which ran through Washington at various azimuths. Johnson and Couch (1970) studied the arrival times of two of those refraction lines, which ran through the northern Washington Cascades and Puget Sound Lowlands. They reported a crustal thickness of 32 km with a P_n velocity of 7.91 km/sec beneath the Cascades and a 29 km thickness with P_n = 8.06 km/sec for the crust under the Puget Sound Lowlands. They also found that crustal thickness increased to the south. Hill (1972), also using the British Columbia explosion as a seismic source, analyzed the arrivals of an unreversed refraction line which ran almost due south through the Columbia Plateau of eastern Washington and into the Blue Mountains of eastern Oregon. He reported an average crustal thickness

of 35 km with a P_n velocity of 8.0 km/sec. He also found, from an analysis of P_n residual values, that the crust beneath the Columbia Plateau had to be either up to 12 km thinner or the P_n velocity had to be up to 0.8 km/sec faster than his reported average value, or some combination of both.

McCollom and Crosson (1975) studied arrival times from regional earthquakes across arrays in western and eastern Washington. Using a modified time-term analysis and apparent velocity measurements they obtained a P_n velocity of 7.72 km/sec west of the Cascades and 8.10 km/sec east. Absolute depths to the Moho were not determined from this analysis although the relative station time-terms indicated a shallow slope of the Moho, thickening toward the Cascades on both sides, of 3° to 5°.

In northern California, Simila (1980) investigated P_n travel-times from regional earthquakes and Nevada Test Site explosions. He found a range of P_n velocity values from 7.98 km/sec to 8.06 km/sec and crustal thicknesses of 26 km beneath the Coast Range and 29-31 km beneath the Cascades.

Langston (1977) studied the timing and relative amplitudes of long-period Ps and Sp conversions and P reverberations from teleseismic events recorded at the World Wide Standard Seismograph station in Corvallis, Oregon. He obtained a P_n velocity of 8.0 km/sec at 21 km depth with a low velocity zone beneath this. His low velocity zone extends to 45 km depth where there is a high velocity contrast which he interprets as evidence of a subducting slab.

Leaver (1982) analyzed a combination of data sets, which included a 1978 U.S.G.S. refraction profile along the crest of the

Oregon Cascades from Mt. Hood to Crater Lake (reversed), 3 regional earthquakes recorded on the U.S.G.S. Oregon Seismic Network, and the Bouguer gravity anomaly map of Thiruvathukal et al. (1970). From this combined data set he determined P_n velocities to be 7.70 km/sec under the Cascades and 7.80 east of the Cascades. His crustal thickness varied from 40 km beneath the northern Oregon Cascades to 48 km beneath the southern Oregon Cascades (Moho dipping to the south).

The combined results of previous investigations (gravity and seismic) indicate that there is a generally thicker crust to the east of the Cascades (35-45 km) than to the west (16-35 km) and a general trend towards higher P_n velocities in the east (7.96-8.10 km/sec) than in the west (7.67-8.0 km/sec).

INSTRUMENTATION AND DATA GATHERING

The Office of Earthquake Studies of the U.S. Geological Survey (U.S.G.S.) instituted a volcanic hazards program in the Oregon Cascades early in 1980. Integral to this program was the installation of a regional seismic network consisting of 32 one Hertz vertical seismometers in and around the Oregon Cascades. The distribution of these staions is shown in Figure 3 and their locations and elevations are given in Table 1. The data from all of these stations are telemetered via telephone lines to the U.S.G.S. in Menlo Park, California and are recorded on analog magnetic tape as well as on film. Sixteen of these stations plus a station in Corvallis have also been recorded on film by the Geophysics Group of the School of Oceanography at Oregon State University. The film is scanned daily and any earthquake activity or explosion is noted and, when possible, located.

When an event of interest was noted on the film, a complete playback from the analog tape of all 32 stations was requested from the U.S.G.S. These playbacks included an analog trace of each station plus a coded time signal that were plotted out at one second per inch. At that scale first arrival times were picked to an accuracy of 0.02 second. Only first arrivals could be picked because the sensitivity of the instruments was set high to record very small, local events. When a regional event large enough to be well recorded by most of the stations occurred, later arrivals would be obscured by the coda of the first arrival which would saturate the recording.

When the location parameters were obtained for these events (as described in a later section) the hand-picked first arrival times

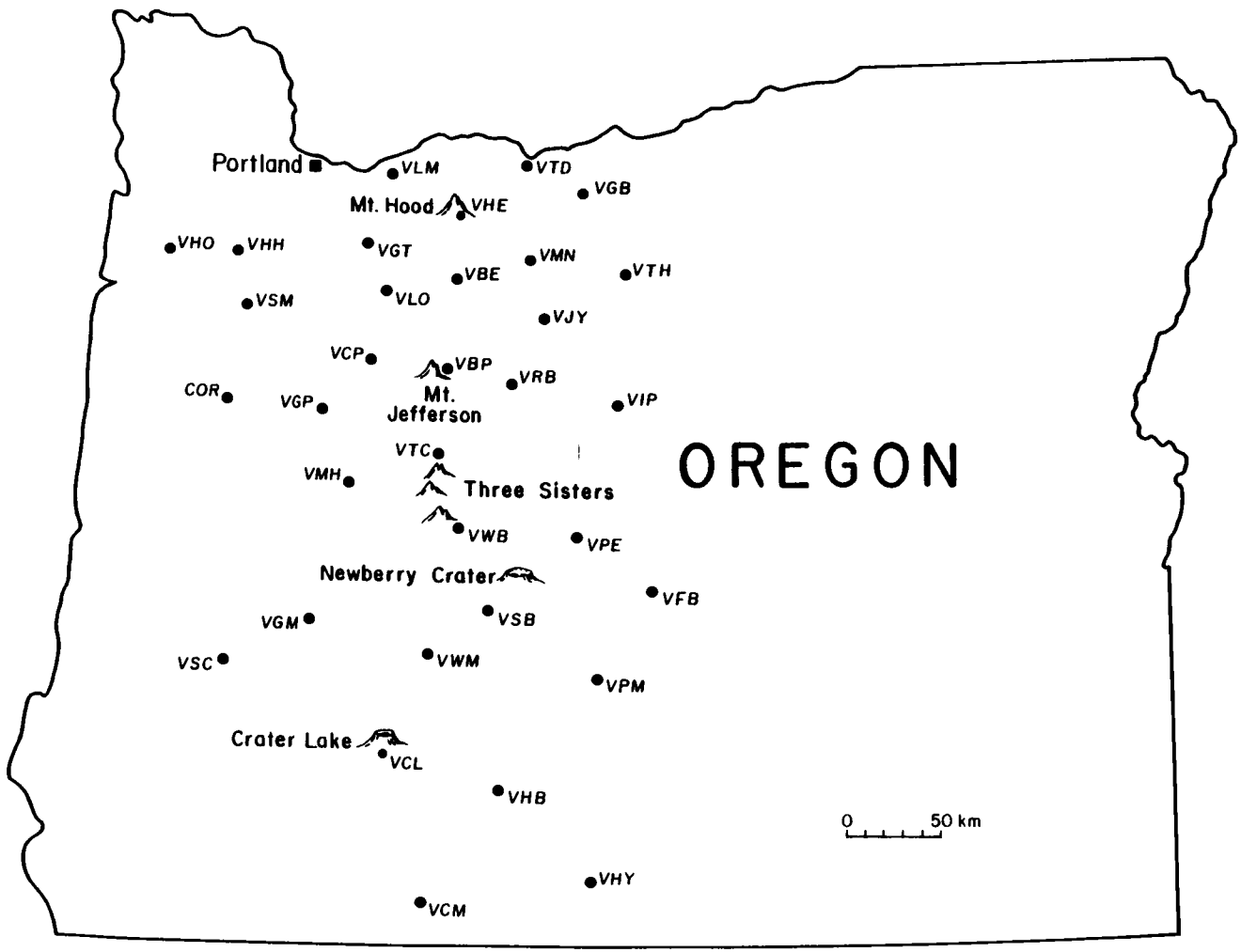

Figure 3. Stations used in this study. 32 stations of the U.S.G.S. Oregon Seismic Network plus a station at Corvallis.

Table 1. U.S.G.S. Oregon Seismic Network Station Locations

Station	Location	Lat (N)	Long (W)	Elev (m)
VGT	Goat Mtn.	45° 8.99'	122°15.92'	993
VLO	Lookout Mt.	44°52.77'	122°23.58'	1351
VCP	Cooper's Ridge	44°40.27'	122° 5.37'	1161
VSM	Salem	44°57.62'	123° 7.65'	290
VHH	High Heaven	45°15.88'	123°18.57'	533
VLM	Little Larch Mtn.	45°32.31'	122° 2.35'	1158
VHE	Mt. Hood East	45°19.72'	121°40.46'	1739
VHO	Mt. Hebo	45°13.15'	123°43.52'	951
VHB	Hamelton Butte	42°47.12'	121°21.00'	1957
VCL	Crater Lake	42°52.71'	122° 7.21'	2048
VGP	Green Peter	44°29.00'	122°34.89'	1212
VMH	Mt. Hagan	44° 8.26'	122°24.44'	902
VGM	Grass Mtn.	43°35.54'	122°32.76'	1561
VCM	Chase Mtn.	42° 5.73'	121°59.33'	1889
VHY	Horsefly Butte	42°15.87'	121° 2.95'	1932
VSC	Scott Mtn.	43°22.35'	123° 3.79'	1295
VGB	Gordon Butte	45°30.94'	120°46.65'	729
VBP	Bald Peter	44°39.66'	121°41.34'	1876
VIP	Ingram Point	44°30.49'	120°37.13'	1731
VJY	Jersey	44°54.13'	120°58.45'	951
VMN	Maupin	45°11.21'	121° 3.18'	555
VTH	The Trough	45°10.87'	120°33.63'	773
VBE	Beaver Butte	45° 3.62'	121°35.21'	1544
VTD	The Dalles	45°32.72'	121°18.69'	305
VFB	Frederick Butte	43°39.51'	120°14.25'	1369
VTC	Trout Creek Butte	44°14.45'	121°39.95'	1690
VWM	Walker Mtn.	43°18.30'	121°42.95	2158
VSB	Spring Butte	42°31.42'	121°20.84'	1664
VPM	Patrick Mtn.	43°11.60'	120°39.98'	1387
VWB	Wanoga Butte	43°54.82'	121°33.27'	1736
VRB	Round Butte	44°36.05'	121°16.21'	743
VPE	Pine Mtn.	43°47.45'	120°56.68'	1932
COR	Corvallis	44°35.16'	123°18.18'	126

were converted to traveltimes by subtracting the origin time of the event. Distances between each station and the event were calculated by a computer program that finds the great circle distance between two points on the earth, taking into account the flattening of the earth. The working data set thus consisted of distances and traveltimes from each event to each station that recorded the event.

DETERMINATION OF EARTHQUAKE LOCATIONS

The selection of earthquakes that were used in this study was made so that they met the following basic criteria: a) the distance between the earthquake and the stations falls in the range where the P_n wave is the first arrival, b) earthquake locations cover as wide an azimuthal range around the array as possible, and c) have a large enough magnitude so that they were well recorded at most of the stations of the array.

During the period of time from May, 1980 to December, 1981 a number of local and regional events that met criteria (b) and (c) were recorded by the array. These events are listed in Table 2. The choice of the distance range over which P_n is considered to be the first arrival (criterion a) is somewhat subjective and will have some effect on the results obtained in this study. This problem will be discussed in more detail in a later section. Figure 4 is a map showing the locations of the earthquakes and seismic stations used in this study.

Included in Table 2 are the sources of the locations of the events used in this study. The Preliminary Determination of Epicenters (PDE)-Earthquake Data Report (EDR) locations are determined by the U.S.G.S. using a network of stations which is much larger in extent and independent of the Oregon network used in this study. Because these locations were determined from an independent data source they were used whenever possible. In the few cases when locations were not available from the PDE-EDR, a location was obtained using data from the hypocenter location computer program HYPOINVERSE (Klein,

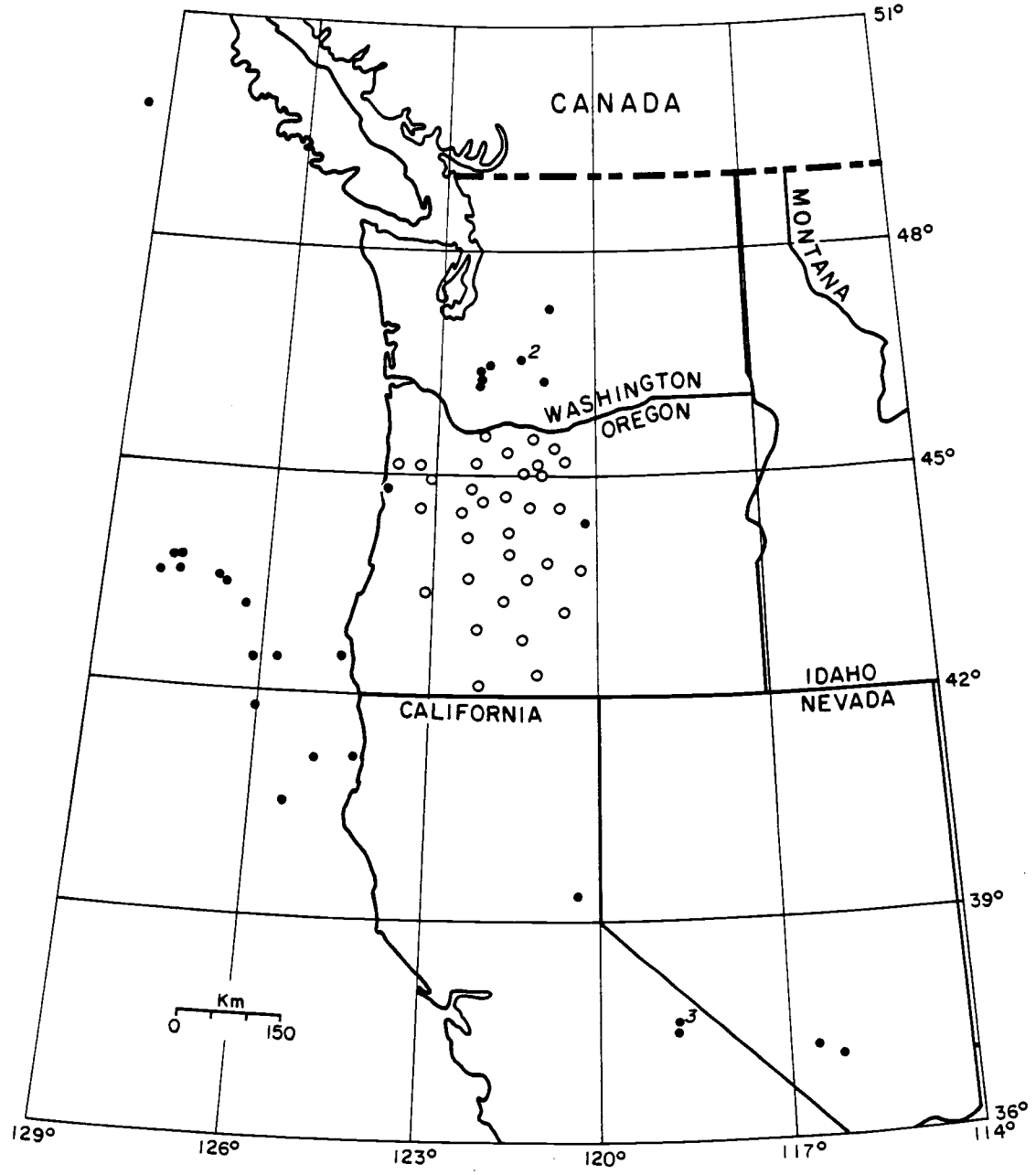

Figure 4. Location map of the events used in this study (•). Shown also is the array of stations (○). A number to the right of an event indicates the number of events occurring at that location.

Table 2. Parameters of Events Used in this Study

Region of Event	Date	Origin Time (GMT)	Lat (N)	Long (W)	Mag.	Source of Location	No. of Stations Recording Event
Mt. St. Helens I	5/16/80	1234:56.3	46.330	122.203	4.6	PDE-EDR	19
Mt. St. Helens II	5/18/80	1532:11.4	46.214	122.195	5.0	PDE-EDR	22
Mammoth Lakes I	5/25/80	1633:44.7	37.600	118.840	6.0	PDE-EDR	20
Mammoth Lakes II	5/25/80	1649:27.3	37.609	118.875	5.8	PDE-EDR	20
Mammoth Lakes III	5/25/80	1944:51.4	37.569	118.820	6.0	PDE-EDR	24
Mammoth Lakes IV	5/25/80	2035:48.5	37.634	118.873	5.5	PDE-EDR	24
Nevada Test Site I	7/25/80	1905:0.08	37.255	116.477	5.6	PDE-EDR	28
Gorda Basin I	8/02/80	2315:41.0	41.836	126.031	4.0	PDE-EDR	25
Gorda Basin II	8/03/80	0824:02.0	42.399	125.708	4.5	PDE-EDR	28
Gorda Basin III	8/03/80	0904:23.4	42.348	126.197	4.5	PDE-EDR	29
Gorda Basin IV	8/03/80	1443:04.2	42.498	124.560	4.5	PDE-EDR	26
Lincoln City, Ore.	9/28/80	2025:28.9	44.780	123.924	-	HYPOINVERSE	26
Eureka, Cal. I	11/08/80	1027:34.0	41.117	124.253	7.0	PDE-EDR	30
Eureka, Cal. II	11/08/80	1232:17.8	41.104	124.946	-	HYPOINVERSE	28
Eureka, Cal. III	11/09/80	0409:08.8	40.501	125.343	5.2	PDE-EDR	30
Blanco F.Z. I	11/18/80	0648:15.8	43.509	126.833	4.0	PDE-EDR	28
Squaw Valley, Cal	11/28/80	1821:13.1	39.305	120.428	5.3	PDE-EDR	28
Sovanco F.Z.	12/17/80	1621:58.8	49.479	129.496	5.7	PDE-EDR	29
White Swan, Wash.	2/02/81	0123:16.8	46.281	120.927	4.0	PDE-EDR	26
Elk Lake, Wash. I	2/14/81	0609:26.3	46.457	122.987	5.0	PDE-EDR	28
Cle Elum, Wash.	2/18/81	0609:37.5	47.237	120.841	4.8	PDE-EDR	26

Table 2. Parameters of Events Used in this Study (continuation)

Region of Event	Date	Origin Time (GMT)	Lat (N)	Long (W)	Mag.	Source of Location	No. of Stations Recording Event
Blanco F.Z. II	3/13/81	0343:12.2	43.757	127.581	-	HYPOINVERSE	22
Blanco F.Z. III	3/20/81	1937:57.0	43.162	126.398	-	HYPOINVERSE	24
Ochoco Mtns. Ore.	3/30/81	2248:09.8	44.420	120.193	-	HYPOINVERSE	18
Blanco F.Z. IV	5/10/81	0413:32.1	43.402	126.711	4.9	PDE-EDR	24
Elk Lake, Wash. II	5/13/81	0500:36.2	46.366	122.252	4.1	PDE-EDR	23
Goat Rocks W.A. I	5/28/81	0856:02.7	46.533	121.416	3.7	PDE-EDR	26
Goat Rocks W.A. II	5/28/81	0910:46.0	46.530	121.406	4.3	PDE-EDR	27
Blanco F.Z. V	6/10/81	1339:29.8	43.711	127.648	4.2	PDE-EDR	22
Blanco F.Z. VI	11/03/81	1347:33.3	43.478	127.890	6.0	PDE-EDR	27
Nevada Test Site II	11/12/81	1500:00.1	37.108	116.050	5.5	PDE-EDR	25
Blanco F.Z. VIII	11/22/81	1137:55.3	43.510	127.597	5.0	PDE-EDR	26

F.Z. - Fracture Zone W.A. - Wilderness Area

1978), the use of which is detailed in the following section.

HYPOINVERSE

HYPOINVERSE was written as a general purpose earthquake location program for minicomputer use. The version in use here accepts up to three crustal models with up to 12 homogeneous layers each, and uses P and S wave first arrival times from up to 70 stations as data. The crustal velocity model used in the program was chosen to be the one determined from surface wave data by Chiburis (1966) and is shown in Table 3. Notice that this model distinguishes between the west and east side of the Cascade Mtns., the east side having a thicker 6.2 km/sec layer and a higher mantle (layer 4) velocity. This model will be further discussed in a later chapter.

Table 3. Crustal Model used in HYPOINVERSE

West of Cascades				East of Cascades			
Layer	Velocity (km/sec)	Depth (km)	Thickness (km)	Layer	Velocity (km/sec)	Depth (km)	Thickness (km)
1	5.5	0.0	5.0	1	5.6	0.0	5.0
2	6.2	5.0	20.0	2	6.2	5.0	30.0
3	6.6	25.0	10.0	3	6.6	35.0	10.0
4	7.67	35.0	∞	4	7.96	45.0	∞

Computationally, HYPOINVERSE uses the singular value decomposition (SVD) technique of inversion (Lawson and Hanson, 1974). This technique allows for eigenvalue truncation so that hypocenter adjustments in poorly constrained directions are prevented. The program starts with a trial hypocenter and origin time which, unless otherwise specified, is put near the station with the first arrival

time. The location routine systematically adjusts the hypocenter location and origin time of the event to obtain a new hypocenter. This adjustment process is iterated until the iteration limit is reached or when either the hypocenter adjustment or the change in the root mean square (RMS) of the traveltime residuals (the difference between observed and calculated traveltimes) becomes small. The program also calculates an error ellipsoid and the errors in the location in the horizontal and vertical directions.

The location technique described above works best when the epicenter of the event is within the array of stations for which arrival time data are available. Due to criterion (a) for event selection, the epicenter of the event was never inside the array of stations used in this study. When locations were attempted on events greater than about 1° away from the array, the horizontal and vertical errors and the RMS became large.

To better understand the problems associated with locating an event outside an array using HYPOINVERSE, a study was undertaken to see where HYPOINVERSE would locate simulated events whose location and origin time were exactly known. Eight stations from the southeast part of the Oregon network were used and locations for 12 simulated events distributed in various locations around the stations were chosen. Traveltimes to each station were calculated for each event using a computer program that calculates the direct traveltime and all of the refracted traveltimes at any distance specified (S. Johnson, personal communication). The crustal velocity model used to calculate the traveltimes was the 'East of Cascades' model (see Table 3) used in HYPOINVERSE for these stations. The shortest

traveltimes among the direct and refracted rays were selected for each station. These times were then input into HYPOINVERSE as first arrival times and locations for the events were obtained from the program. The results are displayed in Figure 5. The true location of event 1 was inside the array. HYPOINVERSE located the event to within 0.4 km of the true location. A very good location, as was expected. Events 2, 3, 4, and 8 were also located very close to their true locations, even though they were outside of the array. The rest of the events were located along the correct azimuth relative to the array, but were always closer to the array than the true locations. When small random errors were introduced into the traveltimes the results described above did not change significantly.

From the results just described, one can conclude that the ability of HYPOINVERSE to locate events outside the array is dependent on the array geometry. Events 2, 3, and 4 had a much wider array aperature (azimuthal coverage of stations) than the other events (with the exception of events 1 and 8) and were therefore better located. Only P wave arrival times were used in this simulation study since S wave arrival times were not available from the observed events data. The lack of S wave arrival times caused the distances to be poorly constrained and HYPOINVERSE put the hypocenter as close to the array as possible and still reasonably fit the P wave arrival times.

A similar simulation study of HYPOINVERSE was performed with an array of ocean bottom seismometers (OBS) located on the Gorda Ridge, off the coast of Oregon (Solano, 1982). This study used first P wave arrivals only and then P and S wave arrival times. When only P wave

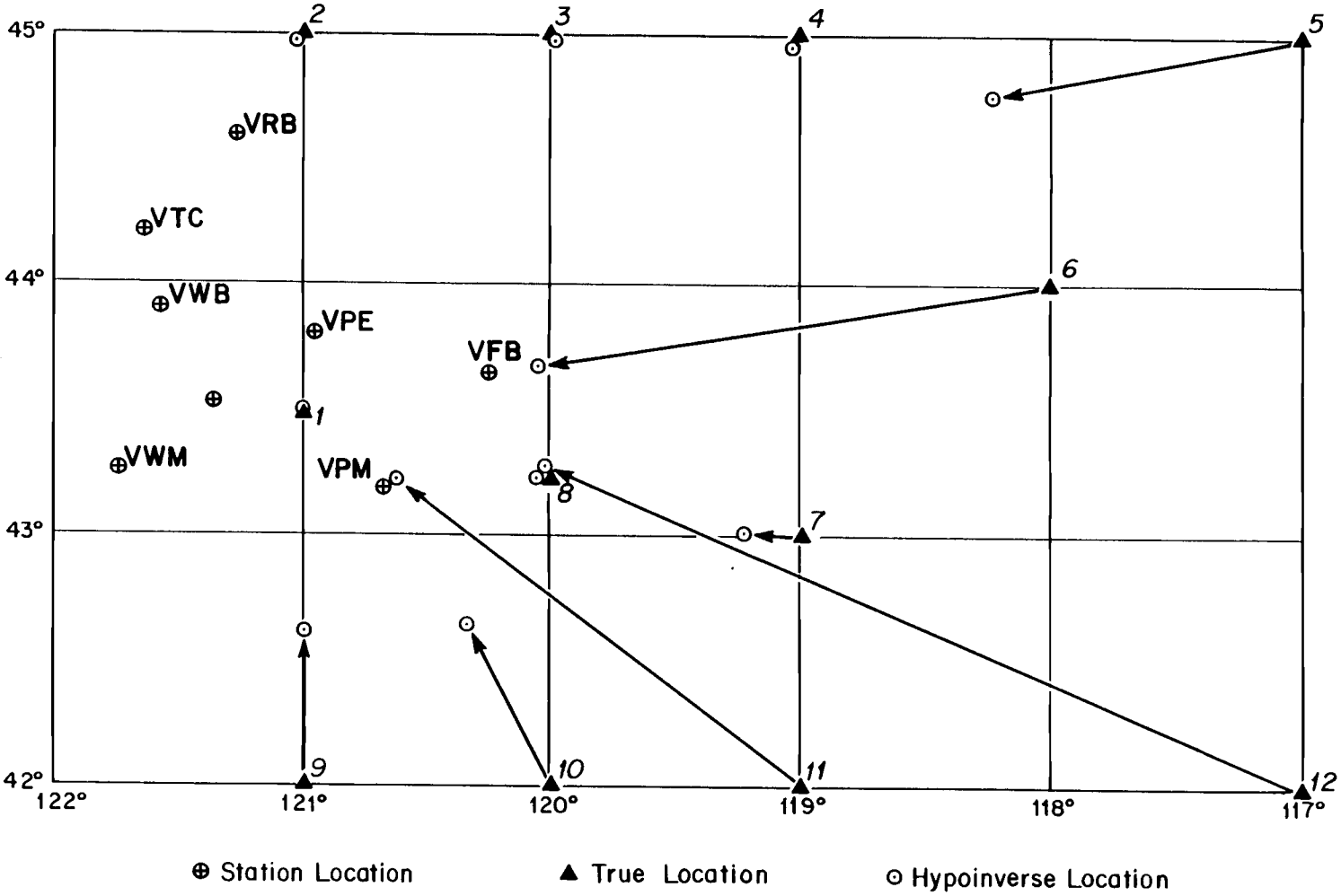

Figure 5. Ability of HYPOINVERSE to locate events. Arrows tie the HYPOINVERSE location with the corresponding true location of the simulated event in the cases where they are not adjacent to each other.

arrival times were used the results were identical to those described above. The program located the events much closer to the array than they actually were, but on the correct aximuth. When S wave arrival times were included, the events that were located close to the array (within 0.5°) were located well by HYPOINVERSE. However, for events located beyond 0.5° away from the array, a problem different to the one found when only P waves were used occurred. The distances were determined to within 10 percent of the true distance, but the azimuths were in some cases up to 20° off of the true azimuth. The fact that the distances were well determined is not surprising since the program weights heavily the S minus P time for distance, when it is available. The errors in the azimuths are more difficult to explain. It is most likely due to a combination of array geometry and location of the trial hypocenter. If the trial hypocenter is in the wrong direction, the program may converge to a local RMS minimum, which may not be the absolute minimum.

Relocation of Events

Because of the problems associated with HYPOINVERSE stated in the preceding section, it was decided to try to improve the locations of the events located by it. The first step in this process was to set up a 2° x 2° grid around the HYPOINVERSE location and consider the location to be at every 0.1° within the grid. For every point in the grid, distances were calculated from the point to each station in the Oregon array. Using the measured traveltimes from the event, a least squares line was fit to the traveltime vs. distance plot for that point. The sum of the squares of the residuals (SSR) between

the calculated (least squares line) and observed traveltimes was determined and plotted for each point (Figure 6). The smallest SSR within the grid should be the best location for the given traveltimes. The difference between the position of the smallest SSR and the center of the grid (the HYPOINVERSE location) gives a measure of the error in the location. The errors ranged from 0.1° to nearly 1° but most were less than 0.3°.

The manner in which errors in location affected the calculated P_n wave velocities (V_{pn}) was a major concern since these velocities would be used in the later analysis of the data. The slope of the least squares line fit to the traveltime vs. distance plot is $1/V_{pn}$. The velocities were therefore also plotted out for each point in the grid (see Figure 7) and for the given error in location, the corresponding error in velocity was measured. The errors in velocity ranged from 0 km/sec to 0.2 km/sec, but most were less than 0.04 km/sec.

Each of the events located by HYPOINVERSE were relocated to the minimum SSR position and its corresponding velocity was used. However, since the errors in location were small and the effects of mislocation on the calculated velocity were very small, it was felt that there was no need to relocate the events for which there were PDE-EDR locations.

Further studies into the location ability of HYPOINVERSE are currently being conducted, but it was felt that the data set represented in Table 2 was a good one for the types of analyses described in the next chapter.

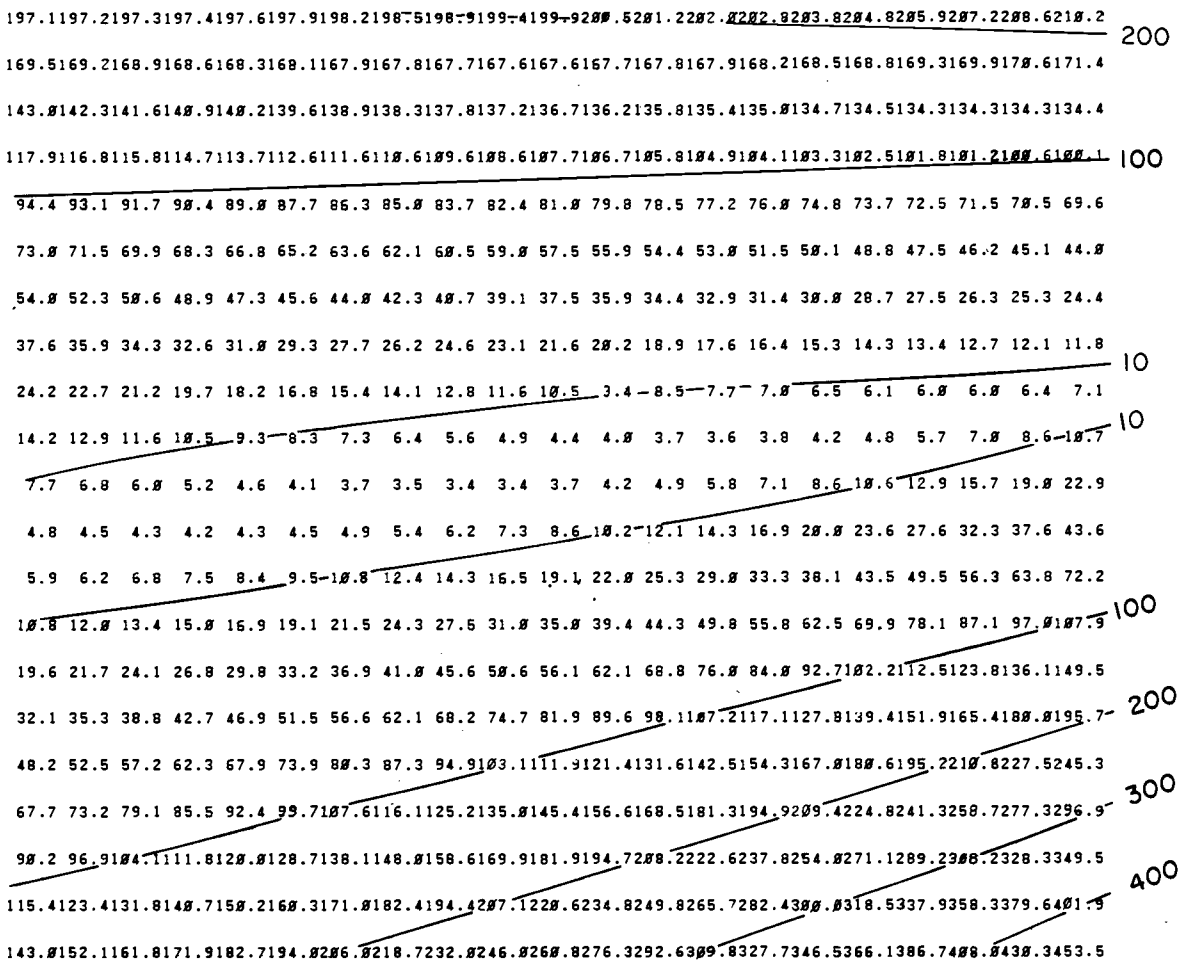

Figure 6. Example of a summation of squared residuals (SSR) grid for the Blanco F.Z. II event. The grid is 2° x 2° and its center is at 43.757°N, 127.431°W. The event was relocated 0.15° west of the center of the grid, which is where the minimum SSR (3.4) is located.

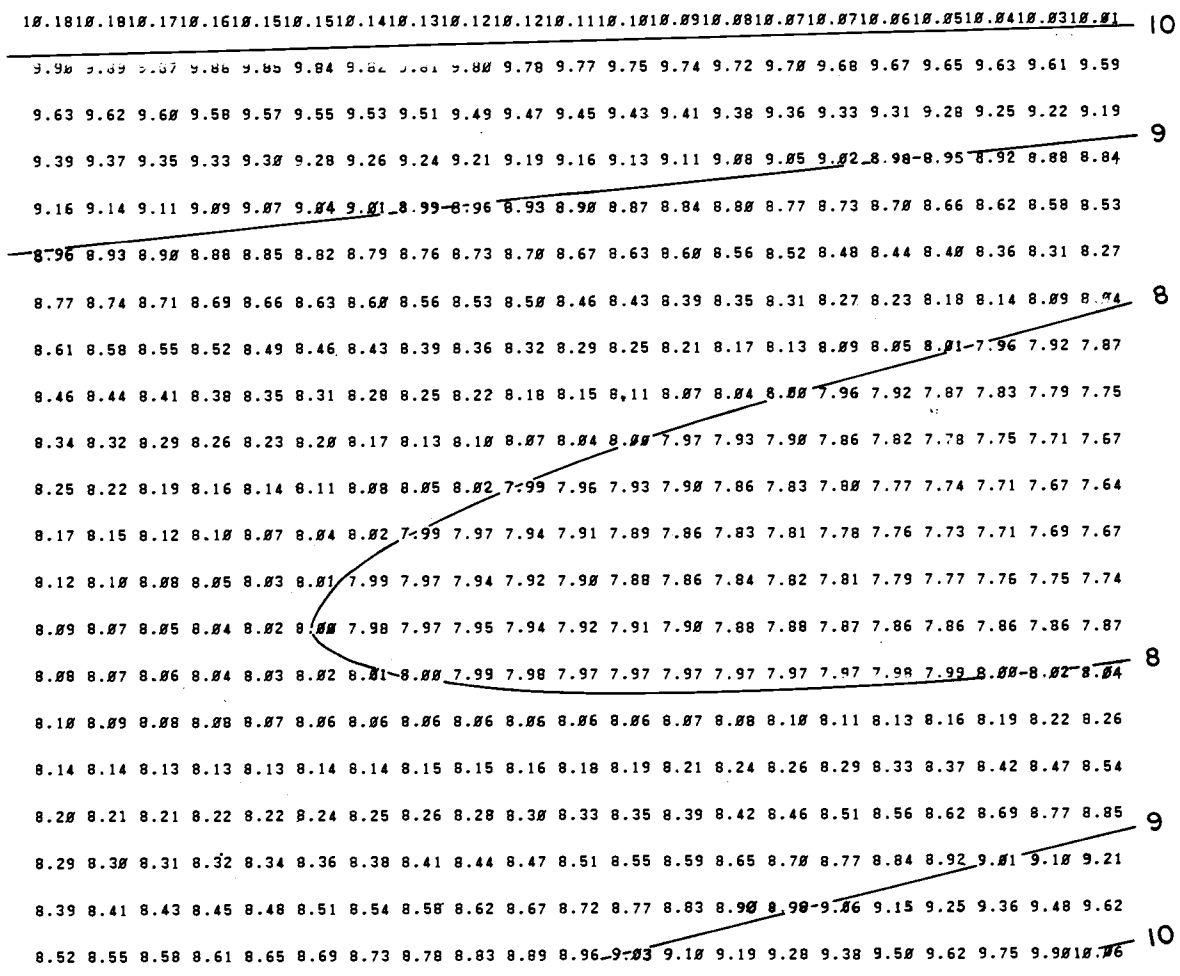

Figure 7. Velocity grid corresponding to the summation of squared residuals (SSR) grid in Figure 6. The velocity at the minimum SSR position (0.15° west of the center) was calculated to be 8.00 km/sec.

P_n WAVE PROPAGATION AND MOHO STRUCTURE

Three different methods of analysis of the traveltime data were employed in this study. The first method involved plotting the traveltimes from each event to each station versus the corresponding distance from the event to the station (hereinafter referred to as a traveltime plot). This was done for each individual event as well as for all of the events as a whole. The second method of analysis, the time-term method, has been in general use since 1960. It allows an areal arrangement of sources and stations and can yield a three-dimensional representation of the underlying refractor structure. In this case the refractor is the Mohorovičić discontinuity that defines the boundary between the crust and the mantle and along which the P_n wave propagates. This method was formulated and developed by Scheidegger and Willmore (1957) and further elaborated upon by Willmore and Bancroft (1960) and Berry and West (1966). A complete description of the theory of the time-term method is given in Appendix A. In the third method of analysis, the velocities that were determined at each station from the traveltime plots of individual events were plotted versus the azimuth from which they came. An analysis of such a velocity vs. azimuth plot can reveal a dipping refractor and/or anisotropy in the refractor velocity, both of which may be present.

Traveltime Analysis

The first step in the analyses of the traveltimes was to plot the traveltimes versus the distances over which they traveled for each individual event. A least squares straight line was then fit

through the data, the slope of which is equal to the reciprocal of the velocity of propagation of the phase being measured. Figure 8 is an example of a traveltime plot of an individual event shown with the least squares line, velocity, correlation coefficient, and root mean square (RMS) of the differences between the line and the data points. An initial inspection of the traveltime plot revealed any potential substantial errors in the picks of first arrival times. These errors occurred when the first arrivals were emergent in character and the uncertainty in the time of arrival was great. If an error of this type was found, the record was rescanned and if the first arrival could be fairly easily picked at another time, that new time was used, otherwise the point was thrown out. These picking errors did not occur very often since most of the events selected had very sharp, impulsive first arrivals and the times could generally be picked to within 0.02 second.

The correlation coefficient and the RMS are measures of how well the data fit the calculated line (i.e. the scatter in the data). If the traveltime data were in a totally random pattern the correlation coefficient would be zero. If the data fit a straight line perfectly the correlation coefficient would equal one. The correlation coefficients of the traveltime plots of the events used in this study ranged from 0.9848 in the worst case to 0.9993 in the best case, but most of the events fell between 0.9970 and 0.9990. These numbers are, of course, relative but they indicate a very good fit to a straight line in all cases. The RMS is comparable to a standard deviation in that it is a measure of the spread in the data about the line. The tightest fit was observed from a Nevada Test Site blast and had an RMS

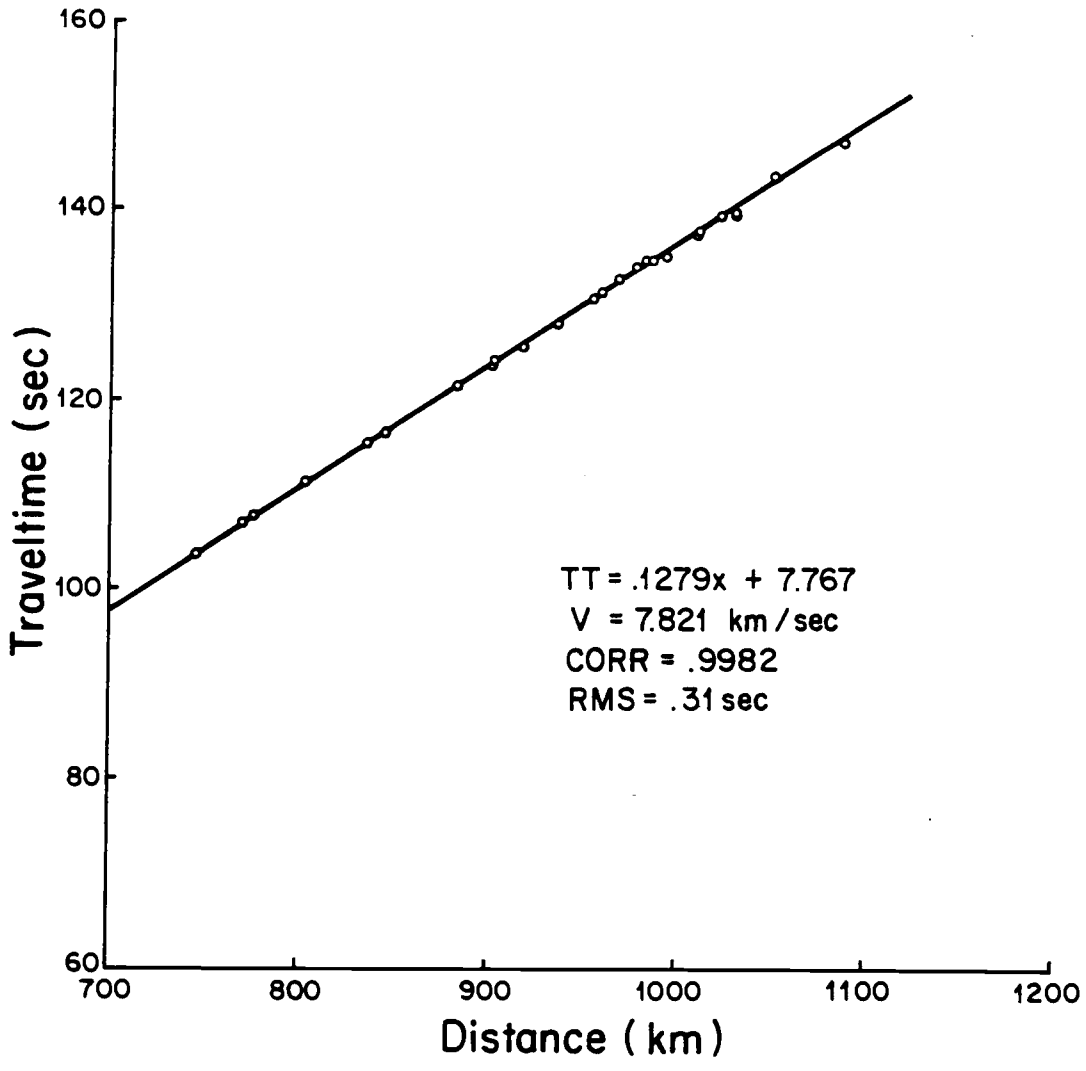

Figure 8. Example of a traveltime plot for an individual event (Nevada Test Site II). Included are the data points, the equation of the least squares line fit through the data, the calculated P_n wave velocity (V), the correlation coefficient (CORR), and the root mean square (RMS) of the traveltime residuals.

of 0.31 second over traveltimes that averaged 120 seconds (0.2% spread). The largest spread was observed from an earthquake in the Gorda Basin which had an RMS of 1.66 seconds over an average traveltime of 55 seconds (3% spread). The RMS also indicated that the data for individual events fit straight lines very well.

For the events initially selected for this study, the velocities ranged from 6.35 km/sec for the Ochoco Mountains event to 8.21 km/sec for the first Eureka event. Some of the events, such as the event in the Ochoco Mountains and the one near Lincoln City, were clearly too near the array for the P_n wave to be the first arrival. When straight lines were fit to the traveltime plots of these events containing non-P_n arrivals, smaller, crustal velocities were observed. Another group of events, all from the State of Washington, exhibited somewhat higher velocities (6.96 - 7.48 km/sec) yet not quite high enough to be considered true P_n velocities. This was due to the fact that these events were located in the distance range where the nearer stations were detecting crustal P waves first and the farther stations were detecting the P_n wave first (i.e. the cross-over distance was within the array). If an estimate of the cross-over distance could be determined, then only arrival times at stations beyond the cross-over distance could be used for the P_n wave investigations.

To obtain an initial estimate of the cross-over distance, a velocity (determined using data from all stations receiving the event) versus distance plot was constructed for one station (VBE). This station was close to the cross-over distance from the Washington events if a standard Moho depth and average crustal and upper mantle velocities are assumed (Telford et al., 1976). This plot is shown in

Figure 9. There is a definite jump in velocities between 250 km and 325 km, indicating that the cross-over point is within this distance range. The initial estimate of the cross-over distance was taken to be 250 km so that all stations that could possibly be detecting P_n waves first would be included.

All of the events used in this study were within 1100 km of the farthest station in the array. The traveltime curve remained linear to this distance, which is interpreted to mean that P_n is the first arrival to at least 1100 km. P_n was therefore considered to be the first arrival in the distance range from 250 km to 1100 km.

The next step in the traveltime analysis was to combine all of the events into one data set to find average values of the Moho velocity and depth for the whole array of stations. Raw traveltimes measured for all of the events, supplemented by data from the refraction line of Berg et al. (1966), were plotted and a single least squares straight line was fit through the data. This plot is shown in Figure 10. The velocity calculated from this single linear fit was 7.611 km/sec with an RMS of 1.74 seconds. This velocity value was somewhat low but it was within the range of previously measured P_n velocities (Herrin and Taggart, 1962) and the RMS seemed reasonable. A definite change in slope was detected in the plot at a distance of about 280 km, which indicated that the data contained arrival times from non-P_n arrivals. In order to better fit the data and further refine the estimation of the cross-over distance, a nonlinear least squares approach was investigated (Mitchell and Hashim, 1977).

In the nonlinear least squares process, contiguous straight lines are fit to the data and an apparent velocity for each line and the

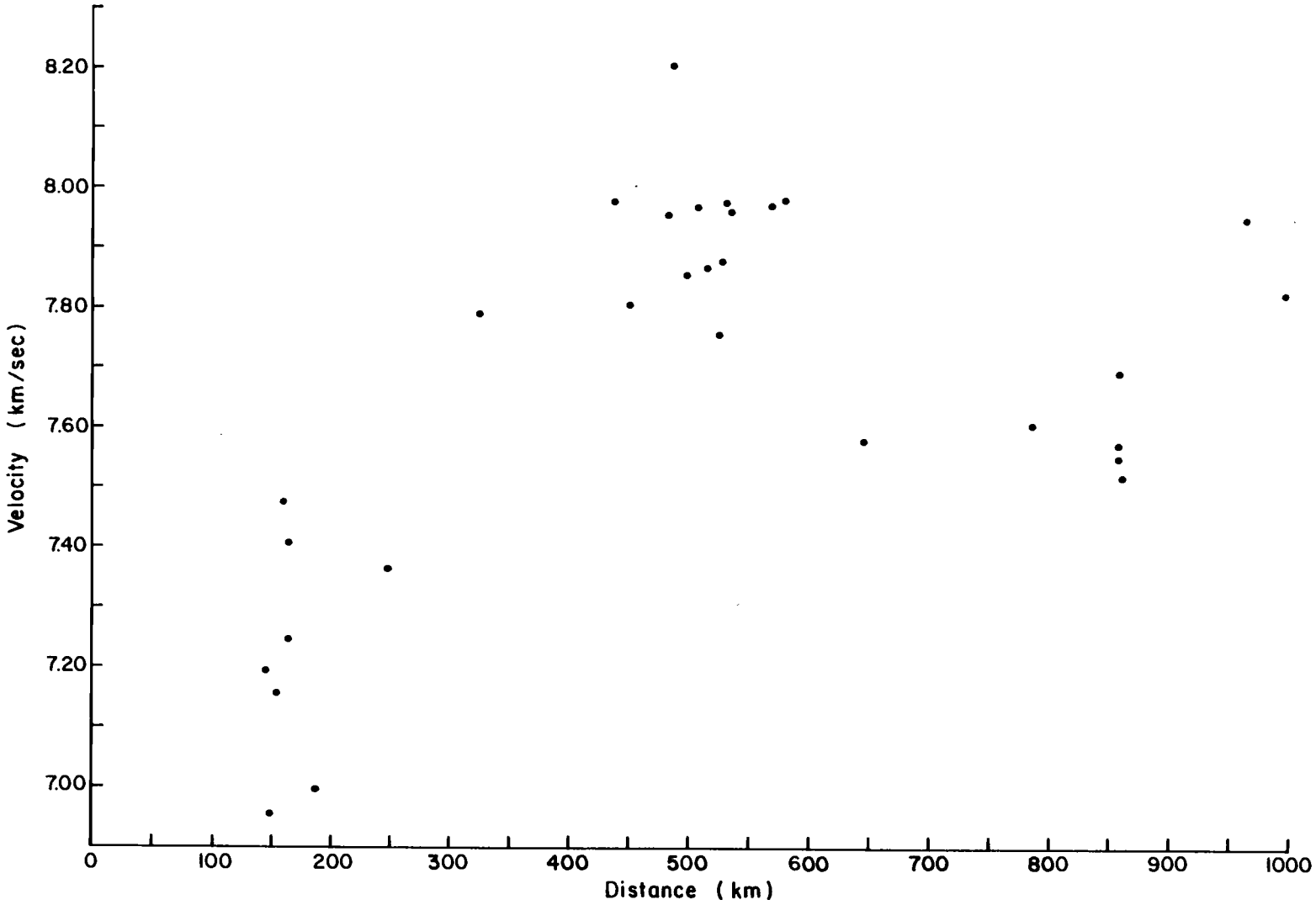

Figure 9. Velocity vs. distance plot for station VBE. Distances are from the events to VBE. Velocities were calculated using the whole array of stations.

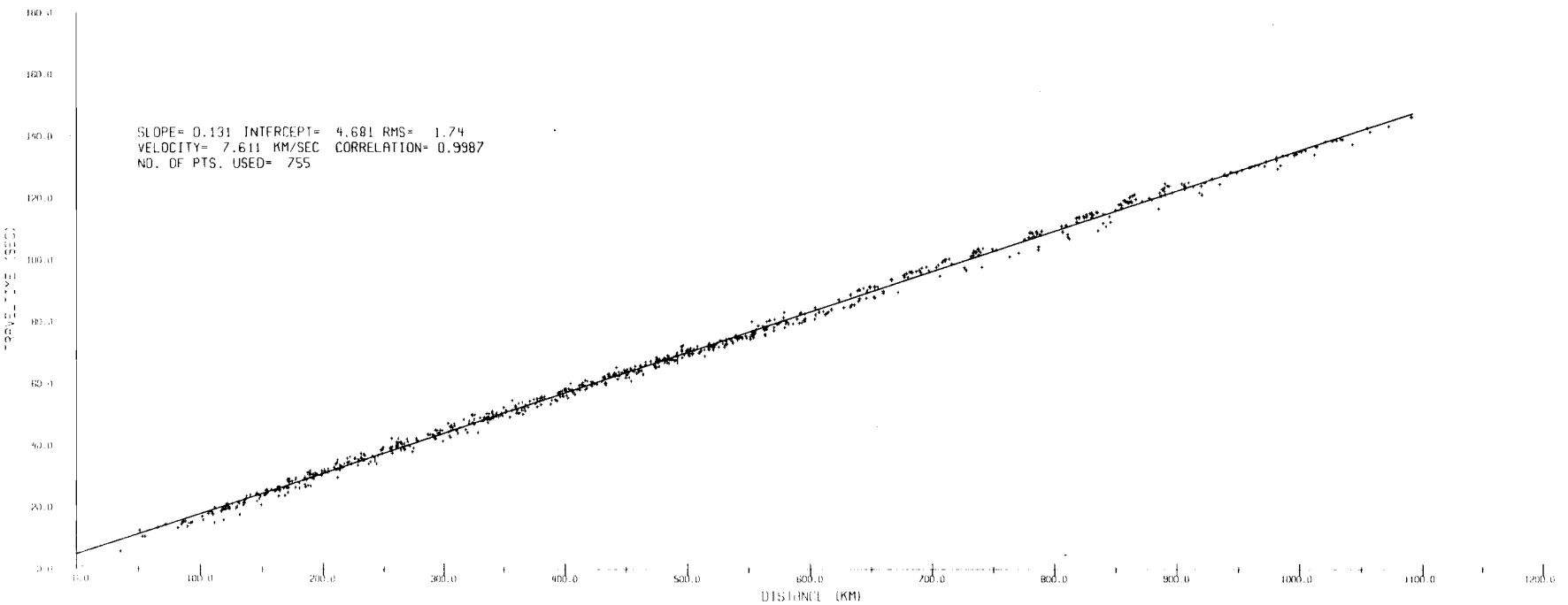

Figure 10. Traveltime plot of all events. A single least squares straight line was fit through the data and the values in the upper left are the parameters associated with the calculation of this line.

points of intersection of the lines are computed. A two-line fit to the data (one layer over a half-space) can be described by the equation

$$t_i = \begin{cases} \dfrac{(x_i - x_1)}{V_1} + t_1 & \text{for } x_i \leq x_1 \\ \dfrac{(x_i - x_1)}{V_2} + t_1 & \text{for } x_i > x_1 \end{cases}$$

where x_1 and t_1 are the coordinates of the point of intersection on the traveltime plot, V_1 and V_2 are the apparent velocities of the upper layer and half-space respectively, and x_i and t_i are the coordinates of the data points. The normal equations for the least squares inversion are

$$t_i = t_{oi} + \frac{\partial t}{\partial a_1}\bigg|_{x=x_i} \Delta a_1 + \frac{\partial t}{\partial a_2}\bigg|_{x=x_i} \Delta a_2 + \frac{\partial t}{\partial x_1}\bigg|_{x=x_i} \Delta t_1 + \frac{\partial t}{\partial x_1}\bigg|_{x=x_i} \Delta x_1$$

where t_{oi} is the value of t at $x=x_i$ for the starting model, $a_1 = 1/V_1$, $a_2 = 1/V_2$, and

$$\frac{\partial t}{\partial a_1} = \begin{cases} x_i - x_1 ; & x_i \leq x_1 \\ 0 ; & x_i > x_1 \end{cases}$$

$$\frac{\partial t}{\partial a_2} = \begin{cases} 0 ; & x_i \leq x_1 \\ x_i - x_1 ; & x_i > x_1 \end{cases}$$

$$\frac{\partial t}{\partial t_1} = 1 \quad ; \text{ for all } x_i$$

$$\frac{\partial t}{\partial x_1} = \begin{cases} -a_1 ; & x_i \leq x_1 \\ -a_2 ; & x_i > x_1 \end{cases}$$

The matrices of the normal equations are inverted to find Δa_1, Δa_2, Δt_1, and Δx_1, which are the changes in the model. The changes in the

model are added to the starting model to obtain the new model. This process is iterated, using the new model as the starting model, until the changes in the model become smaller than some preassigned values. This method requires that an initial guess of the model parameters be made. An intelligent guess can be decided upon by a visual inspection of the data in the traveltime plot. It was found that as long as the initial guess was reasonably close to the visually determined cross-over point and velocities, variations in the starting model did not affect the outcome of the final model.

The nonlinear least squares method was applied to the data represented in Figure 10 and the results can be seen in Figure 11. The upper layer velocity (V_1) is an average lower crustal velocity and was calculated to be 6.825 km/sec. The Moho velocity (V_2), calculated to be 7.664 km/sec, was slightly higher than that obtained by the single line fit. The RMS was smaller than the RMS for the single line fit, but the changes in both the Moho velocity and the RMS were not dramatic. This method does yield an estimate of the depth to the Moho, however. With values for V_1, V_2 and the cross-over distance (x_1), the depth (z) can be determined from the relation $z = (x_1/2)[(V_2-V_1)/(V_2+V_1)]^{\frac{1}{2}}$ (Telford et al., 1976). With V_1 = 6.825 km/sec, V_2 = 7.664 km/sec, and x_1 = 200 km, the depth to the Moho was calculated to be 24 ±4 km, which previous studies indicate is a somewhat low value for an average depth beneath the array of stations (see Previous Geophysical Studies chapter).

Since the calculated Moho depth was smaller than expected and the P_n velocity was lower than previous studies had found, it was decided to try to improve the fit to the traveltime data by correcting the data

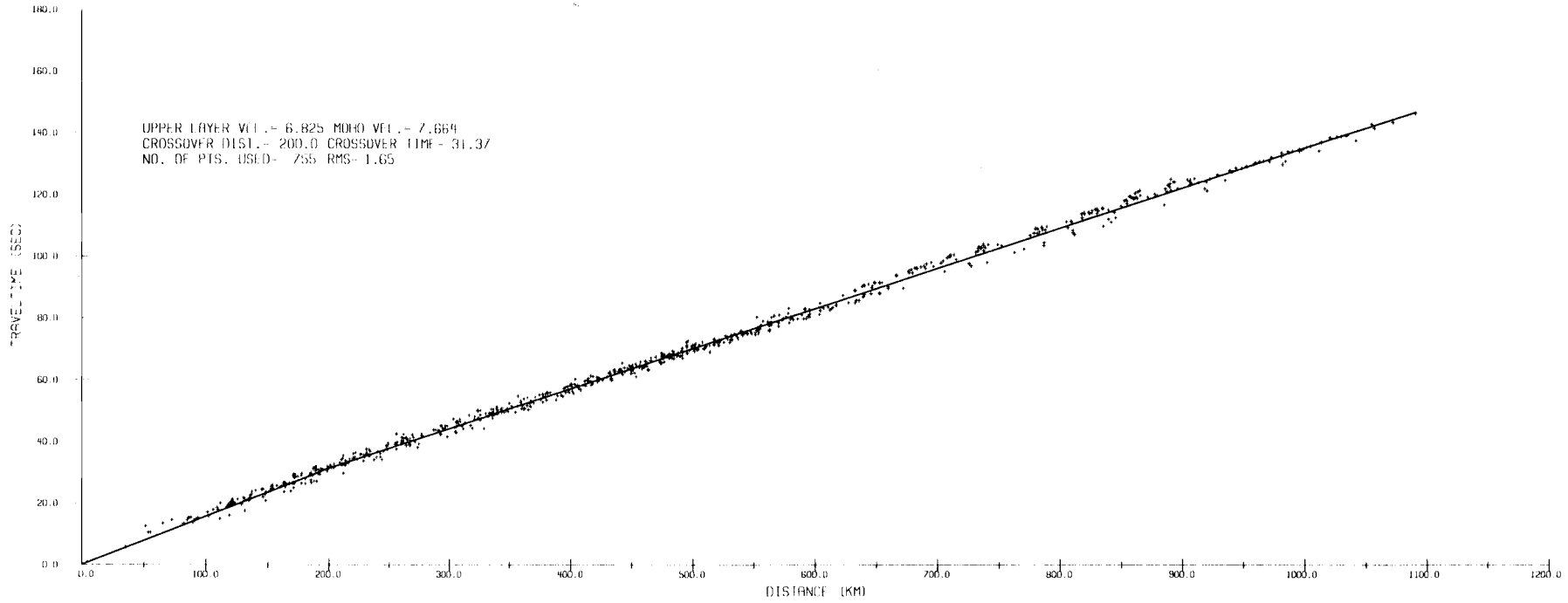

Figure 11. Nonlinear least squares fit to the traveltime plot of all events. Two straight lines were simultaneously fit through the data. The velocities are the reciprocals of the slopes of the lines and the crossover distance and time are the coordinates of the point of intersection of the two lines.

for source effects. These source effects, which include errors in the calculated origin time and hypocenters of the events, were corrected for by subtracting the source terms derived from time-term analysis (see Appendix A and the section on time-term analysis) from the travel-time of each event. The source terms essentially remove the time for the wave to travel from the hypocenter of the event to the refractor and the errors common to the traveltimes to all stations. After the source terms were subtracted from the traveltimes another traveltime plot was constructed and fit with a single least squares straight line (Figure 12). A marked improvement in the RMS (0.89 sec) and correlation coefficient (0.9995) were noted as the source terms reduced the spread in the data, especially at large distances. The source term subtraction also resulted in a slightly higher value for P_n velocity (7.671 km/sec) than that calculated without source terms subtracted. It was thought that a nonlinear fit to the corrected data would further improve the fit to the data. The results of the nonlinear fit are shown in Figure 13. As can be seen, there was a significant increase in the P_n velocity (7.756 km/sec) and cross-over point coordinates (249.8 km and 32.5 secs) along with improvement in the RMS (0.43 sec) over those obtained using uncorrected data. With these values of V_1, V_2, x_1 the average depth to the Moho was calculated to be 32 ±3 km. Due to the better fit of the traveltime data using the nonlinear fitting technique on corrected data, more confidence can be placed in the 32 km depth than in the smaller 24 km depth obtained from uncorrected data.

Having now obtained average values for P_n velocity and depth to

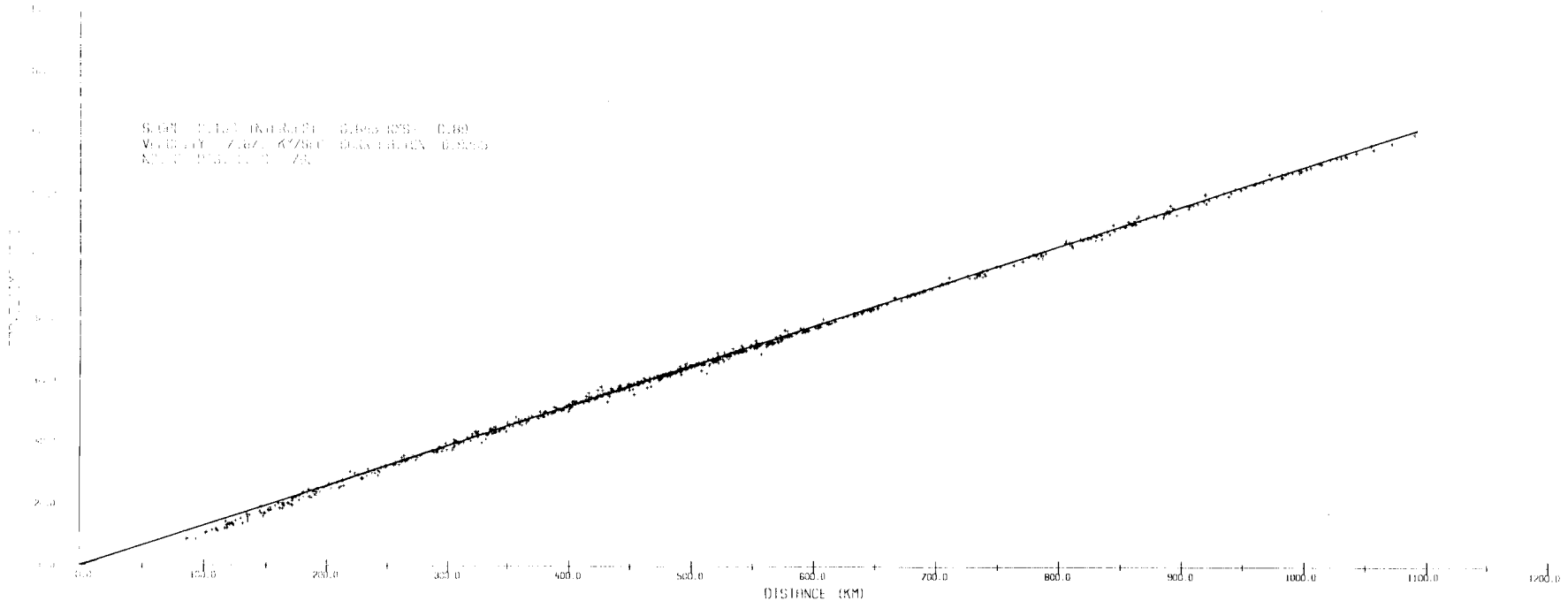

Figure 12. Traveltime plot of all events corrected for source effects by subtracting source terms derived from time-term analysis. Single straight line fit to the data.

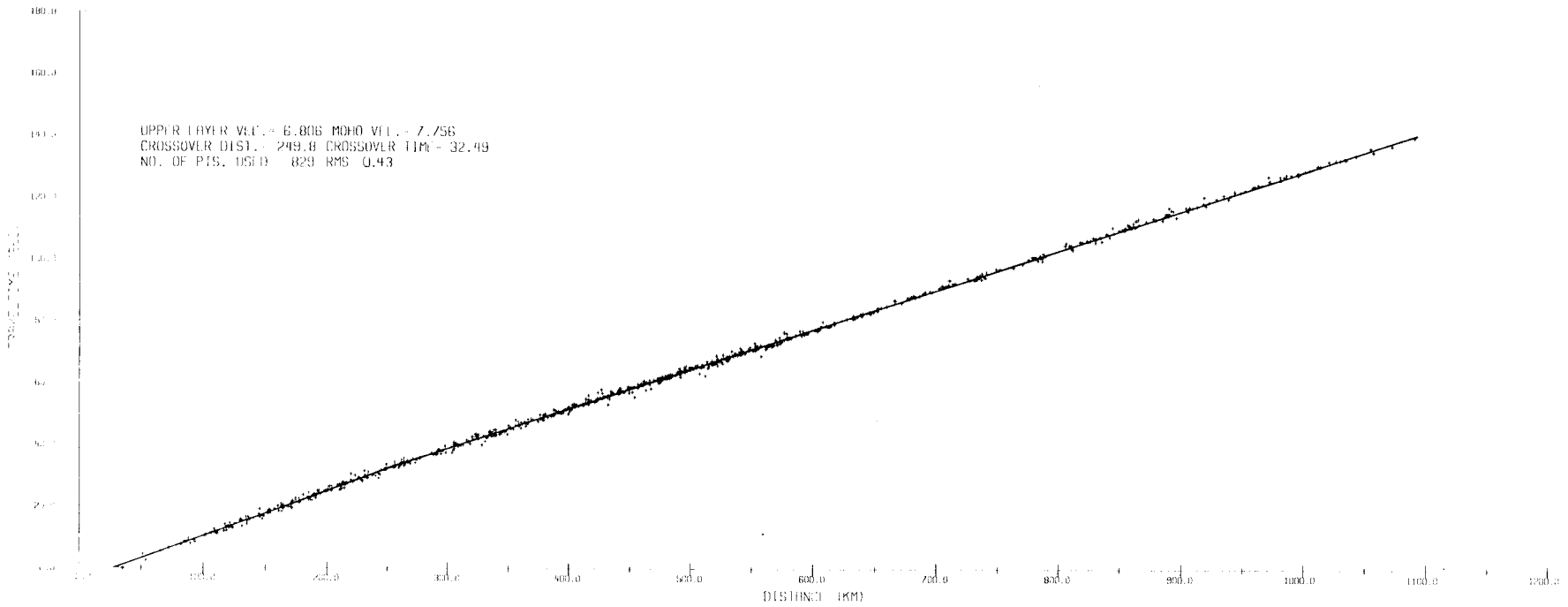

Figure 13. Nonlinear least squares fit to the traveltime plot of all events corrected for source effects.

Moho for the whole array, the next step was to search for differences in these values west and east of the Cascades. To split the data set into west and east subsets, both the stations of the array and the events were split into west and east. Table 4 lists the stations and events contained in each subset. The Blanco Fracture Zone and Gorda Basin events were not included in the West subset because most of their travelpaths were along oceanic crust and may therefore give a distorted picture of the continental crustal thickness.

The same procedures were performed on each subset as were previously described for the whole data set. The results for the West subset are shown in Figure 14. The P_n velocity of 7.975 km/sec is substantially higher than the average P_n velocity obtained for the whole array (7.756 km/sec) and is closer to P_n velocity values obtained in other regions (Herrin and Taggart, 1962). With V_1 = 6.000 km/sec, V_2 = 7.975 km/sec, and x_1 = 115.2 km the Moho depth was calculated to be 22 ±4 km, which is in good agreement with the previous results of Langston (1977) (21 km), Simila (1980) (26 km), and Berg et al. (1966) (16 km) for the region west of the Cascades. Figure 15 shows the results for the East subset. The P_n velocity calculated for this subset (7.751 km/sec) is nearly identical to the whole array average P_n velocity (7.756 km/sec) and is much lower than that obtained for the West. The Moho depth calculated for this subset was 37 km, which is in good agreement with Hill (1972) who studied P_n propagation beneath eastern Washington and Oregon and found a crustal thickness of 35 ±3.5 km. It is somewhat shallower, however, than the depth reported by Chiburis (1966), who calculated a crustal thickness of 45 km from observations of surface waves traveling across eastern Oregon.

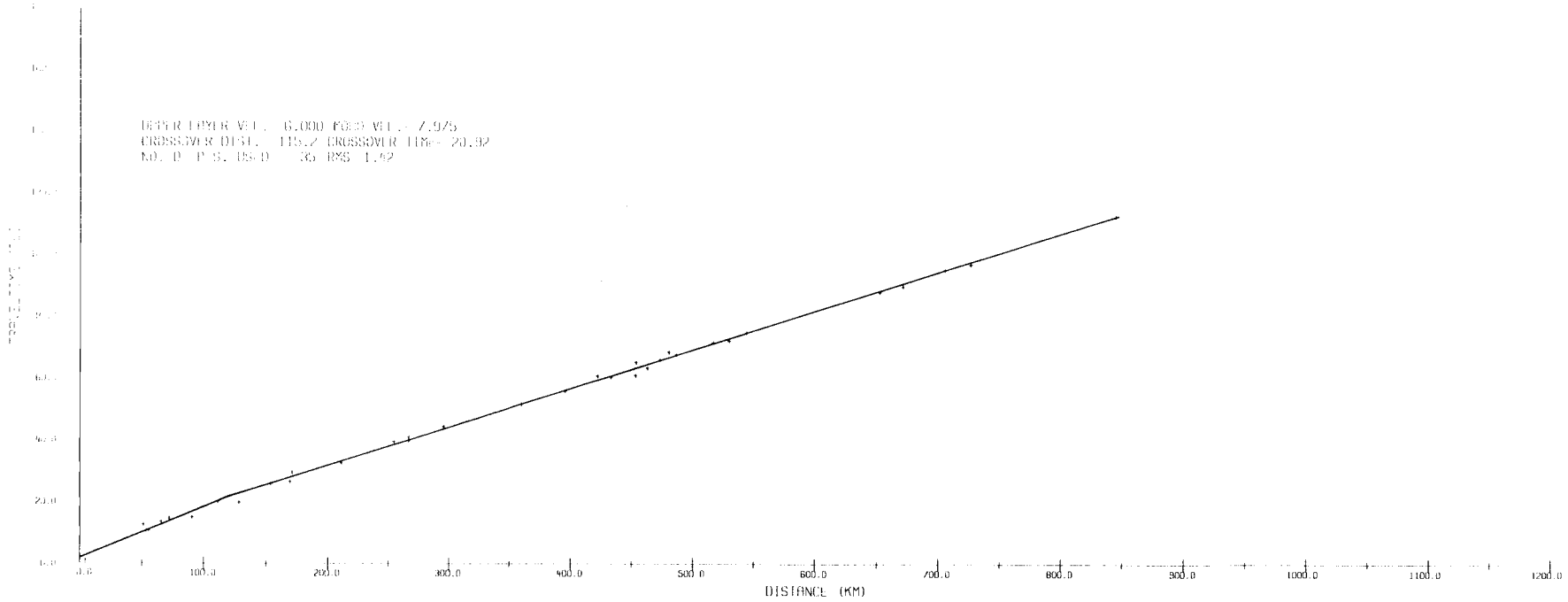

Figure 14. Traveltime plot for the West subset of stations and events. Nonlinear least squares fit to the data.

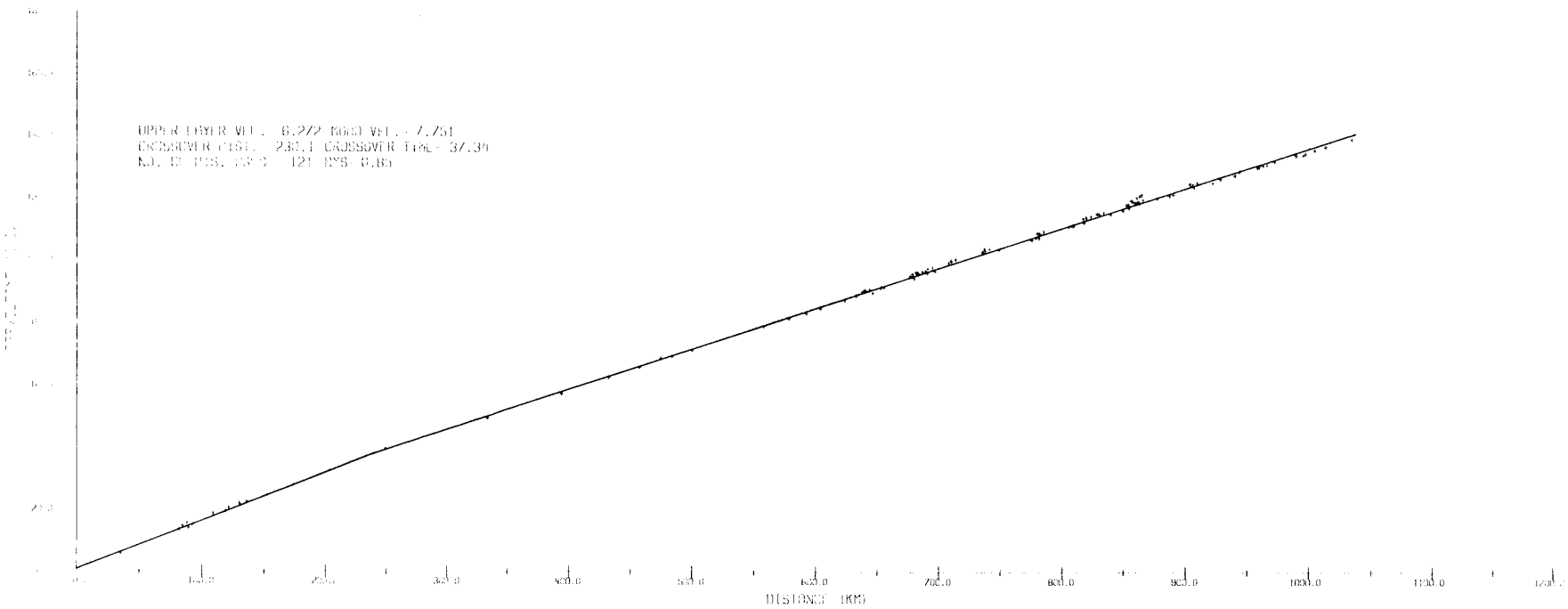

Figure 15. Traveltime plot for the East subset of stations and events. Nonlinear fit to the data.

Table 4. Stations and Events Used in the West and East Data Subsets

West Subset Stations		East Subset Stations	
VSM, VHH, VHO, VGP, VSC, COR		VHB, VHY, VGB, VBP, VIP, VJY, VMN, VTH, VRB, VGE, VTD, VFB, VTC, VWM, VSB, VPM, VWB, VPE	
Events		Events	
Lincoln City	9/28/80	Mammoth Lakes I	5/25/80
Eureka, Cal. I	11/08/80	Mammoth Lakes II	5/25/80
Eureka, Cal. II	11/08/80	Mammoth Lakes III	5/25/80
Eureka, Cal. III	11/09/80	Mammoth Lakes IV	5/25/80
Sovanco F. Z.	12/17/80	Nevada Test Site I	7/25/80
Berg et al. (1966) Refraction line		Squaw Valley, Cal.	11/28/80
		Ochoco Mtns.	3/30/80
		Nevada Test Site II	11/12/81

Time-Term Analysis

In order to obtain a more detailed picture of the Moho structure beneath the array, the time-term method of seismic refraction analysis was employed (see Appendix A for a description of the method). The advantages of the time-term method are that the equations can be solved without requiring the sources and receivers to be laid out in any particular pattern, that the maximum amount of information is extracted from the data, and that the requirements for making simplifying assumptions about the geological structure (such as describing the structure in terms of plane layers) are minimized. The disadvantages of the method include erroneous results if the assumptions of the method (such as small refractor dip) are violated, and an uncertainty in the interpretation of the results. Lateral variations in time-terms can result from a lateral variation in either crustal

velocity or thickness or a combination of both, and one must make assumptions as to which is the cause.

The time-term method yields a set of source terms and receiver terms, and a refractor velocity. A time-term, whether it be a source or receiver term, is the time for a wave to travel either from the source to the refractor or from the refractor to the receiver along the refracted path minus the time for it to travel the horizontal component of that path at the refractor velocity. The source and receiver terms are only known relative to each other (i.e. to within an additive constant) unless either one or more of the sources occupy a receiver position or the velocity structure beneath a source or receiver is known. In this study no source and receiver positions were coincidental. Thus, to obtain absolute values of the time-terms, from which relative depths to the Moho beneath each station could be determined, the crustal velocity structure of Leaver (1982) was modified to fit the crustal thickness and P_n velocity determined from the traveltime analysis of this study (Figure 16a) and utilized. The receiver time-term for this model was calculated to be 2.64 seconds. Since the time-term calculated using the crustal model shown in Figure 16a is the time-term of the 'average' crust under the array, it was equated with the average of the calculated receiver terms. To obtain the absolute time-terms, the average time-term was subtracted from each receiver time-term and 2.64 seconds was added to the result.

To eliminate the effect on the receiver terms of differing station elevations, three separate elevation correction schemes were applied to the data. In each case they were applied to the data

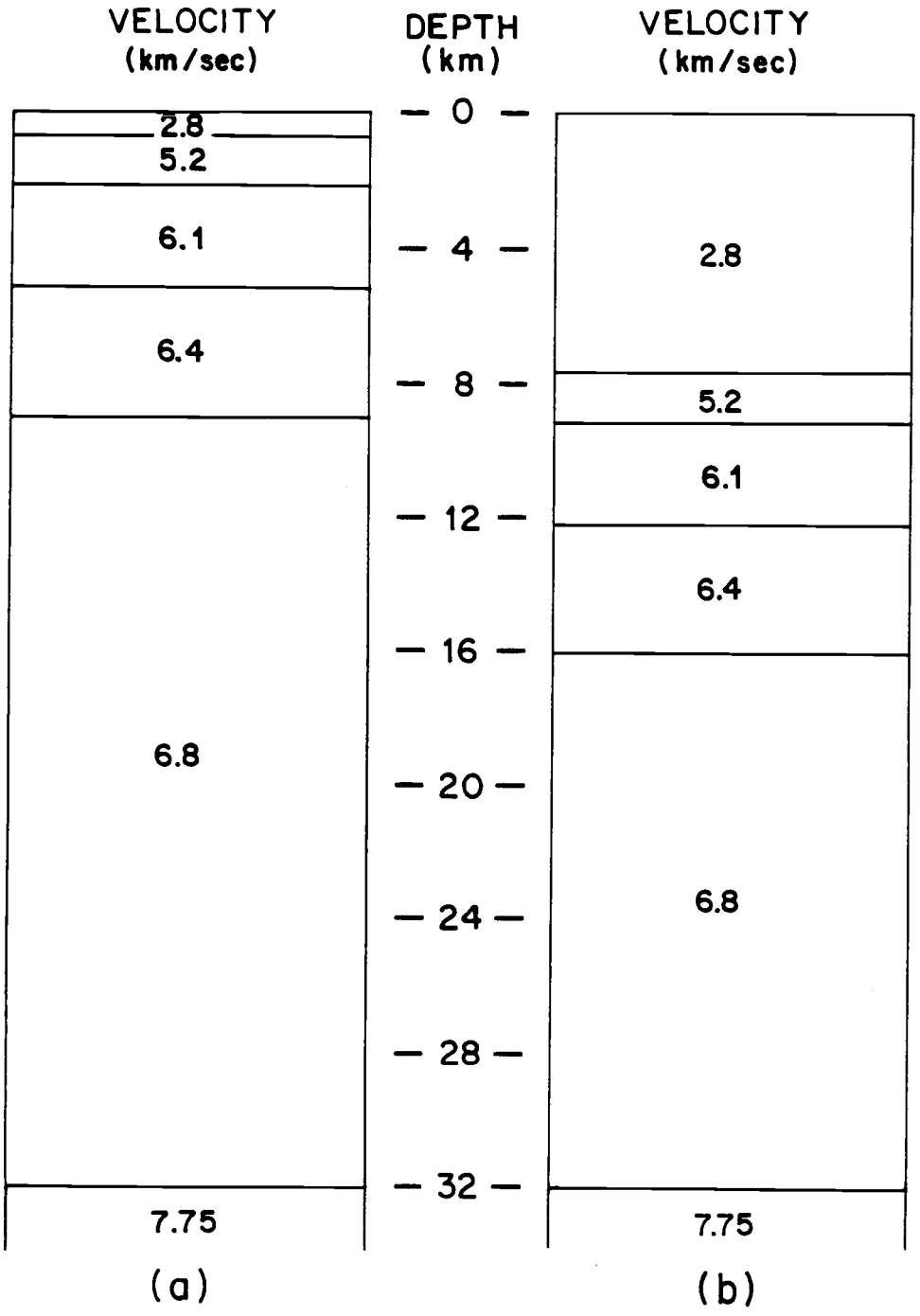

Figure 16. a) Modified crustal velocity model of Leaver (1982) used in calculation of absolute time-terms.
b) Crustal velocity model used in the calculation of absolute time-terms for the Willamette Valley (VSM, COR) and Coast Range (VHO, VHH) stations.

before the time-terms were calculated and therefore their effects were included in the relative time-terms, before they were converted to absolute time-terms.

The first elevation correction scheme was to consider the top two layers in the modified Leaver model (2.8 km/sec and 5.2 km/sec) to follow the topography. The time that was required for a wave to travel through the portion of these layers that was above sea level was subtracted from the total traveltime. The time-terms were then computed and converted into absolute time-terms. The receiver terms were then plotted on a station location map and contoured (Figure 17). The time-terms were generally larger along the crest of the Cascades, dropping off to either side. The exception to this generality occurred for the stations in the Willamette Valley (VSM and COR) and to a lesser extent for those in the Coast Range (VHH and VHO). The time-terms for these stations were higher than the other western stations around them. The most likely explanation for the large time-terms at Willamette Valley and Coast Range stations was that the waves covered a greater portion of their travelpath through low velocity sedimentary rocks than was accounted for by the model and elevation corrections. To correct this problem, the depth to the bottom of the low velocity layer (2.8 km/sec) was increased to 7.6 km, the estimated thickness of sedimentary rocks in the Willamette Valley and Coast Range (Newton, 1969, Snavely et al., 1969). This Willamette Valley crustal velocity model (Figure 16b) was then used to calculate the absolute time-terms for VSM, COR, VHH, and VHO. The contour map with the revised time-terms for these four stations is shown in Figure 18. With the corrections included, these stations

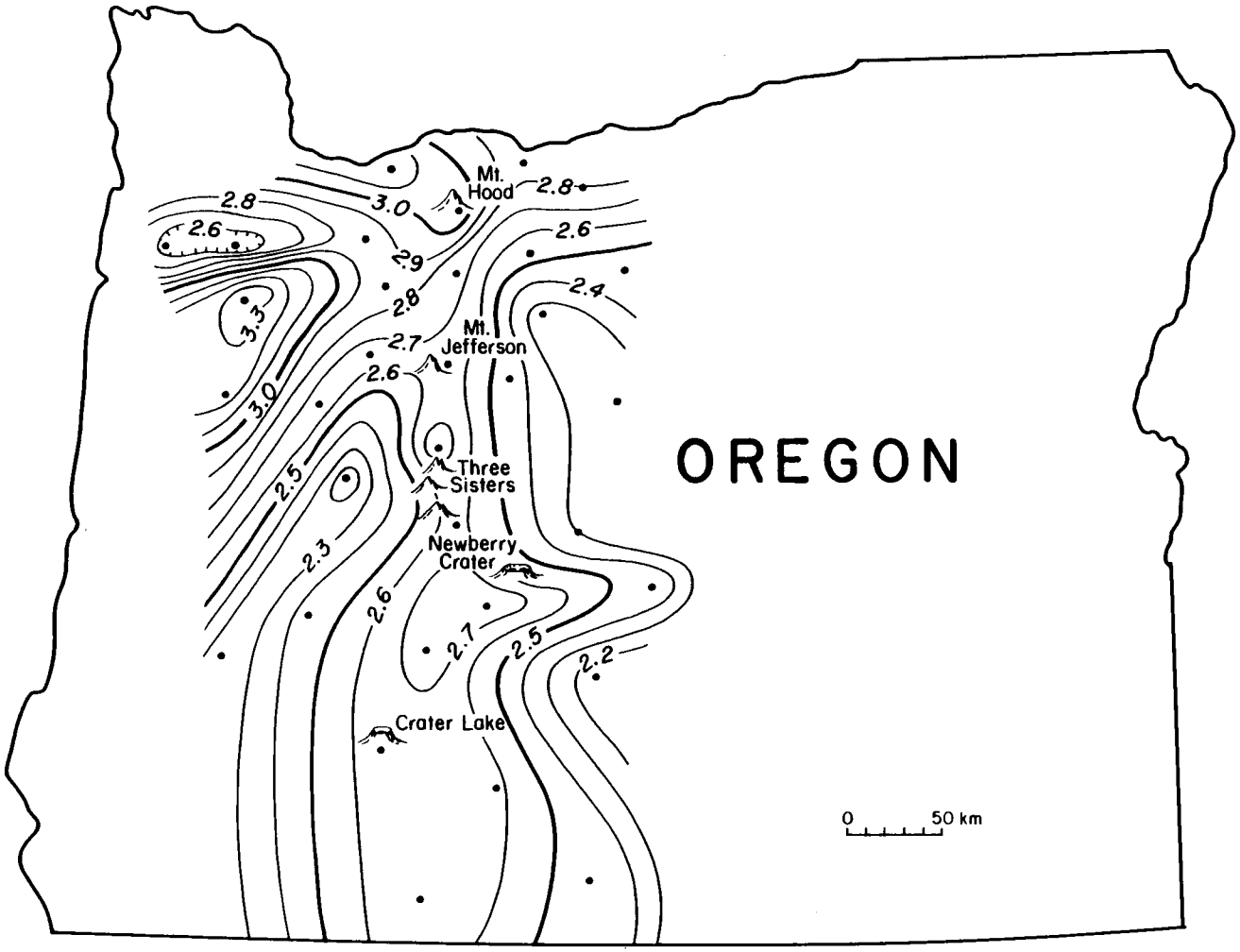

Figure 17. Contour map of receiver time-terms with the first elevation correction scheme. The model in Figure 16a was used for all stations in calculating absolute time-terms.

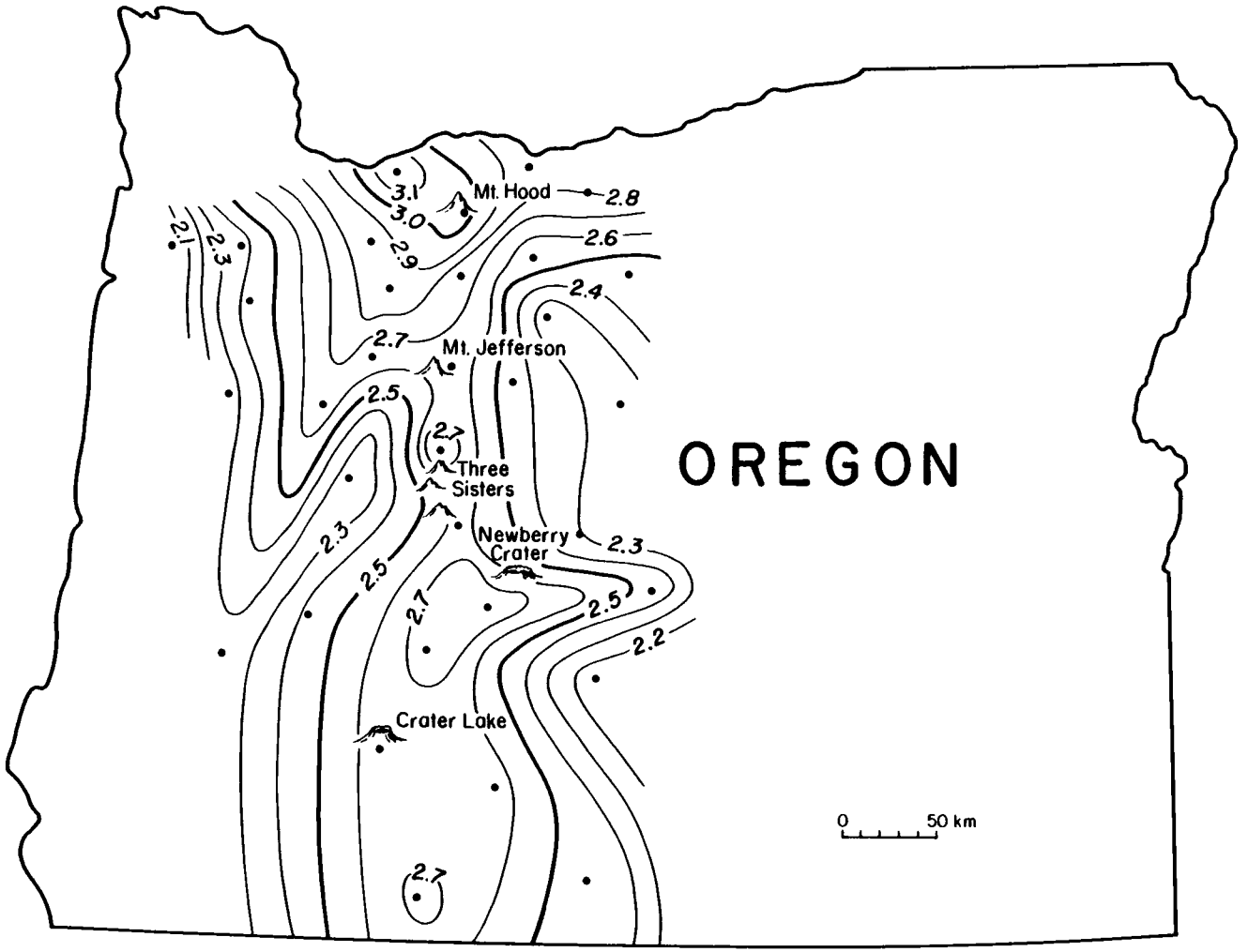

Figure 18. Time-term contour map with first elevation correction scheme. The model in Figure 16b was used for stations VHO, VHH, VSM, and COR.

conformed with the general pattern of high time-terms along the crest of the Cascades, decreasing to either side.

The second elevation correction scheme was to use a single velocity of the material above sea level for all the stations. The velocity was obtained from the slope of the line calculated by minimizing the RMS of the residuals between the fraction of the time-terms associated with the elevation on a time-term vs. elevation plot and the line. The RMS velocity calculated from the uncorrected time-terms was 6.562 km/sec and was used to calculate the traveltime from sea level to each station. This elevation traveltime was then subtracted from the total traveltime and a new set of time-terms was calculated from the revised traveltimes. The absolute time-terms were then determined using the appropriate models in Figure 16 as in the previous elevation correction scheme. The contour map for this second elevation correction scheme is shown in Figure 19. The pattern is very similar to the first elevation correction scheme (Figure 18) with slight differences occurring on the western margin of the array.

The third elevation correction scheme was to calculate the velocity of the material above sea level for each station from the residual gravity anomaly at the station and the Ludwig, Nafe and Drake (1970) empirical relation between compressional wave velocity and density. A residual gravity anomaly (RGA) is obtained for each station by subtracting the long-wavelength regional gravity field (attributed to variations in the thickness of the crust) from the complete Bouguer gravity field (Pitts, 1979). The resulting short-wavelength RGA is due to variations in the density of the upper curst. RGA's have been mapped throughout Oregon by Thiruvathukal et al.

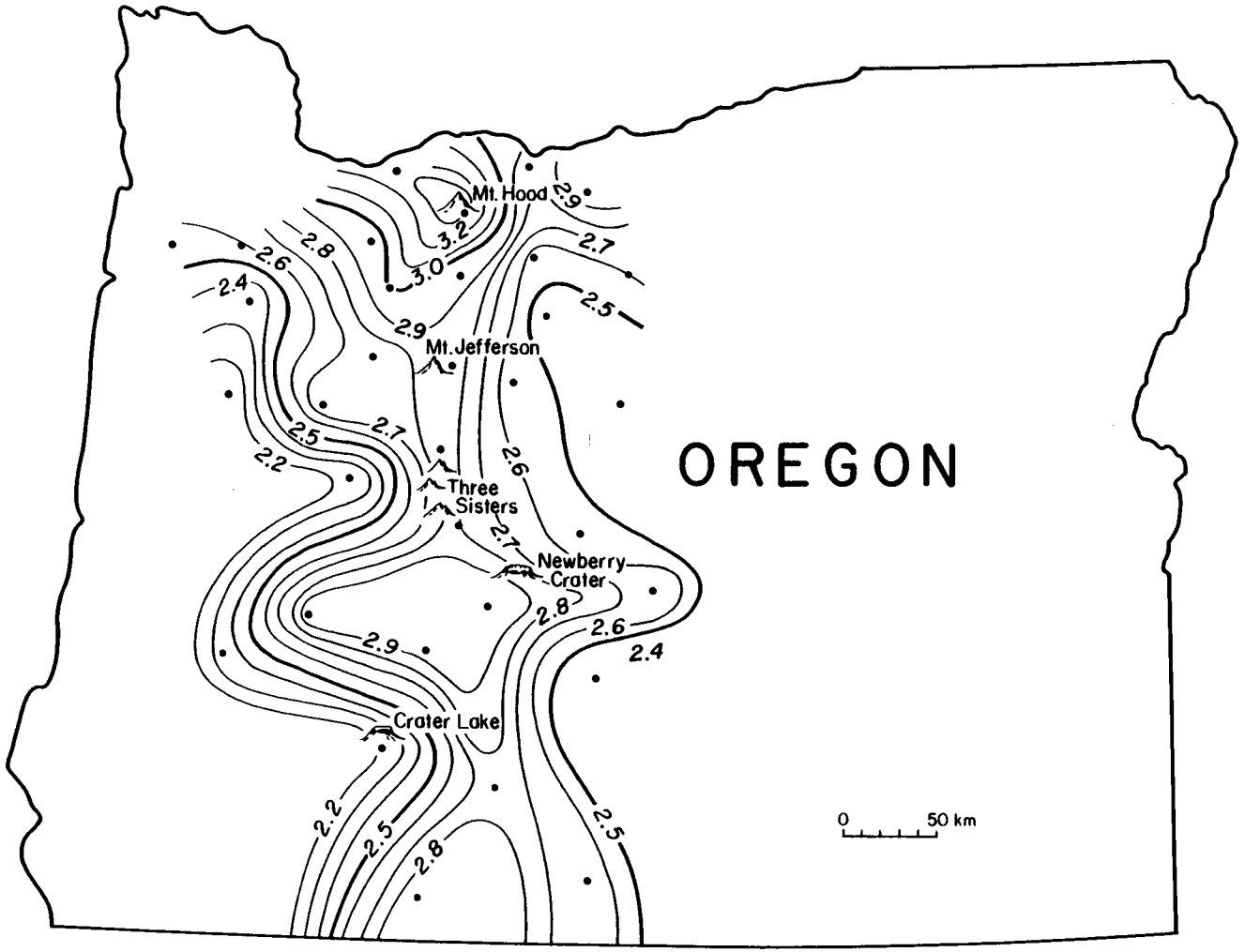

Figure 19. Time-term contour map with second (RMS velocity) elevation correction scheme.

(1970) and in more detail in the northern Oregon Cascades by Braman (1981), the central Oregon Cascades by Pitts (1979), and the southern Oregon Cascades by Veen (1982). Since incoming waves at each station are nearly vertical by the time they reach the upper crust, the RGA values were taken from these maps at the position of each station in the array.

The RGA is proportional to the difference in density between the density used to calculate the Bouguer gravity field and the true dnesity of the upper crustal material. This relation is $\Delta\rho$ = (true density - Bouguer reduction density) = RGA/$2\pi\gamma h$ where h is the elevation and γ is the universal gravitational constant. The Bouguer reduction density used in the Cascade studies was 2.43 g/cm^3, therefore the true density equals $(2.43 + \Delta\rho)$g/cm^3. The P wave velocity was then obtained from the Ludwig, Nafe and Drake (1970) empirical curve (Figure 20). For computational purposes the curve was approximated by two straight lines and a parabola, which are described by the following equations

$$V = 3.5(2.43 + \Delta\rho) - 3.73 \quad \text{for } \Delta\rho > +0.30$$

$$V = 5.54(2.43 + \Delta\rho) - 9.25 \quad \text{for } -0.21 \leq \Delta\rho \leq +0.30$$

$$V = [(2.43 + \Delta\rho)^2 - 2.8(2.43 + \Delta\rho) + 2.64]/0.472 \quad \text{for } \Delta\rho < -0.21.$$

V will be in km/sec if the RGA is in milligals, h is in kilometers, and γ = 6.672. An individual velocity for each station was thus obtained for the material between the station and sea level. These velocities were then used in the same manner as in the previous elevation correction schemes to correct the traveltimes before time-term calculation. Absolute time-terms for each station were again computed

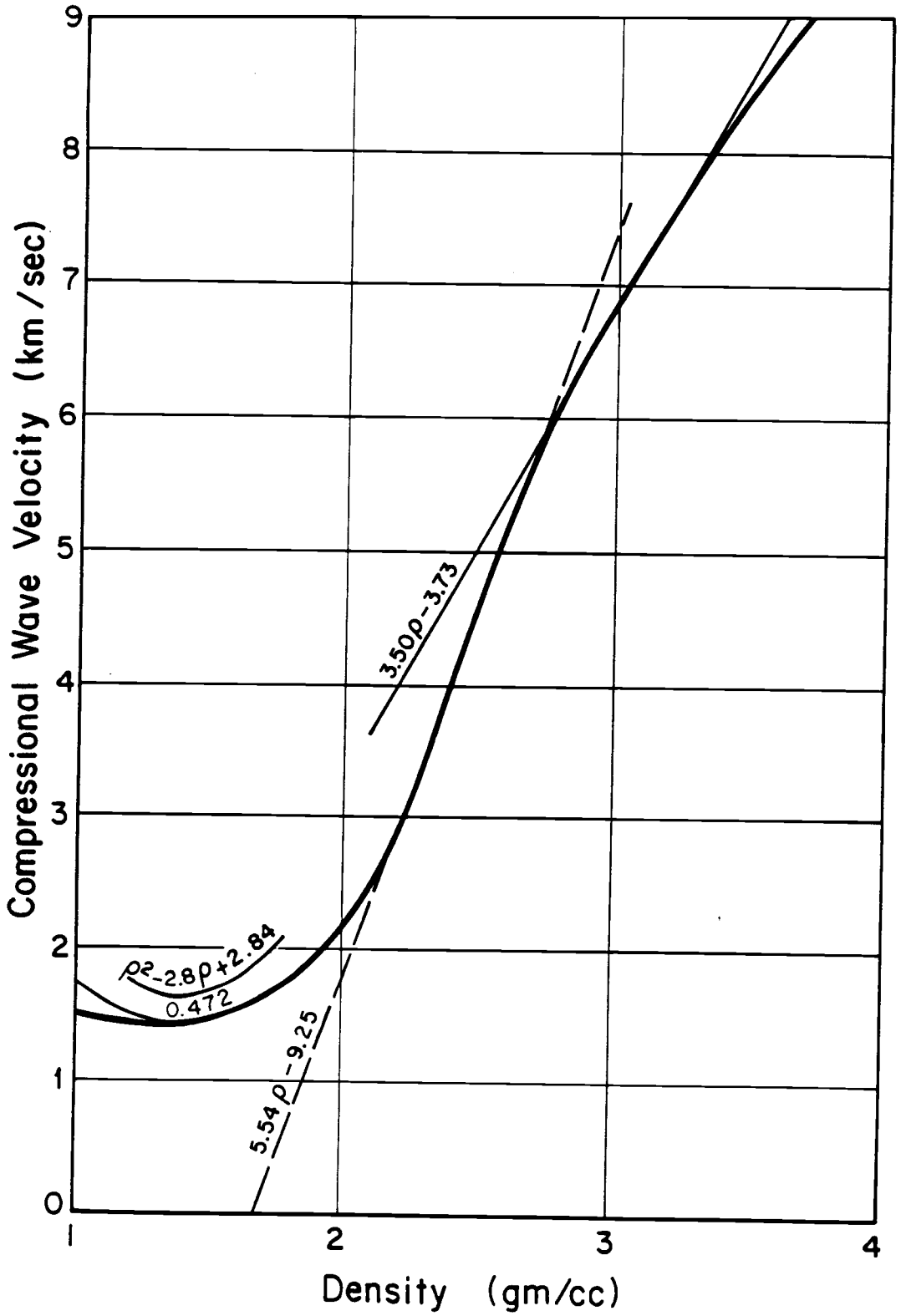

Figure 20. Graph of the Ludwig, Nafe, and Drake empirical relation between compressional wave velocity and density (Ludwig, Nafe, and Drake, 1970). The curve was fit with two straight lines and a parabola for computational purposes.

using the appropriate models in Figure 16 and the resulting contour map for this elevation correction scheme is shown in Figure 21. This map is also very similar to those obtained using the previous two elevation correction schemes, but it was considered to be the most reliable because each station had an individual correction velocity determined from an independent data set.

The spatial variation in the time-terms seen in Figure 21 can be considered to be due to either a lateral variation in crustal velocities or variations in the depth to the Moho or a combination of both. Assuming the variations are due strictly to variations in Moho depth, a crustal thickness map (Figure 22) was constructed using a time-term conversion factor of depth (km) = 13.4 (time-term) (see Appendix A). Standard deviations were calculated for each time-term and an average standard deviation of 0.17 second was found in each of the elevation correction schemes. This corresponds to an error of approximately 2 km in the Moho depth estimations.

Velocity vs. Azimuth Analysis

When the traveltime plots of individual events were made and the P_n velocities determined from them, it was observed that events southwest of the array generally showed higher velocities than events coming from other azimuths. To determine possible causes for this variation in velocity with azimuth of approach, a plot was made of the P_n velocity determined for each individual event versus the azimuth of approach, for each station. To make sure that only P_n waves were being dealt with, any event or part of an event with distances less than 250 km were not used. This requirement eliminated

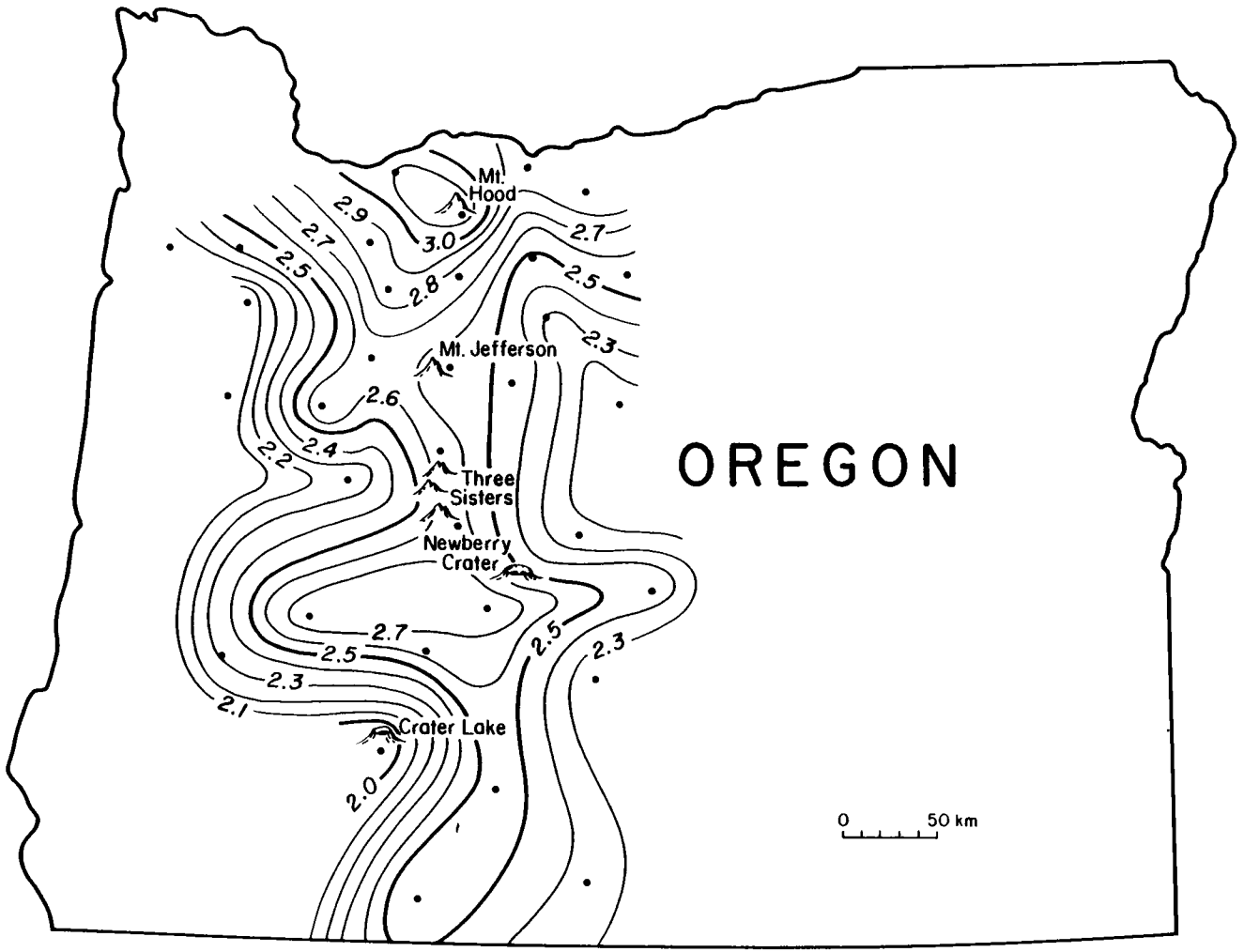

Figure 21. Time-term contour map with third (residual gravity anomaly) elevation correction scheme.

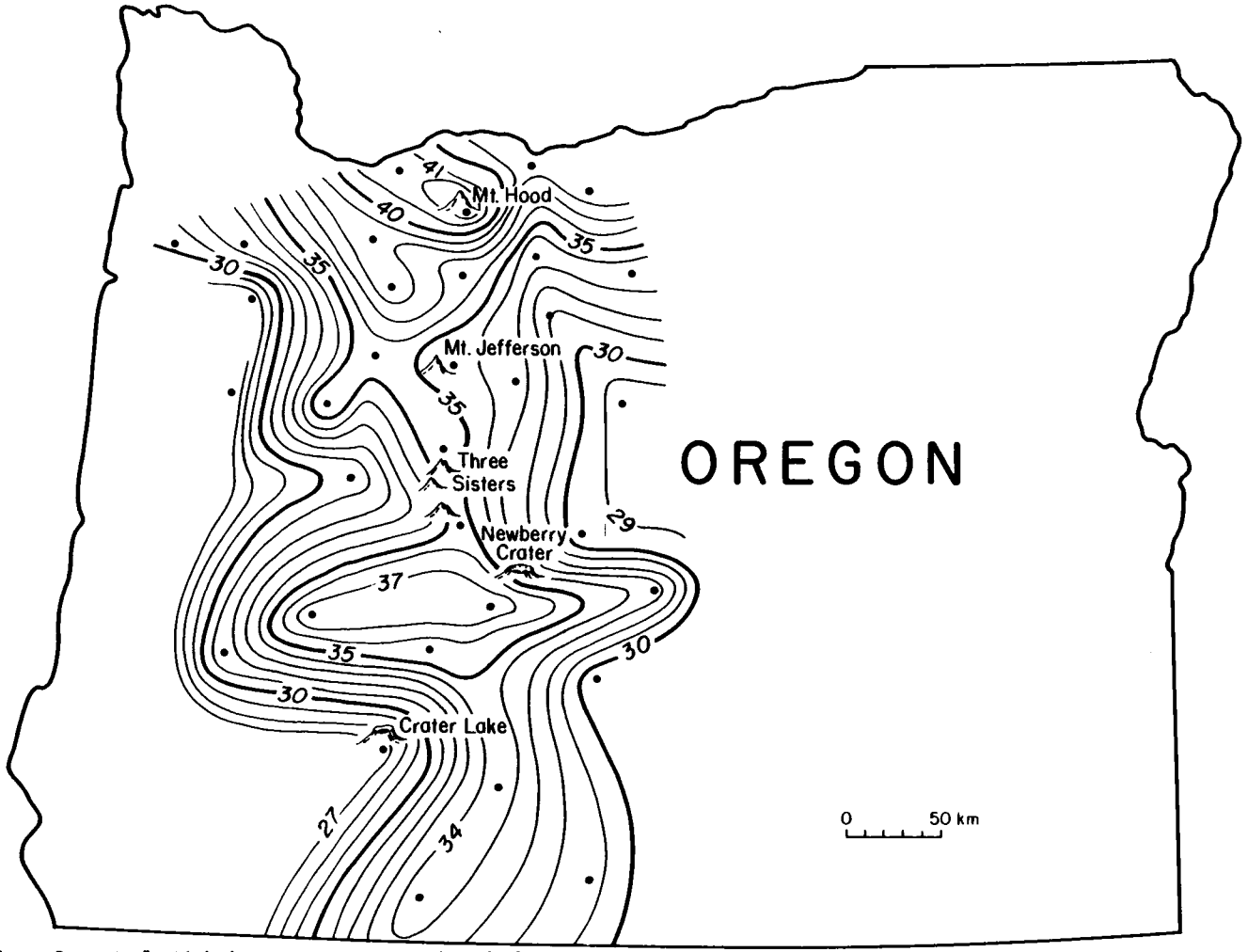

Figure 22. Crustal thickness map obtained from the conversion of the time-terms in Figure 21 to depths to Moho using the conversion factor: depth = 13.45 x (time-term). This conversion assumes that the lateral variations seen in the time-terms are due strictly to lateral variations in the thickness of the crust. (see Appendix A).

the Mt. St. Helens events, the Lincoln City event, and the Ochoco Mtns. event. The P_n velocity was recalculated for the White Swan, Elk Lake, Cle Elum, and Goat Rocks events, using only the stations greater than 250 km from the event. All other events were used unchanged. The events were grouped in three directions; one group coming from the north, one coming from the southwest and one coming from the southeast (see Figure 4).

If the variation in velocity with azimuth is due to a dipping Moho, then the velocity vs. azimuth plot should fit a single wavelength sine curve whose peak is at the azimuth of true dip. A least squares sine-wave of the form $V = V_M + B \sin (AZ + \phi)$, where V_M is the Moho velocity, B is the amplitude of the sine-wave, AZ is the aximuth, and ϕ is a phase angle that shifts the peak of the sine-wave to the azimuth of true dip, was fit to the data. Figure 23a shows the velocity vs. azimuth plot and least squares sine-wave fit for station VWM. VWM was selected because the values obtained for it were typical of the values obtained for all the stations. The ranges of values were 7.546-7.771 km/sec for V_M, 0.124-0.370 km/sec for B, and 206-266 degrees for azimuth of dip. The B value will give the magnitude of the Moho dip for a given upper layer velocity. The dip is plotted over a reasonable range of upper layer velocities for station VWM in Figure 23b. An upper layer velocity of 6.825 km/sec (from traveltime analysis) gives a Moho dip of approximately 3.5° to the southwest. The magnitude of the dip seems reasonable, but the fact that all of the stations have the Moho dipping to the southwest suggests that a dipping Moho may be an incorrect interpretation of the variation in velocity with azimuth. A general southwest

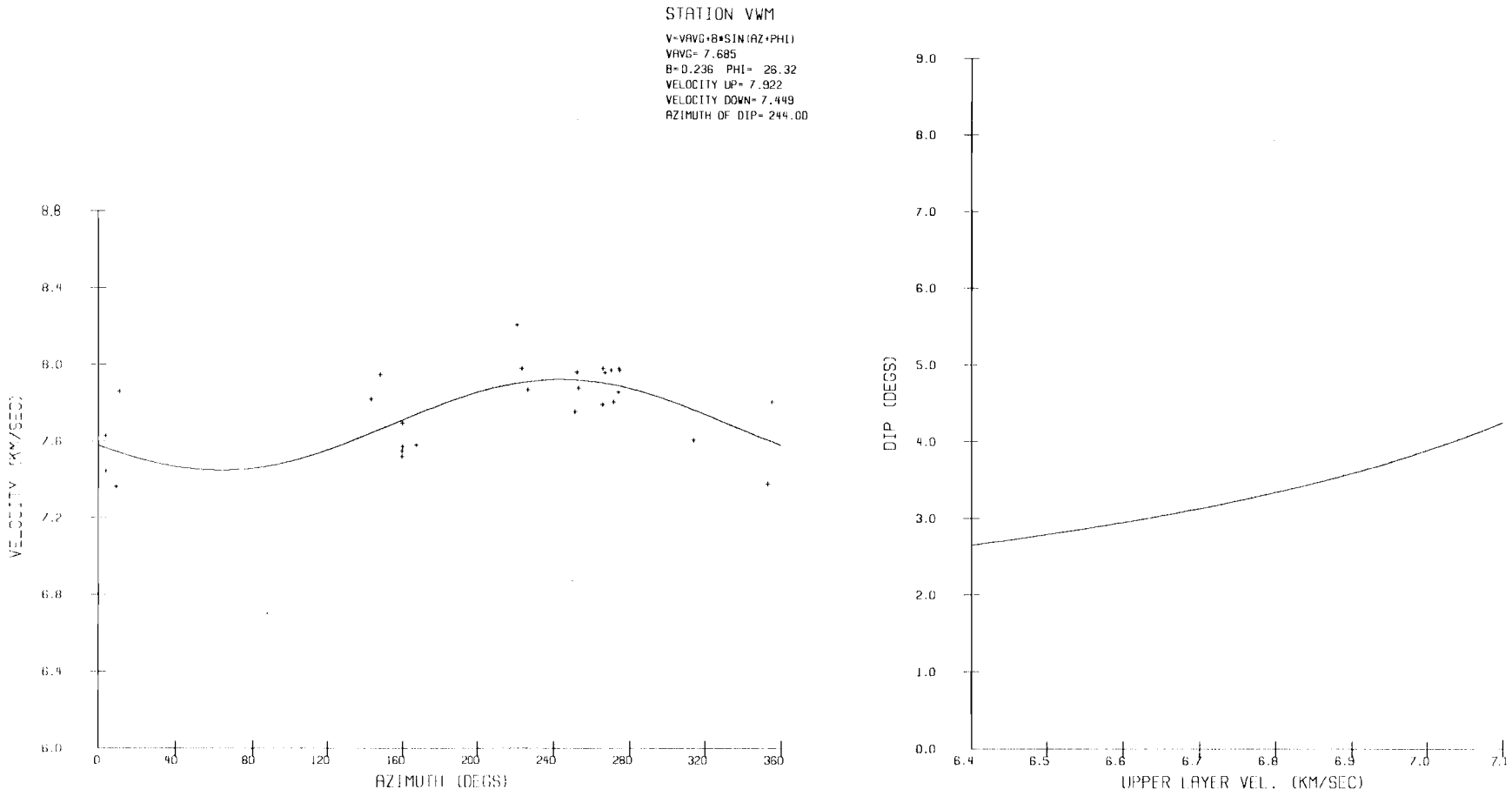

Figure 23. a) Velocity vs. azimuth plot for station VWM. Included are the data points and the parameters of the least squares sine curve fit through the data.
b) Magnitude of the dip of the Moho beneath station VWM as determined from the amplitude of sine curve in Figure 23a, plotted as a function of upper layer velocity.

dip to the Moho is not supported by the time-term results of this study nor by the results of previous regional gravity studies (Thiruvathukal et al., 1970; Pitts, 1979; Braman, 1981; Veen, 1982) and previous seismic studies (Dehlinger et al., 1965; Chiburis, 1966; Langston, 1981), all of which find an east to southeast dip to the Moho.

An alternate interpretation of the variation in velocity with azimuth is velocity anisotropy in the upper mantle. A number of authors have suggested that the upper mantle exhibits a form of anisotropy known as transverse isotropy (Crosson and Christensen, 1969; Crampin and Bamford, 1977; Bamford et al., 1979). Transversely isotropic media possess an axis of symmetry such that all planes containing the axis are equivalent. The velocity vs. azimuth variation can thus be described by a transversely isotropic upper mantle with a horizontal symmetry axis pointing in the direction of maximum velocity. A complete cycle of variation will occur in 180° of azimuth. Therefore the velocity vs. azimuth data was fit with a sine curve of half the wavelength of the dipping layer case. The equation that was used to describe this sine curve is $V^2 = V_{avg.}^2 + B\cos(2\theta) + C\cos(4\theta)$ where V is the observed velocity, $V_{avg.}$ is the average Moho velocity, θ is the azimuth measured from the symmetry axis, and B and C are constants related to the elastic parameters of the material. $V_{avg.}$, B, and C were determined for each station by a least squares fit to the data. Station VWM was again chosen to illustrate the fit of the calculated sine curve to the data and is shown in Figure 24. In general, the fits of these double wavelength sine curves were as good or better than the fits of the single wavelength sine curves (Figure

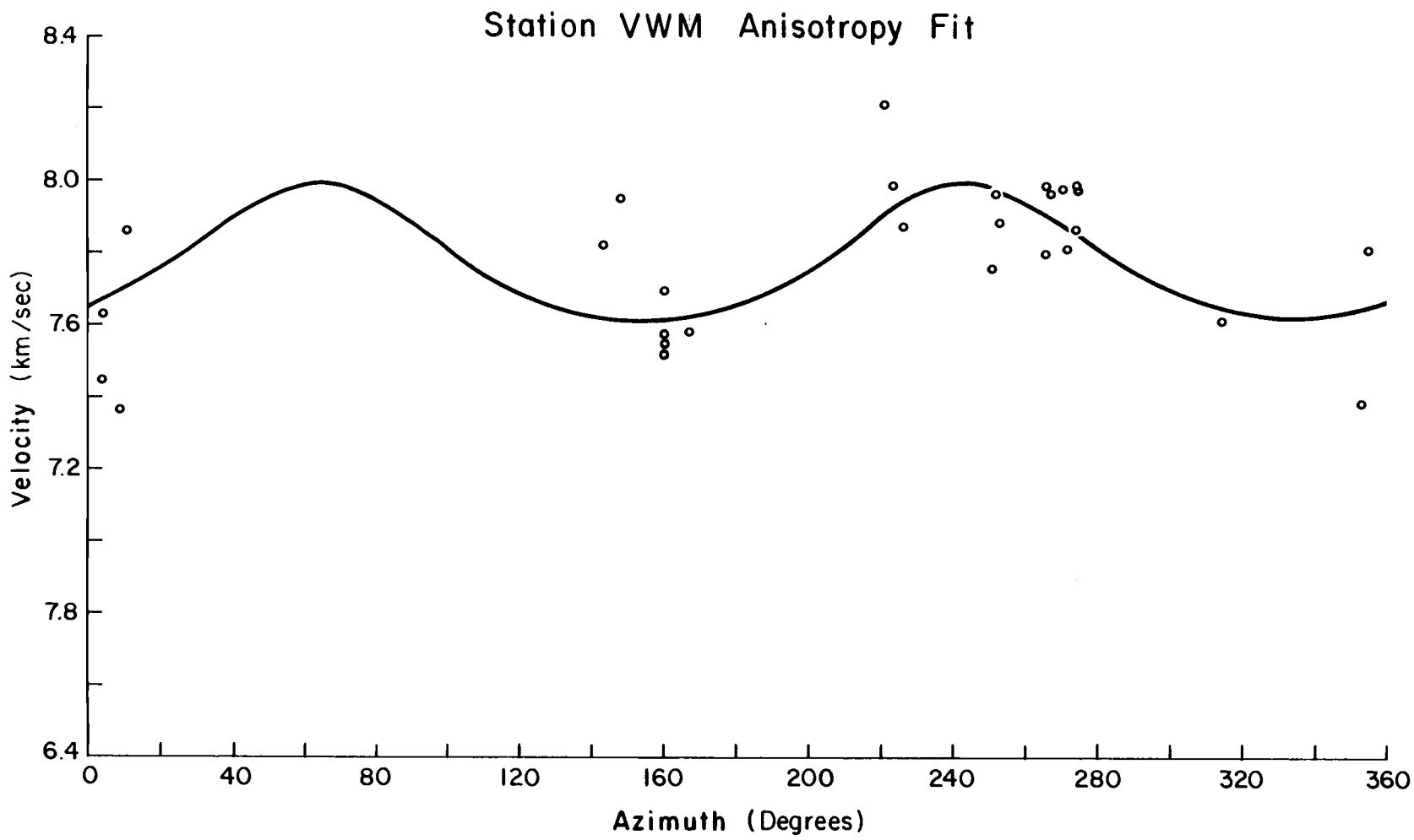

Figure 24. Anisotropy fit to the velocity vs azimuth plot for station VWM. The equation of the calculated least squares curve through the data is: $V^2 = (7.778)^2 + 2.875 \cos(2\theta) + 0.454 \cos(4\theta)$ where θ is measured from the symmetry axis.

23a). Once $V_{avg.}$, B, and C were determined from the least squares fit, a percentage of anisotropy was calculated from the equation: % anisotropy = $\{2[(V^2_{avg.} + B + C)^{\frac{1}{2}} - V_{avg.}]/V_{avg.}\} \times 100$. The percent anisotropy values calculated for each station were plotted on a map shown in Figure 25. The double-headed arrows indicate the orientation of the symmetry (fast) axis. For most of the stations, the axis was oriented generally southwest-northeast. The map shows that anisotropy is generally higher to the east. It also shows a prominent area of low anisotropy centered at Newberry Crater. Discussion of these results are given in the next chapter.

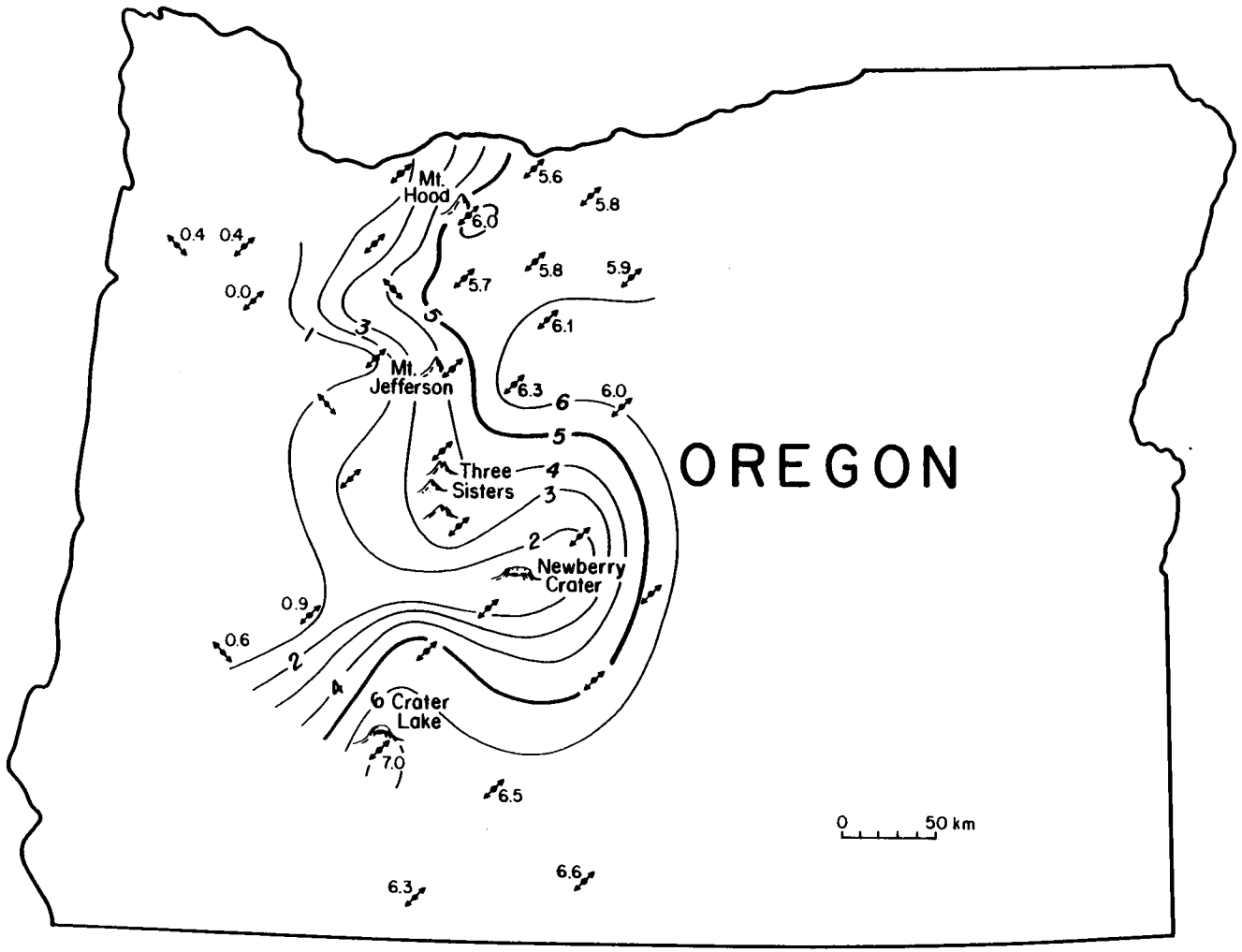

Figure 25. Contour map of percent velocity anistropy of the upper mantle. The orientation of the symmetry (fast) axis is indicated by the double-headed arrows at each station.

DISCUSSION AND SUMMARY

In interpreting the crustal thickness map derived from time-term analysis (Figure 22) one must keep in mind the assumptions of the method (see Appendix A) and the assumption that the variations in the time-terms were strictly due to variations in crustal thickness. For the time-term method to work ideally, the array of stations should be surrounded completely by sources and at least one position should be occupied by both a source and a receiver. In this study, even though as wide an azimuthal coverage as possible was attained, some gaps in azimuth did occur (see Figure 4). Most notable is the lack of sources coming directly from the east. This lack of eastern sources makes the eastern edge of the crustal thickness map less reliable than the rest of the map.

The crustal thickness map shows that the crust is thicker along the crest of the Cascades than to either side. This agrees with the results of the time-term study of McCollom and Crosson (1975), who found the crust in Washington thickening toward the Cascades from both sides. This thickening indicates the possible existence of a 5-6 km thick isostatic crustal root beneath the Cascades. From density modeling by previous gravity investigations of the Cascades (Braman, 1981; Veen, 1982) and from the average P wave velocities found in this study, 2.85 g/cm^3 and 3.32 g/cm^3 are considered reasonable values for the average crustal and upper mantle densities respectively. With these densities and with an average elevation for the crest of the Cascades of 1.6 km, a root of approximately 10 km would be needed for the Cascades to be fully isostatically compensated.

The observed root (5-6 km) thus indicates that the Cascades are 50-60% compensated. This agrees with the gravity survey of Thiruvathukal et al. (1970) who found the Cascades to be not fully compensated and a root that was 'minor' in depth and extent.

The crustal thickness on the west edge of the map (27 km) is in fair agreement with the crustal thickness value of 22 km calculated for the west subset in the traveltime analysis. It is also in good agreement with the values obtained from previous seismic studies of 29 km (Johnson and Couch, 1970) and 26 km (Simila, 1980) and by previous gravity studies of 25 km (Dehlinger, Couch and Gemperle, 1968), 20-30 km (Thiruvathukal, 1970), and 25-30 km (Veen, 1982). The indicated crustal thickness on the eastern edge of the map (29-30 km) is in poor agreement with the value obtained for the east subset of the traveltime analysis (37 km) and also with the previous studies of this area (45 km by Chiburis, 1966; 40-45 km by Thiruvathukal, 1970; 35 km by Hill, 1972). This poor agreement is most likely due to the previously stated lack of eastern sources, but another possible explanation is that the average crustal velocity in the eastern section is higher than that of the model used to determine the absolute time-terms. This will result in smaller than expected time-terms and thus shallower Moho depths will occur (from the constant crustal velocity assumption).

Crustal velocity variations can also explain the apparent thickening of the crust in the vicinities of Newberry Crater and Mt. Hood. High heat flow values have been reported in both these areas (Higgins and Waters, 1968; Blackwell and Steele, 1979; Blackwell, 1981; Williams et al., 1982). Their sources may be magma or near molten material in the curst which slows seismic waves as they pass through

the material. This in turn will increase the time-terms and make the crust appear thicker than it is. If high temperature material is the cause of the apparent crustal thickening, it is interesting to note that the apparent crustal thickening (high temperature) extends from Mt. Hood northwestward toward the direction of Mt. St. Helens, indicating a possible connection between the two volcanoes. This high temperature interpretation is supported by the anisotropy analysis. The percent anisotropy contour map (Figure 25) shows low anisotropy values around Newberry Crater and northwest of Mt. Hood. In areas of high temperature the alignment of crystals (which is thought to be the cause of anisotropy in the mantle) is less well developed (Christensen and Crosson, 1968). There may also be fewer crystals to begin with if the mantle material is partially molten.

A high temperature or partially molten upper mantle would also explain the low P_n velocity found by both the traveltime analysis (7.756 km/sec) and the time-term analysis (7.746 km/sec) and is supported by the generally high heat flow found for the entire Cascade area (Blackwell et al., 1978).

In summary, the traveltime analysis found a thin crust (22 km) and normal velocity Moho (7.975 km/sec) west of the Cascades, a thicker crust (37 km) and lower velocity (7.751 km/sec) east of the Cascades, and a low velocity (7.756 km/sec) and average crustal thickness of 32 km for the whole array. Time-term analysis showed a possible isostatic root associated with the Cascades which does not fully compensate them, and the possibility of partially molten material in the areas of Mt. Hood and Newberry Crater. The velocity vs. azimuth

analysis found anisotropy in the upper mantle, with the fast direction generally southwest-northeast, and also further supported partially molten material in the Mt. Hood and Newberry Crater areas.

BIBLIOGRAPHY

Aki, K., and P. G. Richards, 1980, Quantitative Seismology, Vols. I and II: San Francisco, W. H. Freeman and Co., 932 p.

Allen, J. E., 1966, The Cascade Range Volcano-Tectonic Depression of Oregon, in Transactions of the Lunar Field Conference, Bend, Oregon, August 1965: Oregon Dept. of Geol. and Min. Inds., pp. 21-23.

Backus, G. E., 1965, Possible Forms of Seismic Anisotropy of the Uppermost Mantle under Oceans: J. Geophys. Res., v. 70, no.14, pp. 3429-3439.

Baldwin, E. M., 1980, Geology of Oregon: Dubuque, Iowa, Kendall-Hunt Pub. Co., 170 p.

Bamford, S. A. D., 1973, An Example of the Iterative Approach to Time-Term Analysis: Geophys. J. R. Astr. Soc., 31, pp. 365-372.

Bamford, D., 1976, Mozaic Time-Term Analysis: Geophys. J. R. astr. Soc., 44, pp. 433-446.

Bamford, D., M. Jentsch, and C. Prodehl, 1979, P_n anisotorpy studies in northern Britain and the eastern and western United States: Geophys. J. R. astr. Soc., 57, pp. 397-429.

Barr, K. G., 1971, The Statistics of the Time-Term Method: Bull. Seism. Soc. Am., 61, no. 6, pp. 1853-1854.

Båth, M., 1978, An Analysis of the Time Term Method in Refraction Seismology: Tectonophysics, 51, pp. 155-169.

Beeson, M. H., and M. R. Moran, 1979, Columbia River Basalt Group Stratigraphy in Western Oregon: Oregon Geology, 41, no. 1, pp. 11-14.

Berg, J. W., L. Trembly, D. A. Emilia, J. R. Hutt, J. M. King, L. T. Long, W. R. McKnight, S. K. Sarmah, R. Souders, J. V. Thiruvathukal, and D. A. Vossler, 1966, Crustal Refraction Profile, Oregon Coast Range: Bull. Seism. Soc. Am., 56, no. 6, pp. 1357-1362.

Berry, M. J., and G. F. West, 1966, An Interpretation of the First-Arrival Data of the Lake Superior Experment by the Time-Term Method: Bull. Seism. Soc. Am., 56, no. 1, pp. 141-171.

Blackwell, D. D., 1981, Hottest U.S. Geothermal Find: News, EOS Trans. AGU, v. 62, no. 37, p. 665.

Blackwell, D. D., D. A. Hull, R. G. Bowen, and J. L. Steele, 1978, Heat Flow of Oregon: Special Paper 4, Oregon Dept. of Geol. and Min. Inds., Portland, Oregon, 42 p.

Blackwell, D. D., and J. L. Steele, 1979, Heat Flow Modeling of the New Mt. Hood Volcano, Oregon, in Geothermal Resource Assessment of Mt. Hood, Oregon: Open File Report 0-79-8, Oregon Dept. of Geol. and Min. Inds., pp. 190-264.

Braman, D. E., 1981, Interpretation of Gravity Anomalies Observed in the Cascade Mountain Province of Northern Oregon: unpublished M.S. Thesis, Oregon State University, Corvallis, Oregon, 144 p.

Burdick, L.D., and D. V. Helmberger, 1978, The Upper Mantle P Velocity Structure of the Western United States: J. Geophys. Res., v. 83, pp. 1689-1712.

Burdick, L. J., and C. A. Langston, 1977, Modeling Crustal Structure Through the Use of Converted Phases in Teleseismic Body-Wave Forms: Bull. Seism. Soc. Am., 67, no. 3, pp. 677-691.

Carts, D. A., and G. A. Bollinger, 1981, A Regional Crustal Velocity Model for the Southeastern United States: Bull. Seism. Soc. Am., 71, no. 6, pp. 1829-1847.

Chiburis, E. F., 1966, Crustal Structures in the Pacific Northwest States from Phase-Velocity Dispersion of Seismic Surface Waves: unpublished Ph.D. Thesis, Oregon State University, Corvallis, Oregon, 170 p.

Christensen, N. I., and R. S. Crosson, 1968, Seismic Anisotropy in the Upper Mantle: Tectonophysics, 6, pp. 93-107.

Cook, K. L., 1967, Rift System in the Basin and Range Province, in The World Rift System: Geological Survey of Canada, Paper 66-14, pp. 246-279.

Crampin, S., and D. Bamford, 1977, Inversion of P-Wave Velocity Anisotropy: Geophys. J. R. astr. Soc. 49, pp. 123-132.

Crosson, R. S., 1972, Symmetry of Upper Mantle Anisotropy: Earth and Planetary Science Letters 15, pp. 423-429.

Crosson, R. S., and N. I. Christensen, 1969, Transverse Isotropy of the Upper Mantle in the Vicinity of Pacific Fracture Zones: Bull. Seism. Soc. Am., 59, no. 1, pp. 59-72.

Dehlinger, P., E. F. Chiburis, and M. M. Collver, 1965, Local Travel-Time Curves and Their Geologic Implications for the Pacific Northwest States: Bull. Seis. Soc. Am., 55, no. 3, pp. 587-607.

Dehlinger, P., R. W. Couch, and M. Gemperle, 1968, Continental and Oceanic Structure from the Oregon Coast Westward Across the Juan de Fuca Ridge: Can. J. of Earth Sci., v. 5, pp. 1079-1090.

Greenfield, R. J., and R. M. Sheppard, 1969, The Moho Depth Variations Under the LASA and their Effect on dT/DΔ Measurements: Bull. Seism. Soc. Am., 59, no. 1, pp. 409-420.

Havskov, J., and E. R. Kanasewich, 1978, Determination of the Dip and Strike of the Moho from Array Analysis: Bull. Seis. Soc. Am., v. 68, pp. 1415-1419.

Herrin, E., and J. Taggart, 1962, Regional Variations in P_n Velocity and their Effect on the Location of Epicenters: Bull. Seism. Soc. Am., 52, pp. 1037-1046.

Herrin, E., and J. Taggart, 1968, Regional Variations in P Travel Times: Bull. Seism. Soc. Am., 58, no. 4, pp. 1325-1337.

Higgins, M. W., and A. C. Waters, 1968, Newberry Caldera Field Trip, in Dole, H. M., editor, Andesite Conference Guidebook: Oregon Dept. of Geol. and Min. Inds., Bull., 62, pp. 59-78.

Hill, D. P., 1972, Crustal and Upper Mantle Structure of the Columbia Plateau from Long Range Seismic-Refraction Measurements: Geol. Soc. Am. Bull., 83, pp. 1639-1648.

Hill, D. P., and L. C. Pakiser, 1967, Seismic Refraction Study of Crustal Structure Between the Nevada Test Site and Boise, Idaho: Geol. Soc. Am. Bull., v. 78, pp. 685-704.

Hunt, C. B., 1974, Natural Regions of the United States and Canada: San Francisco, W. H. Freeman and Co., 725 p.

James, D. E., T. J. Smith, and J. S. Steinhart, 1968, Crustal Structure of the Middle Atlantic States: JGR, 73, no. 6, pp. 1983-2006.

Johnson, S. H. and R. W. Couch, 1970, Crustal Structure in the North Cascade Mountains of Washington and British Columbia from Seismic Refraction Measurements: Bull. Seism. Soc. Am., 60, no. 4, pp. 1259-1269.

Klein, F. W., 1978, Hypocenter Location Program HYPOINVERSE, U.S. Geol. Survey Open-file Report 78-694, 113 p.

Kohler, W. M., J. H. Healey, and S. S. Wegener, 1982, Upper Crustal Structure of the Mount Hood, Oregon Region as Revealed by Time Term Analysis: JGR, 87, no. B1, pp. 339-355.

Langston, C. A., 1977, Corvallis, Oregon, Crustal and Upper Mantle Receiver Structure from Teleseismic P and S Waves: Bull. Seism. Soc. Am., 67, no. 3, pp. 713-724.

Langston, C. A., 1979, Structure Under Mount Rainier, Washington, Inferred from Teleseismic Body Waves: JGR, 84, no. B9, pp. 4749-4762.

Langston, C. A., 1981, Evidence for the Subducting Lithosphere Under Southern Vancouver Island and Western Oregon from Teleseismic P Wave Conversions: JGR, 86, B5, pp. 3857-3866.

Lawson, C. L., and R. J. Hanson, 1974, Solving Least Squares Problems: Englewood Cliffs, New Jersey, Prentice-Hall, Inc., 340 p.

Leaver, D. S., 1982, A Refraction Study of the Oregon Cascades: unpublished M.S. Thesis, University of Washington, Seattle, Washington, 67 p.

Ludwig, W. J., K. E. Nafe, and G. L. Drake, 1970, Seismic Refraction: The Sea, H. Maxwell, editor, New York, John Wiley, v. 4, pt. 1, pp. 53-84.

McBirney, A. R., 1978, Volcanic Evolution of the Cascade Range: Ann. Rev. Earth Planet. Sci, 6, pp. 437-56.

McCollom, R. L., and R. S. Crosson, 1975, An Array Study of Upper Mantle Velocity in Washington State: Bull. Seism. Soc. Am., 65, no. 2, pp. 467-482.

McKenzie, D., and B. Julian, 1971, Puget Sound, Washington, Earthquake and the Mantle Structure Beneath the Northwestern United States: Geol. Soc. Am. Bull., v. 82, pp. 3519-3524.

Mitchell, B. J., and B. M. Hashim, 1977, Seismic Velocity Determinations in the New Mexico Seismic Zone: A New Method Using Local Earthquakes: Bull. Seism. Soc. Am., 67, no. 2, pp. 413-424.

Murdock, J. N., and L. H. Jaksha, 1981, The P Wave Velocity of the Uppermost Mantle of the Rio Grande Rift Region of North Central New Mexico: JGR, 86, no. B8, pp. 7055-7063.

Newton, V. C., 1969, Subsurface Geology of Lower Columbia and Willamette Basins, Oregon, Oil and Gas Investigations no. 2: Oregon Dept. of Geol. and Min. Inds., 121 p.

Northrop, J., 1970, Accuracy of Earthquake Epicenters on the Gorda Ridge: Bull. Seism. Soc. Am., 60, no. 1, pp. 265-267.

Otsuka, M., 1966, Aximuth and Slowness Anomalies of Seismic Waves Measured on the Central California Seismographic Array, Part II, Interpretations: Bull. Seism. Soc. Am., 56, no. 3, pp. 655-675.

Pacific Geoscience Centre, 1978, Juan de Fuca Plate Map: Relief: Pacific Geoscience Centre, Sidney, Brit. Columbia.

Peck, D. L., A. B. Griggs, H. G. Schlicker, F. G. Wells, and H. M. Dole, 1964, Geology of the Central and Northern Parts of the Western Cascade Range in Oregon: U. S. Geol. Survey Prof. Paper 449, 56 p.

Pitts, G. S., 1979, Interpretation of Gravity Measurements Made in the Cascade Mountains and Adjoining Basin and Range Provinces in Central Oregon: unpublished M.S. Thesis, Oregon State University, Corvallis, Oregon, 186 p.

Priestly, K., and J. Brune, 1978, Surface Waves and the Structure of the Great Basin of Nevada and Western Utah: J. Geophys. Res., v. 83, no. B5, pp. 2265-2272.

Raikes, S. A., 1980, Regional Variations in Upper Mantle Structure Beneath Southern California: Geophys. J. R. astr. Soc., 63, pp. 187-216.

Reiter, L., 1970, An Investigation into the Time Term Method in Refraction Seismology: Bull. Seism. Soc. Am., 60, no. 1, pp. 1-12.

Richter, C. F., 1958, Elementary Sesimology: San Francisco, W. H. Freeman and Co., 768 p.

Rinehart, V. J., 1964, Investigation of Twelve Earthquakes off the Oregon and Northern California Coasts: unpublished M.S. Thesis, Oregon State University, Corvallis, Oregon, 41 p.

Rite, A., and H. M. Iyer, 1981, Oregon Seismicity: 1981 [Abs.]: EOS Trans. AGU, v. 62, no. 45, p. 966.

Scheidegger, A. E., and P. L. Willmore, 1957, The Use of a Least Squares Method for the Interpretation of Data from Seismic Surveys: Geophysics, Vol. XXII, no. 1, pp. 9-22.

Shor, G. G., Jr., P. Dehlinger, H. K. Kirk, and W. S. French, 1968, Seismic Refraction Studies off Oregon and Northern California: J. Geophys. Res., v. 73, pp. 2175-2194.

Simila, G. W., 1980, Seismic Velocity Structure and Associated Tectonics of Northern California: unpublished Ph.D. Dissertation, University of California, Berkeley, California, 180 p.

Snavely, P. D., Jr., H. C. Wagner, and N. S. MacLeod, 1969, Geology of Western Oregon North of the Klamath Mountains: Oregon Dept. of Geol. and Min. Inds., 64, pp. 32-46.

Solano-Borrego, A. E., 1982, Microseismicity on the Gorda Ridge: unpublished M.S. Thesis, Oregon State University, Corvallis, Oregon, 76 p.

Taylor, S. R., 1980, Crust and Upper Mantle Structure of the Northeastern United States: unpublished Ph.D. Thesis, Mass. Inst. Technol., Cambridge, Mass., 288 p.

Taylor, S. R., 1982, Three Dimensional Crust and Upper Mantle Structure at the Nevada Test Site: UCRL-86664 Preprint, Lawrence Livermore Lab., 63 p.

Telford, W. M., L. P. Geldart, R. E. Sheriff, and D. A. Keys, 1976, Applied Geophyiscs: New York, Cambridge University Press, 860 p.

Thiruvathukal, J. V., J. W. Berg, Jr., D. F. Heinrichs, 1970, Regional Gravity of Oregon: Geol. Soc. Am. Bull., 81, pp. 725-738.

Veen, C. A., 1982, Gravity Anomalies and Their Structural Implications for the Southern Oregon Cascade Mountains Adjoining Basin and Range Province: unpublished M.S. Thesis, Oregon State University, Corvallis, Oregon, 86 p.

Vetter, U., and J. Minster, 1981, P_n Velocity Anisotropy in Southern California: Bull. Seis. Soc. Am., 71, no. 5, pp. 1511-1530.

Weaver, C. S., S. M. Green, and H. M. Iyer, 1982, Seismicity of Mount Hood and Structure as Determined from Teleseismic P Wave Delay Studies: JGR, 87, no. B4, pp. 2782-2792.

Wegener, S. S., W. D. Mooney, and J. H. Healy, 1980, A Long-Range Seismic Refraction Study of the High Cascades, Oregon: EOS Trans. AGU, v. 61, no. 6, p. 71.

Wells, F. G., and D. L. Peck, 1961, Geologic Map of Oregon West of the 121st Meridian: Oregon Dept. of Geol. and Min. Inds., Portland, Oregon.

Williams, D. L., D. A. Hull, H. D. Ackermann, and M. H. Beeson, 1982, The Mt. Hood Region: Volcanic History, Structure, and Geothermal Energy Potential: JGR, 87, no. B4, pp. 2767-2781.

Willmore, P. L., and A. M. Bancroft, 1960, The Time Term Approach to Refraction Seismology: Geophys. J., v. 3, pp. 419-432.

APPENDICES

APPENDIX A

The idea behind the time-term method is that the travel time for a refracted ray between the $i^{\underline{th}}$ source point and the $j^{\underline{th}}$ station may be written as

$$t_{ij} = \frac{\Delta_{ij}}{V} + a_i + a_j$$

where Δ_{ij} is the distance between the $i^{\underline{th}}$ source point and the $j^{\underline{th}}$ station measured along the surface, V is the velocity of propagation in the underlying refractor, and a_i and a_j are the 'time-terms' associated with the source and station respectively. The assumptions of this equation are that 1) the velocity of the upper layer varies only with depth (at least under the source and station); 2) the velocity of the base refractor is constant; and 3) the slope and curvature of the refracting surface is small. If these conditions are satisfied one can take a set of travel times for an array of N sources and stations, assume that the time-term for a particular site (source or station) will be constant in all travel times in which it appears, and then determine the values of a_i (i = 1, 2,..., N) and V that will give a best "least squares" fit to the observed data.

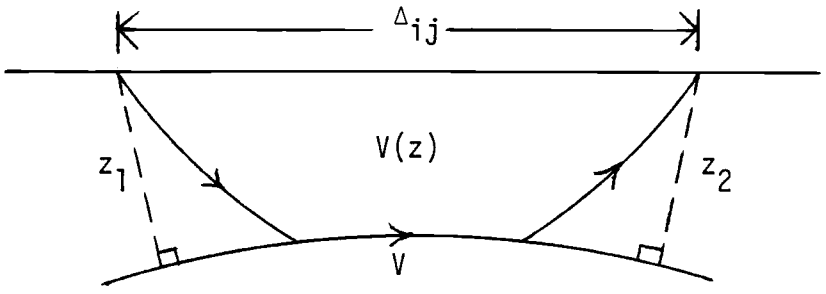

If t_{ij} is the theoretical travel time and T_{ij} is the observed travel time, then the difference between the observed and theoretical travel times, R_{ij}, is the residual of that particular observation:

$$R_{ij} = T_{ij} - t_{ij}$$

$$= T_{ij} - \frac{\Delta_{ij}}{V} - a_i - a_j$$

letting $X_{ij} - T_{ij} - \frac{\Delta_{ij}}{V}$ we have

$$R_{ij} = X_{ij} - a_i - a_j \qquad (1)$$

which is called an "observational equation".

If there are N sites, then there is the possibility of having N(N-1) ovservations, and therefore N(N-1) observational equations. This would correspond to both a source and a station at each site and all sites far enough apart for a head wave to be generated. There will be only N+1 unknowns, however; the N time-terms and the refractor velocity V. To reduce the number of equations to the number of unknowns, the time-terms and refractor velocity are selected so as to minimize the sum of the squares of the residuals R_{ij}. Since it is probable that not all the possible T_{ij} exist, a factor γ_{ij} is introduced such that:

$$\gamma_{ij} = 1 \quad \text{when } T_{ij} \text{ exists as data}$$

$$= 0 \quad \text{when it does not exist}$$

and

$$\gamma_{ii} \equiv 0 \text{ by definition.}$$

The sum of the squares of the residuals, I, can thus be written

$$I = \sum_{i=1}^{N} \sum_{j=i}^{N} [X_{ij} - a_i - a_j]^2 \gamma_{ij}$$

$$= \sum_{i=1}^{N} \Big[\sum_{j=1}^{N} X_{ij}^2 \gamma_{ij} + a_i^2 \sum_{j=1}^{N} \gamma_{ij} + \sum_{j=1}^{N} a_j^2 \gamma_{ij} - 2a_i \sum_{j=1}^{N} X_{ij} \gamma_{ij} - 2 \sum_{j=1}^{N} a_j X_{ij} \gamma_{ij} + 2a_i \sum_{j=1}^{N} a_j \gamma_{ij} \Big].$$

For I to be a minumum with respect to each time-term

$$\frac{\partial I}{\partial a_i} = 0 = \Big[0 + 2a_i \sum_{j=1}^{N} \gamma_{ij} + 0 - 2 \sum_{j=1}^{N} X_{ij} \gamma_{ij} - 0 + 2 \sum_{j=1}^{N} a_j \gamma_{ij}\Big]$$

or

$$\sum_{j=1}^{i-1} a_j \gamma_{ij} + a_i \sum_{j=1}^{N} \gamma_{ij} + \sum_{j=i+1}^{N} a_j \gamma_{ij} = \sum_{j=1}^{N} X_{ij} \gamma_{ij} \qquad (2)$$

since $\gamma_{ii} = 0$.

This is the $i^{\underline{th}}$ equation of a set of N simultaneous linear equations. The complete set of equations can best be expressed in matrix notation

$$[c_{ij}][a_j] = [\bar{x}_i]$$

and therefore

$$[a_j] = [c_{ij}]^{-1}[\bar{x}_i]$$

where

$$c_{ij} = \gamma_{ij},\ i \neq j\ ;\ c_{ii} = \sum_{j=1}^{N} \gamma_{ij}\ ;\ \bar{x}_i = \sum_{j=1}^{N} X_{ij}\gamma_{ij}. \qquad (3)$$

N normal equations can now be formed and, while equation (2) shows the form of a single equation most clearly, (3) is the set of

equations one would use to program a computer to handle the data and form the normal equations. Once the normal equations have been formed, a solution can be obtained by inverting the coefficient matrix $[c_{ij}]$ and cross-multiplying the data matrix $[\bar{x}_i]$ with it to yield the time-term matrix $[a_j]$.

Scheidegger and Willmore (1957) used cracovians to perform the inversion, which they said are well suited for the hand calculator. But since one often deals with large data sets, the limits of practicality of using a hand calculator are quickly surpassed. The inversion is best performed on a computer since nearly all computers have library programs designed to perform matrix inversions.

Now, expanding $[a_j] = [c_{ij}]^{-1}[\bar{x}_i]$ gives

$$[a_j] = [c_{ij}]^{-1}[\bar{T}_{ij}] - [c_{ij}]^{-1}\frac{[\bar{\Delta}_{ij}]}{V}$$

since $[\bar{x}_i] = [\bar{T}_{ij}] - \frac{[\bar{\Delta}_{ij}]}{V}$.

The $r^{\underline{th}}$ time-term can then be written

$$a_r = e_r - \frac{f_r}{V}$$

where e_r is an element of $[c_{ij}]^{-1}[\bar{T}_{ij}]$ and f_r is an element of $[c_{ij}]^{-1}[\bar{\Delta}_{ij}]$.

If the number of data is greater than the number of unknowns, a "least squares" velocity, V, may be calculated. The sum of squared residuals can now be written

$$I = \sum_{j=1}^{N}\sum_{i=1}^{N}\left[T_{ij} - \frac{\Delta_{ij}}{V} - e_i - \frac{f_i}{V} - e_j - \frac{f_i}{V}\right]^2\gamma_{ij}.$$

Expanding this expression, differentiating it with respect to $\frac{1}{V}$, collecting terms and equating the result to zero, gives:

$$V = \frac{\sum_{j=1}^{N}\sum_{i=1}^{N}[\Delta_{ij}-f_i-f_j]^2\gamma_{ij}}{\sum_{j=1}^{N}\sum_{i=1}^{N}[\Delta_{ij}-f_i-f_j][T_{ij}-e_j-e_i]\gamma_{ij}}$$

The matrix $[c_{ij}]$ is non-singular and the solution unique only if one or more source locations coincide with a station location. If this is not the case, then the time-terms are determinate only to within an additive constant. This constant may be chosen to fit the known geology at some point, or to minimize implausible breaks in the time-term pattern.

To get an idea of the quality of the data and the errors produced by the method, Berry and West (1966) formulated the following standard deviations:

1. Standard deviation of a time-term's data $\bar{\sigma}_t$ given by

$$\bar{\sigma}_t^2 = \frac{\sum_{s=1}^{N} R_{st}^2\gamma_{st}}{\sum_{s=1}^{N}\gamma_{st} - 1} ,$$

which is an approximate formula since the time-terms always appear in pairs in the observational equations (not normally distributed). What this gives is a measure of the scatter of the observational data about the true values (i.e. indicates the consistency of the data for a given site).

2. Standard deviation of a time-term, σ_t given by

$$\sigma_t = \frac{\bar{\sigma}_t}{\sqrt{\sum_{s=1}^{N} \gamma_{st}}} ,$$

which gives the amount by which the time-term may deivate from the value which it would have had if its data had been error free (i.e. the reliability of a time-term).

3. Standard deviation of a solution, given by

$$\sigma^2 = \frac{\sum_{i=1}^{N}\sum_{j=1}^{N} R_{ij}^2 \gamma_{ij}}{\sum_{i=1}^{N}\sum_{j=1}^{N} \gamma_{ij} - N} ,$$

which is again an approximate formula but is a useful quantity for comparing the degree of fit of various solutions. It will be a minimum for the best fitting velocity V, and when calculated for other velocities gives an indication of the rate of convergence of the solution upon this velocity.

If the velocity of the upper layer is known (as a function of depth), then one can convert time-terms to depth using the following definition of a time-term

$$a(H) = \int_0^H \frac{[V(H)^2 - V(z)^2]^{\frac{1}{2}}}{V(H)\ V(z)} dz$$

where a(H) is the time-term of the boundary at depth H, V(H) is the velocity of the material directly beneath that boundary (the base refractor), and V(z) is the velocity at depth z.

For a single layer of thickness d_1, constant velocity V_1, and

time-term to bottom boundary a_1 over a half space, we have

$$d_1 = a_1 \frac{V_1 V_2}{[V_2^2 - V_1^2]^{\frac{1}{2}}} = a_1 K[V_2, V_1] \quad ,$$

$K[V_2, V_1]$ being the time-term conversion factor.

The thickness of a second layer in a model of two layers over a half space is

$$d_2 = \{a_2 - [d_1 / K(V_3, V_1)]\} K[V_3, V_1].$$

For a model of n layers over a half space the total depth H to the bottom boundary will be

$$H = \sum_{j=1}^{n} d_j = \sum_{j=1}^{n} \{[a_j - \sum_{i=1}^{j-1} d_i / K(V_{j+1}, V_i)] K[V_{j+1}, V_i]\}.$$

APPENDIX B

Listings of the computer programs written for this study are given in this appendix. The listings include: program RELOC with its subroutines TTDIST and DISTAZ, which was used in the examination of earthquake locations; program TOTTT with its subroutines TTTPLT, NLINEA, and PIVOT, which was used in the traveltime analysis; program TIMETERM, used in the time-term analysis; and program VELAZ, used in the velocity vs. azimuth analysis. Subroutine ECL is a package of input/output subroutines which includes INFILE AND OUTFIL.

All programs were written in FORTRAN IV for use on the Prime 550 computer system. The plotting routines are in the IRVING plotting library found on Prime.

```
C   PROGRAM RELOC
C---CREATES A 2X2 DEG. GRID ABOUT A GIVEN EPICENTER. AT EACH 0.1 DEGREE
C---IT CALCULATES THE SUMMATION OF SQUARED RESIDUALS(SSR) AND VELOCITY
C---FROM OBSERVED TRAVELTIMES AS IF THE EPICENTER WAS LOCATED AT THAT
C---POINT. INPUT FILE CONTAINS THE LATITUDE & LONGITUDE OF THE GIVEN
C---EPICENTER AND THE OBSERVED TRAVELTIMES.
C---THE FIRST OUTPUT FILE CONTAINS THE VELOCITY GRID, THE SECOND OUTPUT
C---FILE CONTAINS THE SSR GRID.
C---USES SUBROUTINES TTDIST AND ECL.
C-------------------------------------------------------------------------
      DIMENSION TT(40),D(40),DELT(40),DELT2(21,21),VA(21,21)
      INTEGER*2 NFI(8),NFO1(8),NFO2(8)
$INSERT SYSCOM>KEYS.F
C---GIVE NAMES OF INPUT & OUTPUT FILES AND OPEN THEM
      CALL INFILE(6,NFI,ILEN1,K1)
      CALL OUTFIL(7,NFO1,ILEN2,K2)
      CALL OUTFIL(8,NFO2,ILEN3,K3)
C---READ LOCATION OF EPICENTER
      READ(6,3)ELAT,ELONG
    3 FORMAT(F6.3,1X,F8.3)
C---READ OBSERVED TRAVELTIMES
      DO 5 J=1,33
      READ(6,4)TT(J)
    4 FORMAT(F6.2)
    5 CONTINUE
C---CLOSE INPUT FILE
      CALL SRCH$$(K$CLOS,NFI,ILEN1,K1,ITYPE,ICODE)
      ELAT=ELAT+1.0
      ELONG=ELONG+1.0
      DO 50 M=1,21
      DO 40 K=1,21
C---FIND DISTANCES AND VELOCITY FOR EACH GRID POINT
      CALL TTDIST(ELAT,ELONG,TT,D,B,V)
      DELT2(M,K)=0.
      VA(M,K)=V
      ELONG=ABS(ELONG)
C---FIND SUMMATION OF SQUARED RESIDUALS FOR EACH GRID POINT
      DO 30 I=1,33
      IF (TT(I).EQ.0.0) GO TO 30
      DELT(I)=TT(I)-((D(I)/V)+B)
      DELT2(M,K)=DELT2(M,K)+(DELT(I)**2)
   30 CONTINUE
C---CONVERT VELOCITY FROM RADIANS/SEC TO KM/SEC
      VA(M,K)=VA(M,K)*6370.8
C---MOVE TO NEXT GRID PT. ON LATITUDE LINE
      ELONG=ELONG-0.1
   40 CONTINUE
C---MOVE TO NEXT LATITUDE LINE
      ELONG=ELONG+2.1
      ELAT=ELAT-0.1
C---WRITE OUT VELOCITY GRID
      WRITE(7,45)(VA(M,K),K=1,21)
   45 FORMAT(21F5.2///)
   50 CONTINUE
C---WRITE OUT SSR GRID
      DO 60 L=1,21
      WRITE(8,55)(DELT2(L,K),K=1,21)
   55 FORMAT(21F5.1///)
   60 CONTINUE
C---CLOSE OUTPUT FILES
      CALL SRCH$$(K$CLOS,NFO1,ILEN2,K2,ITYPE,ICODE)
      CALL SRCH$$(K$CLOS,NFO2,ILEN3,K3,ITYPE,ICODE)
      STOP
      END
```

```
      SUBROUTINE TTDIST(ELAT,ELONG,TT,D,B,V)
C---CALCULATES DISTANCES FROM A GIVEN EPICENTER TO EACH STATION OF THE
C---OREGON SEISMIC NETWORK AND THE VELOCITY OF THE WAVE.
C---INPUTS ARE THE LATITUDE(ELAT) AND LONGITUDE(ELONG) OF THE EPICENTER
C---OF THE EVENT AND THE TRAVELTIMES TO THE STATIONS(TT).
C---OUTPUTS ARE THE DISTANCES(D) AND THE VELOCITY(V).
C---STLAT AND STLON ARE THE LATITUDES AND LONGITUDES RESPECTIVELY OF
C---THE STATIONS OF THE NETWORK.
C---USES SUBROUTINE DISTAZ.
C-----------------------------------------------------------------------
      DIMENSION STLAT(33),STLON(33)
      DIMENSION XKMSQ(40),PDTXY(40),TTSQ(40),TT(40),D(40)
      DATA STLAT/45.150,44.879,44.671,44.960,45.265,45.538,45.329,45.21
     19,42.786,42.878,44.483,44.138,43.592,42.095,42.264,43.372,45.516,
     244.661,44.508,44.902,45.187,45.181,45.060,45.545,43.658,44.241,43
     3.305,43.524,43.193,43.914,44.601,43.791,44.568/
      DATA STLON/-122.265,-122.393,-122.089,-123.127,-123.309,-122.039,
     1-121.666,-123.725,-121.349,-122.120,-122.581,-122.407,-122.546,-1
     221.989,-121.049,-123.063,-120.777,-121.689,-120.619,-120.974,-121
     3.053,-120.560,-121.587,-121.311,-120.237,-121.666,-121.716,-121.3
     447,-120.666,-121.554,-121.270,-120.945,-123.303/
      RAD=57.29578
      N=0
      XSUM=0.0
      XSQSUM=0.0
      YSQSUM=0.0
      YSUM=0.0
      PDTSUM=0.0
      ELONG=-ELONG
      DO 20 I=1,33
      IF(TT(I).EQ.0.0) GO TO 20
      N=N+1
      CALL DISTAZ(ELAT,ELONG,STLAT(I),STLON(I),XDEG,AZ,AZINV)
      D(I)=XDEG/RAD
      XKMSQ(I)=D(I)**2
      TTSQ(I)=TT(I)**2
      PDTXY(I)=D(I)*TT(I)
      XSUM=XSUM+D(I)
      YSUM=YSUM+TT(I)
      XSQSUM=XSQSUM+XKMSQ(I)
      YSQSUM=YSQSUM+TTSQ(I)
      PDTSUM=PDTSUM+PDTXY(I)
   20 CONTINUE
      XAVE=XSUM/N
      YAVE=YSUM/N
      SLNUM=((XSUM*YSUM)/N)-PDTSUM
      SLDEN=((XSUM**2)/N)-XSQSUM
      SLOPE=SLNUM/SLDEN
      V=1.0/SLOPE
      B=YAVE-(SLOPE*XAVE)
      RNUM=PDTSUM-((XSUM*YSUM)/N)
      RDEN=SQRT((XSQSUM-((XSUM**2)/N))*(YSQSUM-((YSUM**2)/N)))
      R=RNUM/RDEN
      RETURN
      END
```

```
      SUBROUTINE DISTAZ(ELAT,ELONG,STLAT,STLON,XDEG,AZ,AZINV)
C---FINDS THE DISTANCE BETWEEN TWO POINTS ALONG THE SURFACE OF THE
C---EARTH, TAKING INTO ACCOUNT THE FLATTENING OF THE EARTH. IT ALSO
C---FINDS THE INCOMING AZIMUTH OF THE PATH AT EACH POINT.
C---INPUTS ARE THE LATITUDE(N+) & LONGITUDE(E+) OF THE TWO POINTS IN
C---DECIMAL DEGREES. OUTPUTS ARE DISTANCE IN DEGREES OF ARC(XDEG), THE
C---AZIMUTH(AZ), AND BACKAZIMUTH(AZINV).
C-----------------------------------------------------------------------
      REAL LAT,LONG
      DR=57.29578
      SLAT=STLAT/DR
      SLONG=STLON/DR
      LAT=ELAT/DR
        LONG=ELONG/DR
      THG=ATAN(.993277*TAN(LAT))
      D=SIN(LONG)
      E=-COS(LONG)
      F=-COS(THG)
      A=F*E
      B=COS(THG)*D
      C=SIN(THG)
      G=-C*E
      H=C*D
      THG=ATAN(.9932773*TAN(SLAT))
      D1=SIN(SLONG)
      E1=-COS(SLONG)
      F1=-COS(THG)
      C1=SIN(THG)
      A1=F1*E1
      B1=-F1*D1
      G1=-C1*E1
      H1=C1*D1
      SC=A*A1+B*B1+C*C1
      SD=SQRT(((A-A1)**2+(B-B1)**2+(C-C1)**2)*((A+A1)**2+(B+B1)
     1 **2+(C+C1)**2)/4.0)
      XDEG=ATAN(SD/SC)*DR
     IF(SC) 1,2,2
    1  XDEG=XDEG+180.0
    2   SS = ((A1-D)**2 +(B1-E)**2+C1**2 - 2.0)
      SC=((A1-G)**2+(B1-H)**2+(C1-F)**2-2.0)
      AZ=ATAN(SS/SC)*DR
      IF (SS) 3,4,5
    3  IF (SC) 6,7,7
    6  AZ=AZ+180.0
      GO TO 4
    7  AZ=AZ+360.
      GO TO 4
    5  IF (SC) 8,4,4
    8  AZ=AZ+180.
    4  SS=((A-D1)**2+(B-E1)**2+C**2-2.0)
      SC=((A-G1)**2+(B-H1)**2+(C-F1)**2-2.0)
      AZINV=ATAN(SS/SC)*DR
      IF (SS) 13,14,15
   13  IF (SC) 16,17,17
   16  AZINV=AZINV+180.0
      GO TO 14
   17  AZINV=AZINV+360.0
      GO TO 14
    15  IF (SC) 18,14,14
   18  AZINV=AZINV+180.0
   14  RETURN
      END
     FUNCTION TAN(THA)
     TAN=SIN(THA)/COS(THA)
     RETURN
     END
```

```
C   PROGRAM TOTTT
C---CALLING PROGRAM FOR SUBROUTINE TTTPLT.
C---READS DISTANCE-TRAVELTIME DATA FROM EVENT FILES LISTED IN COMMAND
C---FILE EQLIST. APPLIES SOURCE-TERM CORRECTIONS TO THE TRAVELTIMES AND
C---PUTS THE DISTANCES AND TRAVELTIMES INTO TWO LARGE ARRAYS ACCEPTABLE
C---TO TTTPLT. TITERM16 CONTAINS THE SOURCE-TERM CORRECTIONS.
C-----------------------------------------------------------------------
$INSERT SYSCOM>KEYS.F
      DIMENSION XKM(1000),TT(1000)
      DOUBLE PRECISION NFILE
C---OPEN COMMAND FILE AND SOURCE-TERM CORRECTION FILE
      CALL SRCH$$(K$READ,'EQLIST',6,1,ITYPE,ICODE)
      CALL SRCH$$(K$READ,'TITERM16',8,2,ITYPE,ICODE)
C---READ NO. OF EVENTS IN COMMAND FILE AND NO. OF STATIONS IN ARRAY
      READ(5,10)NE,NS,CD
10    FORMAT(I2,1X,I2,1X,F5.0)
      K=33
      DO 60 I=1,NE
C---READ AN EVENT FILENAME AND A SOURCE-TERM CORRECTION FOR THE EVENT
      READ(5,35)NFILE
      READ(6,30)STC
30    FORMAT(E10.3)
      WRITE(1,33)NFILE,STC
33    FORMAT(A8,2X,F5.2)
35    FORMAT(A8)
C---OPEN THE EVENT FILE
      CALL SRCH$$(K$READ,NFILE,8,3,ITYPE,ICODE)
      IF(NFILE-'BERG965 ')38,52,38
C---READ DISTANCE-TRAVELTIME DATA FROM THE EVENT FILE AND APPLY
C---THE SOURCE-TERM CORRECTION
38    DO 50 J=1,NS
      READ(7,40)XKM(J),TT(J)
40    FORMAT(8X,F8.3,10X,F6.2)
      IF(XKM(J).EQ.0.0)GO TO 50
      K=K+1
      XKM(K)=XKM(J)
      TT(K)=TT(J)-STC
50    CONTINUE
      GO TO 58
52    DO 55 L=1,9
      READ(7,40)XKM(L),TT(L)
      K=K+1
      XKM(K)=XKM(L)
      TT(K)=TT(L)-STC
55    CONTINUE
C---CLOSE THE EVENT FILE
58    CALL SRCH$$(K$CLOS,NFILE,8,3,ITYPE,ICODE)
C---READ NEXT EVENT FROM COMMAND FILE
60    CONTINUE
C---CLOSE COMMAND AND SOURCE-TERM CORRECTION FILES
      CALL SRCH$$(K$CLOS,'EQLIST',6,1,ITYPE,ICODE)
      CALL SRCH$$(K$CLOS,'TITERM16',8,2,ITYPE,ICODE)
      MM=K-33
C---RENUMBER ELEMENTS IN THE ARRAYS FOR INPUT TO TTTPLT
      DO 70 M=1,MM
      XKM(M)=XKM(M+33)
70    TT(M)=TT(M+33)
      CALL TTTPLT(XKM,TT,MM)
      STOP
      END
```

```
      SUBROUTINE TTTPLT(XKM,TT,K)
C---FITS EITHER A SINGLE LEAST SQUARES STRAIGHT LINE OR TWO LEAST
C---SQUARES STRAIGHT LINES SIMULTANEOUSLY TO DISTANCE-TRAVELTIME DATA
C---AND PLOTS THE DATA OUT ON A TRAVELTIME VS. DISTANCE GRAPH.
C---XKM IS THE DISTANCE ARRAY IN KILOMETERS.
C---TT IS THE TRAVELTIME ARRAY IN SECONDS.
C---K IS THE NUMBER OF POINTS IN THE ARRAYS.
C---USES SUBROUTINE NLINEA FOR THE NONLINEAR FIT AND THE IRVING LIBRARY
C---FOR PLOTTING.
C-----------------------------------------------------------------------
      DIMENSION XKM(1000),TT(1000),XIN(1000),YIN(1000),TTSQ(1000)
      DIMENSION XKMSQ(1000),TTCAL(1000),RESID(1000),PDTXY(1000)
C---CHOOSE LINEAR OR NONLINEAR FIT
      WRITE(1,2)
    2 FORMAT('TYPE 1 FOR NONLINEAR FIT, 2 FOR LINEAR FIT')
      READ(1,3)INL
    3 FORMAT(I1)
      IF(INL.EQ.1)GO TO 30
C---IF LINEAR FIT, GIVE DISTANCE RANGE TO BE PLOTTED
      WRITE(1,5)
    5 FORMAT('LOWER & UPPER CUTOFF PTS. OF PLOT: (F5.0,1X,F5.0)')
      READ(1,10)CD,UCD
   10 FORMAT(F5.0,1X,F5.0)
C---CALCULATE THE LINEAR LEAST SQUARES LINE
      N=0
      XSUM=0.0
      XSQSUM=0.0
      YSQSUM=0.0
      YSUM=0.0
      PDTSUM=0.0
      WRITE(1,15)K
   15 FORMAT(I6)
      DO 20 I=1,K
      IF(XKM(I).LE.CD.OR.XKM(I).GE.UCD) GO TO 20
      N=N+1
      XKMSQ(I)=XKM(I)**2.0
      TTSQ(I)=TT(I)**2.0
      PDTXY(I)=XKM(I)*TT(I)
      XSUM=XSUM+XKM(I)
      YSUM=YSUM+TT(I)
      XSQSUM=XSQSUM+XKMSQ(I)
      YSQSUM=YSQSUM+TTSQ(I)
      PDTSUM=PDTSUM+PDTXY(I)
      XIN(N)=XKM(I)/50.
      YIN(N)=TT(I)/20.
   20 CONTINUE
      WRITE(1,21)N
   21 FORMAT(I6)
      XAVE=XSUM/N
      YAVE=YSUM/N
      SLNUM=((XSUM*YSUM)/N)-PDTSUM
      SLDEN=((XSUM**2.0)/N)-XSQSUM
      SLOPE=SLNUM/SLDEN
      V=1.0/SLOPE
      B=YAVE-(SLOPE*XAVE)
      SQRES=0.0
      DO 25 J=1,K
      IF(XKM(J).LE.CD.OR.XKM(J).GE.UCD) GO TO 25
      TTCAL(J)=(SLOPE*XKM(J))+B
      RESID(J)=TT(J)-TTCAL(J)
      SQRES=SQRES+RESID(J)**2
   25 CONTINUE
      RMS=SQRT(SQRES/N)
      RNUM=PDTSUM-((XSUM*YSUM)/N)
      RDEN=SQRT((XSQSUM-((XSUM**2.0)/N))*(YSQSUM-((YSUM**2.0)/N)))
      R=RNUM/RDEN
      GO TO 38
   30 N=K
```

```
C---CALCULATE THE NONLINEAR LEAST SQUARES LINES
      CALL NLINEA(XKM,TT,N,X1,T1,AV1,AV2)
      SQRES=0.
      DO 35 L=1,N
      IF(XKM(L).GT.X1)GO TO 32
      TTCAL(L)=AV1*XKM(L)
      GO TO 33
   32 TTCAL(L)=(AV2*(XKM(L)-X1))+T1
   33 RESID(L)=TT(L)-TTCAL(L)
      SQRES=SQRES+RESID(L)**2
      XIN(L)=XKM(L)/50.
      YIN(L)=TT(L)/20.
   35 CONTINUE
      RMS=SQRT(SQRES/N)
      V1N=1./AV1
      V2N=1./AV2
C---PLOT THE TRAVELTIME DATA AND LINE FITTING PARAMETERS
   38 CALL PLOTS(0,0,99)
      CALL PLOT(0.,0.,-3)
      CALL AXES(0.,0.,0.,1200.,0.02,50.,100.,4HF6.1,0.,'DISTANCE (KM)',
     213)
      CALL AXES(0.,0.,0.,180.,0.05,20.,20.,4HF5.1,90.,'TRAVELTIME (SEC)
     1',16)
      DO 40 I=1,N
      CALL SYMBOL(XIN(I),YIN(I),0.05,4,0.,-1)
   40 CONTINUE
      IF(INL.EQ.1)GO TO 45
      CALL SYMBOL(1.0,7.0,0.15,'SLOPE=',0.,6)
      CALL NUMBER(1.9,7.0,0.15,SLOPE,0.,4HF5.3)
      CALL SYMBOL(2.7,7.0,0.15,'INTERCEPT=',0.,10)
      CALL NUMBER(4.1,7.0,0.15,B,0.,4HF6.3)
      CALL SYMBOL(5.0,7.0,0.15,'RMS=',0.,4)
      CALL NUMBER(5.7,7.0,0.15,RMS,0.,4HF5.2)
      CALL SYMBOL(1.0,6.75,0.15,'VELOCITY=',0.,9)
      CALL NUMBER(2.25,6.75,0.15,V,0.,4HF6.3)
      CALL SYMBOL(3.2,6.75,0.15,'KM/SEC  CORRELATION=',0.,20)
      CALL NUMBER(5.9,6.75,0.15,R,0.,4HF6.4)
      GO TO 50
   45 CALL SYMBOL(1.0,7.0,0.15,'UPPER LAYER VEL.=',0.,17)
      CALL NUMBER(3.3,7.0,0.15,V1N,0.,4HF5.3)
      CALL SYMBOL(4.1,7.0,0.15,'MOHO VEL.=',0.,10)
      CALL NUMBER(5.5,7.0,0.15,V2N,0.,4HF5.3)
      CALL SYMBOL(1.0,6.75,0.15,'CROSSOVER DIST.=',0.,16)
      CALL NUMBER(3.2,6.75,0.15,X1,0.,4HF5.1)
      CALL SYMBOL(4.0,6.75,0.15,'CROSSOVER TIME=',0.,15)
      CALL NUMBER(6.05,6.75,0.15,T1,0.,4HF5.2)
      CALL SYMBOL(4.0,6.5,0.15,'RMS=',0.,4)
      CALL NUMBER(4.6,6.5,0.15,RMS,0.,4HF4.2)
   50 CALL SYMBOL(1.0,6.5,0.15,'NO. OF PTS. USED=',0.,17)
      XN=FLOAT(N)
      CALL NUMBER(3.3,6.5,0.15,XN,0.,4HF4.0)
      CALL PLOT(0.,0.,40)
      RETURN
      END
```

```
      SUBROUTINE NLINEA(X,T,N,X1,T1,AV1,AV2)
C---SOLVES SIMULTANEOUSLY FOR TWO VELOCITIES AND THE CROSS-OVER PT.
C---ON A TRAVELTIME VS. DISTANCE PLOT GIVEN A STARTING MODEL.
C---USES SUBROUTINE PIVOT.
C---INPUTS ARE DISTANCE(X), TRAVELTIME(T), AND NO. OF POINTS(N).
C---OUTPUTS ARE THE CROSS-OVER POINT COORDINATES(X1,T1) AND THE SLOPES
C---OF THE TWO LINES.
C-----------------------------------------------------------------------
      DIMENSION A(4,4),F(4),X(1000),T(1000),TTCAL(1000),RESID(1000)
C---READ IN THE STARTING MODEL
      WRITE(1,5)
5     FORMAT('INPUT STARTING MODEL:V1,V2,T1,X1(F5.3,1X,F5.3,1X,F5.2,1X,
     1F5.1)')
      READ(1,7)V1,V2,T1,X1
7     FORMAT(F5.3,1X,F5.3,1X,F5.2,1X,F5.1)
      AV1=1./V1
      AV2=1./V2
C---INITIALIZE THE MATRIX EQUATION ARRAYS
8     DO 15 K=1,4
      DO 10 L=1,4
10    A(K,L)=0.
15    F(K)=0.
C---BUILD THE MATRIX EQUATION ARRAYS
      DO 40 I=1,N
      IF(X(I).GT.X1)GO TO 20
      TM=AV1*(X(I)-X1)+T1
      F(1)=F(1)+((X(I)-X1)*(T(I)-TM))
      F(4)=F(4)+(-AV1*(T(I)-TM))
      A(1,1)=A(1,1)+((X(I)-X1)**2)
      A(1,3)=A(1,3)+(X(I)-X1)
      A(1,4)=A(1,4)+(-AV1*(X(I)-X1))
      A(3,4)=A(3,4)-AV1
      A(4,4)=A(4,4)+(AV1**2)
      GO TO 30
20    TM=AV2*(X(I)-X1)+T1
      F(2)=F(2)+((X(I)-X1)*(T(I)-TM))
      F(4)=F(4)+(-AV2*(T(I)-TM))
      A(2,2)=A(2,2)+((X(I)-X1)**2)
      A(2,3)=A(2,3)+(X(I)-X1)
      A(2,4)=A(2,4)+(-AV2*(X(I)-X1))
      A(3,4)=A(3,4)-AV2
      A(4,4)=A(4,4)+(AV2**2)
30    F(3)=F(3)+(T(I)-TM)
40    CONTINUE
      A(3,3)=FLOAT(N)
C---MAKE THE ARRAY SYMMETRICAL
      DO 55 J=1,4
      DO 50 K=1,4
50    A(K,J)=A(J,K)
55    CONTINUE
      NP=4
      NN=4
C---INVERT & SOLVE FOR CHANGES IN THE MODEL
      CALL PIVOT(A,F,NP,NN)
C---CALCULATE NEW MODEL
      AV1=AV1+F(1)
      AV2=AV2+F(2)
      T1=T1+F(3)
      X1=X1+F(4)
      TS=T1-(AV1*X1)
      WRITE(1,555)TS
555   FORMAT(F10.4)
      SQRES=0.
      DO 59 M=1,N
      IF(X(M).GT.X1)GO TO 56
      TTCAL(M)=AV1*X(M)+TS
      GO TO 57
56    TTCAL(M)=(AV2*(X(M)-X1))+T1
```

```
57      RESID(M)=T(M)-TTCAL(M)
        SQRES=SQRES+RESID(M)**2
59      CONTINUE
        RMS=SQRT(SQRES/N)
        V1N=1./AV1
        V2N=1./AV2
C---WRITE OUT NEW MODEL TO THE TERMINAL & CHECK IF YOU WANT TO ITERATE
        WRITE(1,60)F(1),F(2),F(3),F(4),X1,T1,V1N,V2N,RMS
60      FORMAT('CHANGES IN THE MODEL ARE:'/'DA1=',E11.4,2X,'DA2=',E11.4,2
       1X,'DT1=',E11.4,2X,'DX1=',E11.4/'THE NEW MODEL IS:'/'X1=',E11.4,2
       2X,'T1=',E11.4,2X,'V1=',E11.4,2X,'V2=',E11.4/'RMS=',E11.4/'TYPE 1
       3FOR ANOTHER ITERATION, 2 TO QUIT')
        READ(1,65)IT
65      FORMAT(I1)
        IF(IT.EQ.1)GO TO 8
        RETURN
        END
```

```
      SUBROUTINE PIVOT(A,F,N,NN)
C---SOLVES THE MATRIX EQUATION [F]=[A][M] FOR [M].
C---[F] IS THE DATA MATRIX (NX1)
C---[A] IS THE COEFFICIENT MATRIX (NXN)
C---[M] IS THE SOLUTION MATRIX (NX1)
C---INPUTS ARE [A], [F], THE DIMENSION OF THE ARRAYS(N), AND THE MAX.
C---DIMENSION OF THE ARRAYS(NN).
C---OUTPUT IS [M], RETURNED TO MAIN PROGRAM THROUGH F.
C---WRITTEN BY M. FEHLER
C-----------------------------------------------------------------------
      COMMON MI(70)
      DIMENSION A(NN,NN),F(NN)
      DO 19 I=1,N
   19 MI(I)=I
C
C L - U DECOMPOSITION
C
      N1=N-1
      DO 9 J=1,N1
      AMAX=0.
      DO 999 I=1,N
      IF (MI(I).LT.J) GO TO 999
      ATEST=ABS(A(I,J))
      IF ( ATEST.LT.AMAX) GO TO 999
      AMAX=ATEST
      II=I
  999 CONTINUE
      J1=J+1
      DO 29 I=1,N
      IF(MI(I).EQ.J) GO TO 30
   29 CONTINUE
   30 MI(I)=MI(II)
      MI(II)=J
      DO 9 I=1,N
      IF (MI(I).LE.J)GO TO 9
      FM=A(I,J)/A(II,J)
      DO 8 K=J1,N
    8 A(I,K)=A(I,K)-FM*A(II,K)
      A(I,J)=FM
    9 CONTINUE
C
C 'G' FROM 'L' AND 'F'
C
      DO 79 J=1,N1
      II=IMAX(J,N)
      DO 79 I=1,N
      IF(MI(I).LE.J) GO TO 79
      F(I)=F(I)-A(I,J)*F(II)
   79 CONTINUE
C
C 'X' FROM 'U' AND 'G'
C
      DO 89 J=1,N
      JJ = N-J + 1
      J1=JJ+1
      II=IMAX(JJ,N)
      IF(J1.GT.N) GO TO 85
      DO 88 K=J1,N
      L=IMAX(K,N)
   88 F(II)=F(II)-F(L)*A(II,K)
   85 F(II)=F(II)/A(II,JJ)
   89 CONTINUE
      CALL ASORTP(F,MI,N)
      RETURN
      END
      FUNCTION IMAX(J,N)
      COMMON MI(70)
      DO 77 I=1,N
```

```
      IF(MI(I).NE.J) GO TO 77
      IMAX=I
      RETURN
   77 CONTINUE
      END
        SUBROUTINE ASORTP(F,M,NT)
C---SUBROUTINE TO RE-ORDER RESULTS OBTAINED IN PIVOT
C---M. FEHLER 2/4/81
        DIMENSION F(NT),M(NT)
        IF(NT.LE.1) RETURN
        N = NT - 1
        DO 30 I = 1,N
        I1 = I + 1
        DO 30 K = I1,NT
        IF(M(I).LE.M(K)) GO TO 30
        TEMP = M(I)
        M(I) = M(K)
        M(K) = TEMP
        TEMP = F(I)
        F(I) = F(K)
        F(K) = TEMP
  30    CONTINUE
        RETURN
        END
```

```
C   PROGRAM TIMETERM
C---SOLVES FOR SOURCE & RECEIVER TIME TERMS GIVEN DISTANCES AND TRAVEL-
C---TIMES FROM GIVEN EARTHQUAKES AND STATIONS.
C---USES SUBROUTINE PIVOT.
C---EQLIST IS THE COMMAND FILE OF EVENTS USED
C---TITERM16 IS THE OUTPUT FILE FOR THE RESULTS
C---GRAVCOR IS THE INPUT FILE OF ELEVATION CORRECTIONS TO TRAVELTIMES
C-------------------------------------------------------------------------
$INSERT SYSCOM>KEYS.F
      DIMENSION B(70,70),D(35,35),T(35,35),ATD(70),NFILE(4),EC(33)
      DIMENSION R(70,70),SD(70)
      REAL N(35)
C---OPEN INPUT & OUTPUT FILES
      CALL SRCH$$(K$READ,'EQLIST',6,6,ITYPE,ICODE)
      CALL SRCH$$(K$READ,'GRAVCOR',7,5,ITYPE,ICODE)
      CALL SRCH$$(K$WRIT,'TITERM16',8,3,ITYPE,ICODE)
C---NE IS THE NO. OF EVENTS IN THE COMMAND FILE
C---NS IS THE NO. OF STATIONS
C---CD IS THE DISTANCE BELOW WHICH DISTS. & TRAVELTIMES ARE NOT USED
      READ(10,2)NE,NS,CD
    2 FORMAT(I2,1X,I2,1X,F5.0)
      JJ=NE+1
C---NM IS THE DIMENSION OF THE MATRIX
      NM=NE+NS
C---INITIALIZING ALL ARRAYS TO ZERO
      DO 5 M=1,NS
    5 N(M)=0.
      DO 20 K=1,NM
      DO 10 L=1,NM
      R(K,L)=0.
   10 B(K,L)=0.
   20 ATD(K)=0.
C---READ ELEVATION CORRECTIONS
      DO 25 K=1,33
      READ(9,22)EC(K)
   22 FORMAT(F10.3)
   25 CONTINUE
C---CLOSE ELEVATION CORRECTION FILE
      CALL SRCH$$(K$CLOS,'GRAVCOR',7,5,ITYPE,ICODE)
      DO 90 J=1,NE
C---READ AN EVENT FILENAME FROM COMMAND LIST
      READ(10,30)NFILE
   30 FORMAT(4A2)
C---OPEN THE EVENT FILE
      CALL SRCH$$(K$READ,NFILE,8,2,ITYPE,ICODE)
      DO 80 I=1,NS
C---READ THE DISTANCES & TRAVELTIMES FROM THE EVENT TO THE STATIONS
      READ(6,40)D(I,J),T(I,J)
   40 FORMAT(8X,F8.3,10X,F6.2)
C---SUBTRACT ELEVATION CORRECTIONS FROM TRAVELTIMES
      T(I,J)=T(I,J)-EC(I)
      IF(D(I,J).GT.CD) GO TO 45
      D(I,J)=0.0
      T(I,J)=0.0
   45 CONTINUE
C---BUILD THE ATA MATRIX & THE ATD VECTOR
      IF(I.EQ.1) GO TO 50
      B(1,NE+I)=B(1,NE+I)+D(I,J)
      ATD(NE+I)=ATD(NE+I)+T(I,J)
      IF(D(I,J).NE.0.) B(J+1,NE+I)=1.
   50 IF(D(I,J).NE.0.) B(J+1,J+1)=B(J+1,J+1)+1.
      IF(D(I,J).NE.0.) N(I)=N(I)+1.
      B(1,1)=B(1,1)+(D(I,J)**2.)
      B(1,J+1)=B(1,J+1)+D(I,J)
      ATD(J+1)=ATD(J+1)+T(I,J)
      ATD(1)=ATD(1)+(D(I,J)*T(I,J))
   80 CONTINUE
C---CLOSE THE EVENT FILE
```

```
      CALL SRCH$$(K$CLOS,NFILE,8,2,ITYPE,ICODE)
C---GO TO THE NEXT EVENT
   90 CONTINUE
C---CLOSE COMMAND FILE
      CALL SRCH$$(K$CLOS,'EQLIST',6,6,ITYPE,ICODE)
C---BUILD MORE OF THE ATA MATRIX
      DO 100 III=2,NS
  100 B(NE+III,NE+III)=N(III)
C---MAKE IT SYMMETRIC
      DO 120 L=1,NM
      DO 110 K=1,NM
  110 B(K,L)=B(L,K)
  120 CONTINUE
      NN=70
C---INVERT THE ATA MATRIX & SOLVE FOR THE TIMETERMS
      CALL PIVOT(B,ATD,NM,NN)
C---INVERT THE FIRST ELEMENT OF THE SOLUTION VECTOR TO OBTAIN THE
C---REFRACTOR VELOCITY.
      ATD(1)=1./ATD(1)
C---CALCULATE STANDARD DEVIATIONS OF THE TIMETERMS
      NM1=NM-1
      K1=NS-1
      DO 220 I=1,NM1
      SRSQ=0.
      N1=0
      IF(I.LE.K1)GO TO 200
      DO 190 J=1,K1
      IF(D(J,I-K1).EQ.0.)GO TO 190
      R(J,I-K1)=T(J,I-K1)-(D(J,I-K1)/ATD(1))-ATD(I-K1+1)-ATD(JJ+J)
      N1=N1+1
      SRSQ=SRSQ+R(J,I-K1)**2
  190 CONTINUE
      SD(I-K1+1)=SQRT(SRSQ/((N1-1)*N1))
      GO TO 220
  200 DO 210 J=1,NE
      IF(D(I,J).EQ.0.)GO TO 210
      R(I,J)=T(I,J)-(D(I,J)/ATD(1))-ATD(J+1)-ATD(JJ+I)
      N1=N1+1
      SRSQ=SRSQ+R(I,J)**2
  210 CONTINUE
      SD(I+JJ)=SQRT(SRSQ/((N1-1)*N1))
  220 CONTINUE
C---WRITE THE REFRACTOR VELOCITY
      WRITE(7,130)ATD(1)
  130 FORMAT('REFRACTOR VELOCITY=',E11.4//'THE SOURCE TERMS ARE:'/)
C---WRITE THE SOURCE TERMS & THEIR STAN. DEVS.
      DO 150 KK=2,JJ
      WRITE(7,140)ATD(KK),SD(KK)
  140 FORMAT(E10.3,3X,F8.4)
  150 CONTINUE
      WRITE(7,155)
  155 FORMAT(/'THE RECEIVER TERMS ARE:'/)
      LL=JJ+1
C---WRITE THE RECEIVER TERMS & THEIR STAN. DEVS.
      DO 170 MM=LL,NM
      WRITE(7,140)ATD(MM),SD(MM)
  170 CONTINUE
C---CLOSE OUTPUT FILE
      CALL SRCH$$(K$CLOS,'TITERM16',8,3,ITYPE,ICODE)
      STOP
      END
```

```
C   PROGRAM VELAZ
C---FITS LEAST-SQUARES SINE WAVE TO VELOCITY VS. AZIMUTH PLOT AND
C---FINDS DIP OF REFRACTOR VS. UPPER LAYER VELOCITY.
C---USES SUBROUTINES PIVOT & ECL AND THE IRVING PLOTTING LIBRARY.
C---INPUT FILE CONTAINS THE AZIMUTH AND VELOCITY DATA.
C-------------------------------------------------------------------------
$INSERT SYSCOM>KEYS.F
      DIMENSION AZ(30),V(30),A(3,3),F(3),Y(181),AZD(30),NSTA(2),NLE(8)
      DIMENSION X(181),XLINE(30),YLINE(30),XPLOT(181),YPLOT(181)
      N=3
      NN=3
C---GIVE NAME OF INPUT FILE AND OPEN IT
      CALL INFILE(7,NLE,ILEN,K)
C---READ NUMBER OF POINTS IN INPUT FILE
      READ(7,10)ND
   10 FORMAT(I2)
      DO 30 I=1,ND
C---READ AZIMUTH, VELOCITY PAIR
      READ(7,20)AZD(I),V(I)
   20 FORMAT(F6.2,1X,F5.3)
C---CONVERT AZIMUTH FROM DEGREES TO RADIANS
      AZ(I)=AZD(I)*(3.14159/180.)
C---SCALE DATA POINTS FOR PLOTTING
      YLINE(I)=(V(I)-6.0)*2.5
      XLINE(I)=AZD(I)/40.0
   30 CONTINUE
C---CLOSE INPUT FILE
      CALL SRCH$$(K$CLOS,NLE,ILEN,3,ITYPE,ICODE)
C---INITIALIZE THE MATRIX EQUATION ARRAYS
      DO 33 K=1,3
      F(K)=0.
      DO 33 L=1,3
      A(K,L)=0.
   33 CONTINUE
C---BUILD THE MATRIX EQUATION ARRAYS
      DO 40 J=1,ND
      A(1,2)=A(1,2)+SIN(AZ(J))
      A(1,3)=A(1,3)+COS(AZ(J))
      A(2,2)=A(2,2)+(SIN(AZ(J))**2)
      A(3,3)=A(3,3)+(COS(AZ(J))**2)
      A(2,3)=A(2,3)+(SIN(AZ(J))*COS(AZ(J)))
      F(1)=F(1)+V(J)
      F(2)=F(2)+(V(J)*SIN(AZ(J)))
      F(3)=F(3)+(V(J)*COS(AZ(J)))
   40 CONTINUE
      A(2,1)=A(1,2)
      A(3,1)=A(1,3)
      A(3,2)=A(2,3)
      A(1,1)=ND
C---INVERT & SOLVE MATRIX EQUATION
      CALL PIVOT(A,F,N,NN)
C---FIND PARAMETERS OF SINE WAVE EQUATION
      B=SQRT((F(2)**2)+(F(3)**2))
      PHI=ATAN(F(3)/F(2))
      PHIDEG=PHI*(180./3.14159)
      VU=0.
      VD=10.0
C---CONSTRUCT SINE CURVE
      DO 50 M=1,181
      Y(M)=F(1)+B*SIN(-(((M-1)*0.0349)+PHI))
      X(M)=FLOAT((M-1)*2)
C---SCALE SINE CURVE FOR PLOTTING
      YPLOT(M)=(Y(M)-6.0)*2.5
      XPLOT(M)=X(M)/40.0
C---FIND MINIMUM & MAXIMUM OF SINE CURVE
      VD=AMIN1(VD,Y(M))
      IF(VU.GT.Y(M)) GO TO 50
      VU=Y(M)
```

```
      DIPAZ=X(M)
   50 CONTINUE
      WRITE(1,55)
   55 FORMAT(1X,'INPUT STATION NAME FOR OUTPUT ON PLOT')
      READ(1,57)NSTA
   57 FORMAT(2A2)
C---INITIALIZE PLOTTING ROUTINES
      CALL PLOTS(0,0,99)
C---PLOT VELOCITY VS. AZIMUTH DATA PTS. AND SINE CURVE
      CALL AXES(0.,0.,0.,360.,0.025,40.,40.,4HF4.0,0.,'AZIMUTH (DEGS)',
     114)
      CALL AXES(0.,0.,6.0,8.8,2.5,0.4,0.4,4HF4.1,90.,'VELOCITY (KM/SEC)
     2',17)
      DO 65 L=1,ND
      CALL SYMBOL(XLINE(L),YLINE(L),0.05,4,0.,-1)
   65 CONTINUE
      CALL PLOT(XPLOT(1),YPLOT(1),3)
      DO 70 J=1,181
      CALL PLOT(XPLOT(J),YPLOT(J),2)
   70 CONTINUE
      CALL SYMBOL(7.5,9.5,0.15,'STATION',0.,7)
      CALL SYMBOL(8.54,9.5,0.15,NSTA,0.,4)
      CALL SYMBOL(7.5,9.2,0.10,'V=VAVG+B*SIN(AZ+PHI)',0.,20)
      CALL SYMBOL(7.5,9.0,0.10,'VAVG=',0.,5)
      CALL NUMBER(8.0,9.0,0.10,F(1),0.,4HF5.3)
      CALL SYMBOL(7.5,8.8,0.10,'B=',0.,2)
      CALL NUMBER(7.7,8.8,0.10,B,0.,4HF5.3)
      CALL SYMBOL(8.3,8.8,0.10,'PHI=',0.,4)
      CALL NUMBER(8.7,8.8,0.10,PHIDEG,0.,4HF6.2)
      CALL SYMBOL(7.5,8.6,0.10,'VELOCITY UP=',0.,12)
      CALL NUMBER(8.6,8.6,0.10,VU,0.,4HF5.3)
      CALL SYMBOL(7.5,8.4,0.10,'VELOCITY DOWN=',0.,14)
      CALL NUMBER(8.75,8.4,0.10,VD,0.,4HF5.3)
      CALL SYMBOL(7.5,8.2,0.10,'AZIMUTH OF DIP=',0.,15)
      CALL NUMBER(8.85,8.2,0.10,DIPAZ,0.,4HF6.2)
      CALL PLOT(11.5,0.,-3)
C---PLOT DIP VS. UPPER LAYER VELOCITY
      CALL AXES(0.,0.,6.4,7.1,10.0,0.1,0.1,4HF4.1,0.,'UPPER LAYER VEL.
     3(KM/SEC)',25)
      CALL AXES(0.,0.,0.,9.0,1.0,1.0,1.0,4HF4.1,90.,'DIP (DEGS)',10)
      CALL PLOT(0.,0.,3)
      DO 80 K=1,71
      V1=6.4+(0.01*(K-1))
      DIP=(B*V1)/((F(1)**2)*SQRT(1-(V1/F(1))**2))
      DIPDEG=(DIP*(180./3.14159))
      VPLOT=(V1-6.4)*10.
      CALL PLOT(VPLOT,DIPDEG,2)
   80 CONTINUE
      CALL PLOT(0.,0.,40)
      STOP
      END
```

```
C---SUBROUTINE PACKAGE ECL
      SUBROUTINE INFILE(J,NLE,ILEN,K)
       INTEGER*2 NLE(8)
$INSERT SYSCOM>KEYS.F
$INSERT SYSCOM>ERRD.F
       IUNIT = J -4
       ITYPE = 0
       IF(J.GT.5) GO TO 10
       WRITE(1,3) J
  3    FORMAT(1X,'CANT OPEN FILE FOR UNIT NUMBER ',I6)
       RETURN
  10   WRITE(1,4) J
   4   FORMAT(1X,'INPUT NAME OF INPUT FILE FOR CHANNEL ',I6)
       CALL CNIN$(NLE,16,ILEN)
       ILEN = ILEN - 1
       K = J - 4
       CALL SRCH$$(K$EXST,NLE,ILEN,IUNIT,ITYPE,ICODE)
       IF(ICODE.NE.E$FNTF) GO TO 20
       WRITE(1,5)
   5   FORMAT(1X,'FILE DOES NOT EXIST, TRY AGAIN ')
       GO TO 10
  20   CALL SRCH$$(K$READ,NLE,ILEN,K,ITYPE,ICODE)
       IF(ICODE.EQ.0) GO TO 30
       WRITE(1,40) ICODE
  40   FORMAT(1X,'ERROR OPENING FILE, CODE = ',I6)
  30   CONTINUE
       RETURN
       END
      SUBROUTINE OUTFIL(J,NLE,ILEN,K)
       INTEGER*2 NLE(8)
$INSERT SYSCOM>KEYS.F
$INSERT SYSCOM>ERRD.F
       IUNIT = J -4
       ITYPE = 0
       IF(J.GT.5) GO TO 10
       WRITE(1,3) J
  3    FORMAT(1X,'CANT OPEN FILE FOR UNIT NUMBER ',I6)
       RETURN
  10   WRITE(1,4) J
   4   FORMAT(1X,'INPUT NAME OF OUTPUT FILE FOR CHANNEL ',I6)
       CALL CNIN$(NLE,16,ILEN)
       ILEN = ILEN - 1
       K = J - 4
  103  CALL SRCH$$(K$EXST,NLE,ILEN,IUNIT,ITYPE,ICODE)
       IF(ICODE.EQ.E$FNTF) GO TO 20
  102  WRITE(1,5)
   5   FORMAT(1X,'FILE ALREADY EXISTS, DO YOU WANT TO DELETE ')
       CALL YESNO(N)
       GO TO (100,10,102) ,N
  100  CALL SRCH$$(K$DELE,NLE,ILEN,K,ITYPE,ICODE)
       GO TO 103
  20   CALL SRCH$$(K$WRIT,NLE,ILEN,K,ITYPE,ICODE)
       IF(ICODE.EQ.0) GO TO 30
       WRITE(1,40) ICODE
  40   FORMAT(1X,'ERROR OPENING FILE, CODE = ',I6)
  30   CONTINUE
       RETURN
       END
      SUBROUTINE YESNO(N)
       READ(1,5) IY
  5    FORMAT(A1)
       IF(IY-'Y ') 10,1,10
  10   IF(IY-'N ') 3,2,3
C---YES ANSWER
  1    N = 1
       RETURN
C---NO ANSWER
  2    N = 2
```